

AN INVESTIGATION OF CYCLIC, IMMISCIBLE
TWO-PHASE FLOW IN POROUS MEDIA

By

EDWARD G. WOODS

Bachelor of Science
Oklahoma State University of
Agriculture and Applied Science
Stillwater, Oklahoma
1959

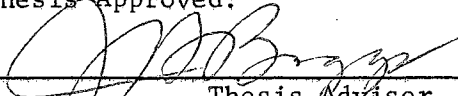
Master of Science
Oklahoma State University of
Agriculture and Applied Science
Stillwater, Oklahoma
1960

Submitted to the Faculty of the Graduate School
of the Oklahoma State University of Agriculture
and Applied Science in partial fulfillment
of the requirements for the degree of
DOCTOR OF PHILOSOPHY
May, 1963

JAN 9 1964

AN INVESTIGATION OF CYCLIC, IMMISCIBLE
TWO-PHASE FLOW IN POROUS MEDIA

Thesis Approved:



Thesis Adviser











Dean of the Graduate School

ACKNOWLEDGEMENT

I wish to thank the Northern Natural Gas Company of Omaha, Nebraska, for their sponsorship of the research program that made this study possible and for supplying core samples from their Redfield, Iowa, storage field. I appreciate the cooperation of E. V. Martinson and his associates in the Underground Storage Department for making information available concerning this storage field. My appreciation also goes to the Faculty of the School of Mechanical Engineering, Oklahoma State University for awarding me the graduate assistantship that made my doctoral study possible.

I offer my thanks to Professor A. G. Comer, research project leader and doctoral committee member, for his constant encouragement and untiring efforts during the course of this research problem. I also appreciate the efforts of Dr. J. H. Boggs, committee chairman, Dr. R. D. Morrison, and Professors E. C. Fitch and E. J. Waller, committee members.

For their discussion of experimental equipment and methods in the initial stages of this problem, I thank Mr. Jack Bobek and associates of the Jersey Production Research Company, Tulsa, Oklahoma, and the late Mr. C. R. Stewart and associates of the Pan American Research Corporation, Tulsa, Oklahoma.

The aid and cooperation of the staff of the Mechanical Engineering Laboratory, the late Professor B. S. Davenport, Professor F. C. McQuiston, J. A. McCandless, George Cooper and L. S. Benjamin in constructing the experimental apparatus is gratefully recognized.

I wish to thank master's candidates H. J. Baker and E. W. Adams and undergraduates James Webb and Tom Groves for their aid with the experimental testing. I thank Mr. F. H. Brinkman and Dr. Keith Coats of the Jersey Production Research Company for their discussion of the partial differential equation for two-phase flow with hysteresis and the frontal equation for withdrawal.

For her aid in preparing this manuscript and for her continued encouragement, I offer my appreciation to my wife Norma. To my parents and the many others who have encouraged and guided me I offer my heartfelt thanks. I also thank Mrs. Mildred Avery and Mrs. Norma Monday for their aid in preparing this manuscript.

TABLE OF CONTENTS

Chapter	Page
I. INTRODUCTION	1
II. PREVIOUS INVESTIGATIONS	4
III. THEORETICAL CONSIDERATIONS.	11
Two-Phase Flow Equations	12
Frontal Development, First Injection	14
Frontal Development, Withdrawal Without Hysteresis	14
Frontal Development, Second Injection Without Hysteresis	18
Two-Phase Flow With Hysteresis	19
Frontal Development With Hysteresis.	20
Withdrawal	20
Injection	22
Water Production	22
Average Saturation	24
Two-Phase Gas Zone, Unsteady-Aquifer Model	25
IV. EXPERIMENTAL APPARATUS	30
Core Assembly.	30
Pressure Measurement	33
Fluid Control System	34
Fluid Measurement.	37
Electrical System	37
Instrument and Control Panel	40
V. EXPERIMENTAL PROCEDURE	43
Drying of Cores	45
Klinkenberg Permeability	45
Saturation of Cores.	46
Water Permeability Tests	47
Saturation Measurement	47
Data Observations.	48
VI. EXPERIMENTAL RESULTS.	49
Porosity	49
Resistance-Saturation Measurements	55
Single-Phase Permeability.	68
Relative Permeability.	72

TABLE OF CONTENTS (CONTINUED)

Chapter	Page
VII. PREDICTED RESERVOIR PERFORMANCE	93
Example Problem.	93
VIII. SUMMARY AND CONCLUSIONS	101
IX. RECOMMENDATIONS FOR FUTURE STUDY	104
BIBLIOGRAPHY	106
APPENDIX	112
A. DERIVATION OF EQUATIONS	112
Material Balance	112
Fractional Flow.	113
Two-Phase Flow	114
Two-Phase Flow With Hysteresis	116
Frontal Development, First Injection	117
Frontal Development, Withdrawal.	118
Frontal Development, Injection After Withdrawal.	120
Water Production	123
Average Saturation	125
Two-Phase Gas Zone, Unsteady Aquifer Model	126
B. COMPUTER PROGRAMS	130
Relative Permeability.	130
Saturation-Resistance.	134
Klinkenberg Permeability, Model II, Bivariate.	137
Relative Permeability Tabulation	140
Fractional Flow-Saturation Distribution.	146
Two-Phase Gas Zone, Unsteady-Aquifer Model	150
Cyclic Two-Phase Flow,	155
C. SYMBOLS	162

LIST OF TABLES

Table	Page
I. Core Sample Specifications	50
II. Porosity	52
III. Saturation-Resistance, Core AL-1-13	62
IV. Saturation-Resistance, Core AL-1-21	63
V. Saturation-Resistance, Core D-1-1	64
VI. Saturation-Resistance, Core M-1-1A	64
VII. Saturation-Resistance, Core M-2-1	65
VIII. Saturation-Resistance, Core N-3-1	66
IX. Single-Phase Permeability	70
X. Relative Permeability, Core AL-1-13	75
XI. Relative Permeability, Core AL-1-21	77
XII. Relative Permeability, Core D-1-1	80
XIII. Relative Permeability, Core M-1-1A (Run 1).	85
XIV. Relative Permeability, Core M-1-1A (Run 2).	86
XV. Relative Permeability, Core M-2-1	89
XVI. Relative Permeability, Core N-3-1	91
XVII. Relative Permeability Computer Program.	132
XVIII. Saturation Resistance Computer Program.	136
XIX. Klinkenberg Permeability Computer Program	142
XX. Relative Permeability Tabulation Computer Program	145

LIST OF TABLES (CONTINUED)

Table	Page
XXI. Fractional Flow-Saturation Distribution Computer Program. ,	148
XXII. Two-Phase Gas Zone, Unsteady-Aquifer Model Computer Program	153
XXIII. Cyclic Two-Phase Flow Computer Program	159

LIST OF FIGURES

Figure	Page
1. Radial Saturation Distribution - w/o Hysteresis.	15
2. Fractional Flow with Frontal and Average Saturations	16
3. Radial Saturation Distribution, Hysteresis Case, $S_{gr} \geq S_f$	21
4. Saturation Distribution at Breakthrough.	23
5. Mathematical Model	26
6. Typical Pressure Gradient, Injection Case.	26
7. Plastic Core Assembly.	31
8. Fluid Flow Diagram	38
9. Gas-Liquid Separator	39
10. Pressure Transducer Electrical Circuit	41
11. Saturation-Resistance, Core AL-1-13.	56
12. Saturation-Resistance, Core AL-1-21.	57
13. Saturation-Resistance, Core D-1-1.	58
14. Saturation-Resistance, Core M-1-1A	59
15. Saturation-Resistance, Core M-2-1.	60
16. Saturation-Resistance, Core N-3-1.	61
17. Klinkenberg Permeability, Core AL-1-21	71
18. Relative Permeability, Core AL-1-13.	74
19. Relative Permeability, Core AL-1-21.	76
20. Relative Permeability, Core D-1-1,	79

LIST OF FIGURES (CONTINUED)

Figure	Page
21. Relative Permeability, Core M-1-1A (Run 1)	83
22. Relative Permeability, Core M-1-1A (Run 2)	84
23. Relative Permeability, Core M-2-1	88
24. Relative Permeability, Core N-3-1	90
25. Relative Permeability, Core N-3-1, Curve Fitted	95
26. Injection-Production Performance, w/o Hysteresis	96
27. Gas-Water Production	97
28. Injection-Production Performance with Hysteresis	99
29. Flow Chart, Relative Permeability	131
30. Flow Chart, Saturation-Resistance	135
31. Flow Chart, Klinkenberg Permeability	141
32. Flow Chart, Relative Permeability Tabulation	144
33. Flow Chart, Fractional Flow-Saturation Distribution	147
34. Flow Chart, Two-Phase Gas Zone, Unsteady-Aquifer Model	151
35. Flow Chart, Cyclic, Two-Phase Flow	157

LIST OF PLATES

Plate	Page
I. Rubber Sleeve Core Assembly	32
II. Constant Rate Liquid Pump	35
III. Pump Transmission and Motor	36
IV. Instrument Panel.	42

CHAPTER I

INTRODUCTION

In recent years the natural gas industry has turned to underground storage in its continuing efforts to develop low cost gas storage facilities in its marketing areas ⁽³⁾. One such development -- gas storage in virgin aquifers -- was initiated because of the absence of depleted oil or gas fields near many of the centers of high gas consumption.

Rigid government regulation of these projects has enhanced the need for adequate description of the performance of these man-made gas fields. The need for this description has brought about several interesting extensions of the fluid-flow-in-porous-media concepts of reservoir mechanics. Included among these fluid flow concepts are the theories of unsteady-state flow and of two-phase flow. The object of this dissertation was a study of a portion of the two-phase flow theory.

The two-phase fluid flow occurring in gas storage reservoirs differs from the two-phase flow conditions that are normally encountered in natural petroleum reservoirs. This difference in flow conditions arises because the geologic formations used for gas storage reservoirs are subjected to a cyclic process of gas injection and withdrawal at common points in the reservoir. In contrast to the gas storage case are processes such as water flooding or gas cycling of a petroleum reservoir. In these oil recovery cases, the displacing fluid is

injected at one point in the reservoir while the produced fluid is withdrawn simultaneously at a different point. The importance of this difference in operation is that the cyclic operation of gas storage reservoirs introduces, within the reservoir, flow conditions under which the relative permeability hysteresis phenomenon has been observed.

The hysteresis phenomenon becomes important in describing gas reservoir behavior because it has the effect of physically trapping, within the reservoir, a volume of gas that is significant economically. Also, an additional volume of gas is not recoverable economically because the production of a large volume of water is required to recover small increments of gas. The gas industry can never divorce its operations from economic considerations. Therefore, it is of particular importance when selecting and operating a gas storage reservoir to estimate accurately this loss of gas which is related to the two-phase relative permeability characteristics of the rock formation.

Relative permeability characteristics vary from formation to formation; thus it is an obvious conclusion that certain formations are more desirable than others for the purpose of gas storage. However, one should be cognizant of the fact that random variations of permeability also occur within formations which add to the complexity of the problem under consideration.

In addition to predicting the volume of gas lost, the two-phase flow concept provides essential data for predicting the rate of water production during gas withdrawal and for predicting the efficiency of the displacement of the water during gas injection. Information concerning water production rate is essential for the efficient selection of production wells in order to minimize the hydrate and line freeze-up

problems occurring at the cold temperatures during which gas demand is highest. The water production information can also be used in sizing equipment to meet the peak load demands for removal and disposal of water from the produced gas. With regard to water displacement efficiency, two-phase flow theory should lead to techniques for the development of underground storage in aquifers which will maximize gas storage volume per unit of rock pore volume.

The key to the solution of many of the problems mentioned above is the rapid advance in computer technology in recent years. These technological advances have made possible and have created an interest in the simulation of industrial processes by mathematical models. By applying mathematical techniques and high speed computers, this study seeks to contribute to the development of such a model for the gas storage process. As theoretical advances are made in the more accurate mathematical description of the reservoir mechanics of the gas storage process, these devices should make possible a rapid and accurate prediction of the storage reservoir behavior under any one proposed set of operating conditions. This ability to predict reservoir behavior would then make possible the comparison of many different operating programs in order to select the most desirable program.

CHAPTER II

PREVIOUS INVESTIGATIONS

The development of two-phase flow theory has progressed rapidly since Buckley and Leverett (4, 35) published their work on "Mechanism of Fluid Displacement in Sands" in 1941. Their work has been extended from linear to radial systems (51, 64) and from water displacement of oil to cases of gas going into and coming out of solution during the displacement of oil by gas (48). Currently, there is also a substantial interest in the field of two-phase flow in the area of miscible displacement of oil from sands (7, 20, 48, 59).

Also of interest is the work that has been done on the effects of gravity and capillary pressure as they affect the two-phase displacement process (15, 19, 26, 39). Of particular importance in these investigations is the fact that the inclusion of the capillary pressure term in the fractional flow equation eliminates the triple value of saturation that occurs in the Buckley-Leverett equation (6). However, its inclusion means resorting to numerical methods and high-speed computers for the solution of the differential equation. The triple value has previously been eliminated by material balance considerations (4, 63) and shock theory (60).

Hawthorne (25) has presented Dietz's theory (14) to determine the tilting of the fluid interface due to gravity effects as one fluid is displaced by another at low rates. It should be noted, however, that

this theory considers a constant saturation of the displacing fluid in the region behind the fluid interface. The assumption of constant saturation is not true in the general case.

West, et al ⁽⁶⁵⁾ have investigated the case of unsteady-state, two-phase flow for a bounded, solution-gas-drive system by the simultaneous, finite difference solution of two second-order, non-linear partial differential equations at each time step. Nevertheless, their solution does not consider frontal displacement or cyclic flow which are both of importance in gas storage operations.

Welge, et al ⁽⁶⁴⁾ have recently extended the radial, two-phase flow model to a radial cone type reservoir. Their work has potential application in describing the gas storage process since most gas storage reservoirs are of a dome-type geologic structure. In its present form, however, this work considers only the fluid injection process and does not consider cyclic flow.

In a recent publication, Sheffield and Brinkman ⁽⁶¹⁾ have presented a two-dimensional, finite difference analysis of the two-phase displacement process with the effects of gravity and capillary pressure being included. Their work, if modified to include hysteresis, has possible application to gas storage problems.

Geffen and co-workers ⁽²³⁾ have noted the hysteresis phenomena of relative permeability functions. They ⁽²⁴⁾ have also studied experimentally the effect of imbibition on the loss of gas in naturally occurring gas reservoirs being produced by water drive. Their investigations showed that from 15 to 50 per cent of the initial gas in place would be lost ultimately in the exterior region of the reservoir which is subjected to water invasion. It is this phenomenon of high gas losses

that makes the present study of particular interest to the gas storage industry.

A valuable contribution to the theory of relative permeability hysteresis has been made by Naar and Henderson (42, 43). They developed a mathematical model based on a bundle of capillaries of random radii that is sliced into sections and rotated by a random angle thereby having capillaries of random radii joined in series as well as in parallel. Based on this model, Naar and Henderson developed an equation for predicting the imbibition non-wetting phase relative permeability curve from the corresponding drainage curve. Difficulty was encountered in that the imbibition behavior is also related to the consolidation characteristics of the porous medium; that is, an unconsolidated sand behaves very differently from a well consolidated sandstone. It is for this reason that tedious experimental techniques still must be resorted to in determining the hysteresis characteristics of a particular porous medium.

Kruger (31) has experimentally investigated the effect of saturation history on the residual gas saturation after water flooding. He found that the residual gas after water flooding increased with increasing initial gas saturation when using a drainage-imbibition process. Also, when the test cores were displaced to residual water saturation then subjected to an imbibition-partial drainage-imbibition process, he found the residual gas saturation to be essentially constant and to be equal to the maximum residual gas saturation. The residual gas saturation was approximately 30 percent for the cores tested. The described behavior of these cores is the same as would be indicated by an examination of relative permeability curves with hysteresis.

Most of the investigations in the area of two-phase fluid flow in porous media have dealt with the recovery of liquid hydrocarbons; but recently, its application to the gas storage process has been recognized (8, 12, 13, 21).

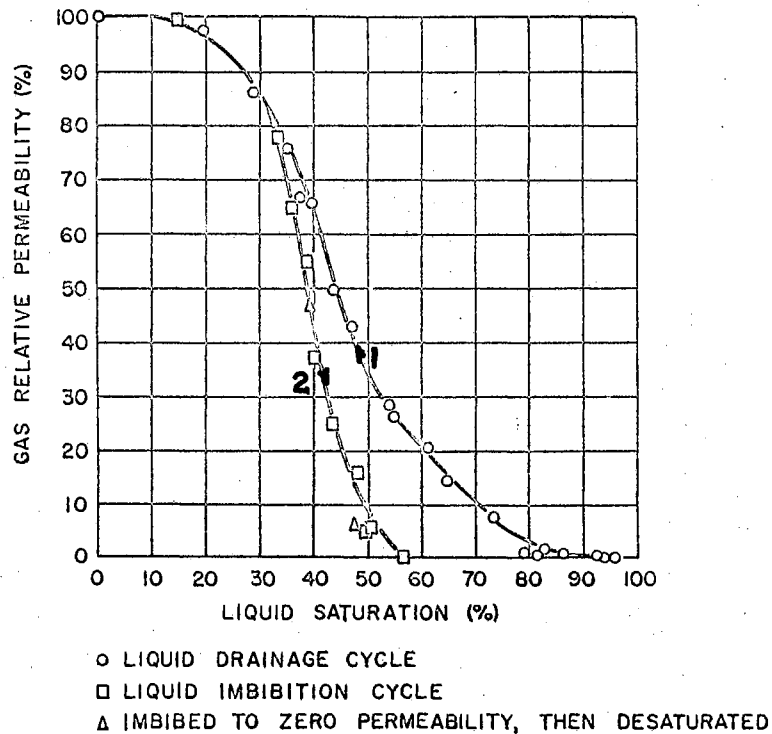
Gardner, et al (21) have noted the importance of hysteresis upon gas storage. Because of the bearing of this article upon this study and because of the complete, concise manner in which it is stated, the following direct quotation is made from their article:

It is the intention of this paper to discuss a factor in the use of aquifers for storing gas which has a profound influence on the economics of storage. This is the necessity of providing "cushion gas"; it stems from a hysteresis in the injection and removal of a non-wetting phase from a porous medium. While the detailed mechanism of this hysteresis is still not fully understood, its consequences are. In brief, it is found that if gas is injected into an aquifer so as to displace water, there remains a certain irreducible volume of water which cannot be displaced. The permeability of the rock to gas during this displacement process is a function of the water saturation. Typically, the relative permeability to gas varies in the manner shown by curve 1 in Fig. 1. When the gas is withdrawn the variation of permeability with water saturation is different; the permeability to gas at a particular saturation is lower than during injection. This is illustrated by curve 2 in Fig. 1. What is important from the standpoint of gas storage is that permeability to gas becomes zero at a gas saturation which may be large. In the example shown in Fig. 1 it is 43 per cent. This means that if gas is injected into an aquifer until the gas saturation exceeds 70 per cent and then attempts are made to remove it, 43 per cent of the pore volume of the rock will contain gas in a form so discontinuous that it is no longer able to flow to a borehole. If gas is again injected it is found that the variation of permeability with saturation now follows the gas withdrawal curves (marked 2 on Fig 1); subsequent production and injection cycles do likewise. In practice, a gas field cannot be produced economically below a saturation somewhat in excess of this trapped residual. This gas volume, greater than 43 per cent of the pore volume in the example cited, is known as "cushion gas." Cushion gas is a phenomenon

only important in the use of aquifers for gas storage, since, in the case of most old gas fields used for storage, the cushion gas is already present as a residual unproduced gas.

If, therefore, a trap structure in a large aquifer is to be used as a reservoir for the storage of natural gas during the summer months and for production during the winter, it is necessary that cushion gas first be injected into the reservoir. In other words, before an aquifer can be used as a reservoir of natural gas it must be conditioned by the pre-injection of some 40 per cent or more of its pore volume of natural gas. This gas is to all intents and purposes lost. In the case of large storage projects the cost of the cushion gas is extremely high and amounts to some 50 per cent of the capital cost of the entire venture.

FIGURE 1
GAS RELATIVE PERMEABILITY FOR BEREA SANDSTONE
ON BOTH LIQUID IMBIBITION AND DRAINAGE CYCLES



(Reproduced from the original source, Ref. 22).

It should be noted that Gardner and co-workers did not deal with the mechanics of flow of the problem, but only considered the problems of mixing and diffusion that arise if a low cost gas such as air or flue gas is used for a cushion gas.

Cornell ⁽¹²⁾ has published a computer program applying the two-phase flow concepts to a linear gas storage reservoir; but he neglected starting the gas withdrawal under the reservoir saturation conditions that existed at the end of the gas injection period. This investigation also did not consider the gas permeability hysteresis phenomena observed by Geffen ⁽²³⁾, by Osaba ⁽⁴⁵⁾, and by Gardner ⁽²²⁾.

An excellent extension of two-phase flow theory was made by Ribe ⁽⁵¹⁾ in studying the "Production Behavior of a Water-Blocked Oil Well." This work developed the radial, two-phase flow equation and applied it to the invasion of an oil sand by water during a work-over operation and then the subsequent removal of the water as the oil was produced. Relative permeability hysteresis was not taken into consideration by Ribe. The writer of this dissertation has been unable to derive Ribe's equation for the gas-water front during withdrawal; however, this may be because his notation is not clearly defined.

Of interest to those persons surveying the two-phase flow literature is a report by Baker ⁽¹⁾ entitled "A Summary of Research of Two-phase, Immiscible Fluid Flow in Porous Media." A "Review of Aquifer Gas Storage Projects" has been presented by Martinson ⁽³⁷⁾. Also, Erickson and Svoboda ⁽¹⁷⁾ have presented geological information of a gas storage reservoir.

Katz and co-workers ^(10, 11, 28, 29, 30, 56, 69) have made a rather extensive investigation into the effect of unsteady aquifer

movement upon the pressure and production performance of gas storage reservoirs. However, their work has not dealt with the actual water displacement process in that a gas zone of constant gas saturation and of essentially constant dimensions has been assumed to exist initially. Also, gas has been considered to be the only flowing phase within the gas storage region; that is, "piston-like" displacement of the water was assumed with all residual water being considered to be immobile.

In a recent publication, the writer of this dissertation and Comer (66) have sought to minimize the limitation of single-phase gas zone flow by incorporating into the unsteady-state model a variable radius, two-phase gas storage region. This model considered only the displacement process during which a single-well radial gas storage reservoir was being developed. However, this model gave a good correlation with the initial development stage of an operating gas storage reservoir.

All of these works that have been reviewed have made important contributions in the fields of two-phase flow and of aquifer storage of natural gas. But, to date, no one has published results of the effect of two-phase flow, with or without relative permeability hysteresis, on the operation of a gas storage reservoir undergoing cyclic injection and withdrawal of gas. It is in this area of two-phase immiscible flow that this dissertation seeks to make a contribution.

CHAPTER III

THEORETICAL CONSIDERATIONS

In using mathematical models to describe the behavior of physical processes, it is necessary to have equations which adequately describe the model. In this chapter, equations are given for describing cyclic, two-phase flow in porous media.

The equations discussed in this chapter are derived in detail in Appendix A. All symbols used in this dissertation are defined in Appendix C and follow those suggested in the AIME Symbols List, Transactions, AIME (1956) 207, 363.

The equations of immiscible two-phase flow in porous media are based on the four fundamental concepts that follow. The material balance or equation of continuity for two-phase flow is given by

$$\nabla \cdot (\rho_i \bar{u}_i) + \phi \frac{\partial}{\partial t} (\rho_i S_i) = 0, \dots i = g, w. \quad (1)$$

Darcy's Law for each phase is represented by

$$\bar{u}_i = \frac{-k k_{ri}(S)}{\mu_i} \nabla (p_i + \rho_i g z). \quad (2)$$

The thermodynamic equation of state for the case of isothermal, incompressible fluid may be written as

$$\frac{\partial \rho_i}{\partial p_i} = 0 \quad (3)$$

The equation for capillary pressure is given by

$$P_c = P_c(S) = P_i - P_j \quad (4)$$

which relates the pressures in the wetting, j , and non-wetting phases, i .

Two-Phase Flow Equations

Equations (1), (2), (3), and (4) can be combined into a pair of general equations for incompressible, immiscible two-phase flow. These two equations are the continuity equations for each phase, i , (20, 65),

$$\nabla \cdot \bar{u}_i + \phi \frac{\partial S_i}{\partial t} = 0, \quad \dots i = g, w \dots \dots \quad (5)$$

and the fractional flow equation

$$f_i = \left[1 - \frac{k_{ri} \bar{u}_t}{k_{rj} u_t} (\nabla P_c + \bar{j} [\rho_g - \rho_w] g) \right] \div \left[1 + \frac{k_{rj} \omega_i}{k_{ri} \omega_j} \right] \dots i = g, w; j = w, g. \dots \quad (6)$$

Except at extremely low flow rates the capillary effects are usually of minor importance and may be neglected (53). Also, if the area under consideration is of limited extent and if the formation thickness is limited, then gravity effects may be neglected without serious error. Since a one-well system is being considered in this study, these assumptions seem justifiable. The validity of these assumptions about capillary pressure and gravity should be investigated for each particular geometrical system that is considered.

With the assumption that gravity and capillary pressure are negligible, the fractional flow equation becomes

$$f_i = \frac{1}{1 + \frac{k_{rj} \mu_i}{k_{ri} \mu_j}}, \dots i = g, w; j = w, g \dots \quad (7)$$

Equations (5) and (7) may be combined when Equation (5) is adapted to a particular geometry.

For linear, incompressible, immiscible flow without gravity and capillary effects, the two-phase flow equation becomes the Buckley-Leverett equation ⁽⁴⁾, as given by Equation (8).

$$\frac{q_t}{\phi A} f'_i \frac{\partial S_i}{\partial x} + \frac{\partial S_i}{\partial t} = 0, \quad i = g, w \dots \quad (8)$$

For the radial case the corresponding equation is

$$\frac{q_t}{2\pi\phi hr} f'_i \frac{\partial S_i}{\partial r} + \frac{\partial S_i}{\partial t} = 0 \dots \quad (9)$$

where $f'_i = df_i/dS$.

Equations (8) and (9) are planar partial differential equations which have no direct analytical solution of the form $S_i = g(r, t)$; however, they yield to solution by the method of characteristics. This method of solution yields the doubly infinite set of curves given by

$$S_i = \text{constant} \dots \quad (10)$$

and

$$r_{i,m} = \left(\frac{\Delta Q f_i}{\pi\phi h} + r_{i,m-1}^2 \right)^{\frac{1}{2}} \dots \quad (11)$$

in which m refers to time, r_i is the radius of a surface of a constant saturation, and ΔQ is the total fluid (gas or gas and water) injected or produced during the ' m 'th time interval. The sign of ΔQ is considered positive for the injection case and negative for the withdrawal case.

The numerical solution of Equation (11) yields a saturation-radius relationship similar to Fig. 1.

Frontal Development, First Injection

The application of Equation (11) and Equation (7) results in a multiple valued saturation distribution at the front which can not exist physically. This condition of a non-unique frontal saturation is remedied by using a material balance procedure to determine the radius of the displacing fluid bank. For a two-phase displacement process the condition to be satisfied for material balance, as shown by Welge (63) for the injection of a non-wetting fluid, is that

$$f'_f = \frac{f_f}{S_f} \quad (12)$$

A graphical interpretation of this condition is that f'_f is the slope of a tangent to the fractional flow curve which passes through the origin. The graphical representation is shown in Fig. 2. The material balance condition is also equivalent to balancing the volumes represented by Regions A and B in Fig. 1.

Frontal Development, Withdrawal Without Hysteresis

The corresponding material balance conditions for two-phase imbibition after displacement are

$$r_* - r_{**} = 0 \quad (13)$$

where r_* and r_{**} are the radii of the upper and lower values of the multi-valued saturation distribution, as shown in Fig. 1, and by material balance that

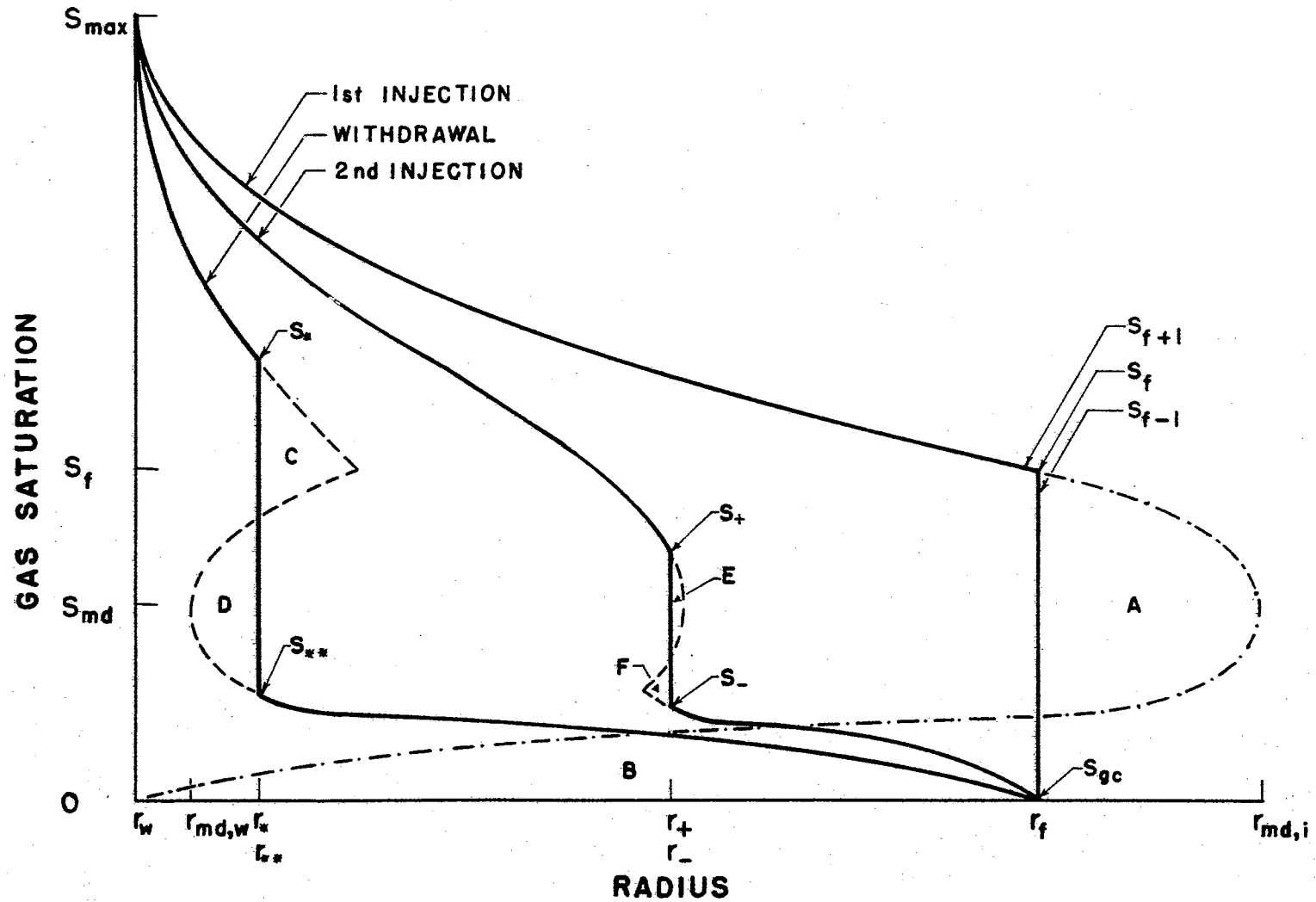


FIG. I RADIAL SATURATION DISTRIBUTION w/o HYSTERESIS

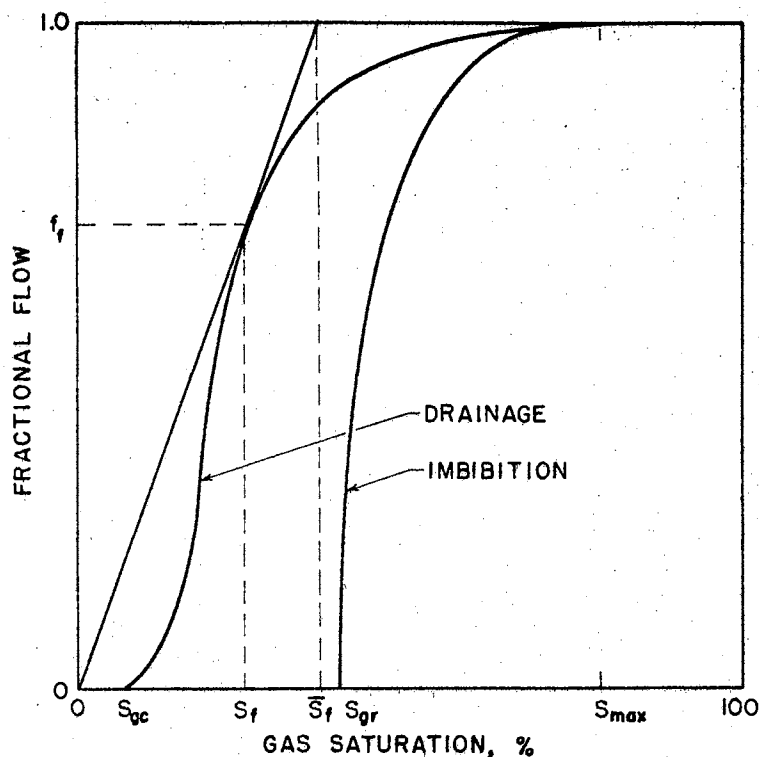


FIG. 2 FRACTIONAL FLOW WITH FRONTAL AND AVERAGE SATURATIONS

$$f'_* = \left\{ f_* - f_{**} + \frac{G_i}{G_p} (f_* - f'_f S_{**}) \right\} \frac{1}{(S_* - S_{**}) \left(1 + \frac{G_i}{G_p} \right)} \quad (14)$$

G_i is the initial volume of gas injected, and G_p is the volume of gas withdrawn (algebraically negative).

The fractional flow function, f , may be calculated from Equation (7) once the experimental relative permeability functions are determined. The derivative of the fractional flow function, f' , may be computed by numerical (57) or graphical methods. Then the saturations at the front, S_* and S_{**} , may be determined by a trial and error solution of Equation (14) for any given fractional volume withdrawn, G_p/G_i . The application of Equation (14) is equivalent to balancing the volumes of C and D in Fig. 1.

Observation of the behavior of the saturation-radius relationship given by Equation (11) in Fig. 1 will show that definite limits can be placed on the values that S_* and S_{**} may assume. For example, consider the relative positions of S_f and S_{f+1} as shown in Fig. 1. These saturations originated from a common surface, the well bore, at the beginning of gas injection; but at the end of the injection period, S_f lies at a greater radius than S_{f+1} because of its greater value of f' . Application of Equation (11) during withdrawal will show that the calculated radius of S_f will always be greater than the radius of S_{f+1} until $Q_p = G_i$. Now consider the relative positions of S_f and S_{f-1} . By material balance (Equation 12), these two saturations are placed on the same radial surface at the end of the injection period. During withdrawal, S_{f-1} will advance toward the well bore more rapidly than S_f because it has a larger value of f' . Therefore, the calculated radius of S_f , during withdrawal, will always be greater than the calculated radius of S_{f-1} . Since S_f has a greater radius than its adjacent values of saturation, it must represent the maximum radius of the Region C in Fig. 1.

Next, observe the behavior of the saturation for which f' is a maximum, S_{md} . By Equation (11) S_{md} will have the maximum rate of advancement toward the well bore because of its fractional flow derivative. At the beginning of withdrawal (end of injection) S_{md} lies on the same radial surface as all $S \leq S_f$. Therefore, because of its rate of travel, the radial position of S_{md} , during withdrawal, will always be less than any $S \leq S_f$ and must then be the minimum radius of the Region D.

Further reflection upon these conditions shows that for Regions C

and D to be equal, S_* must lie between S_f and a higher saturation, $S(r_{md,w})$, having the same radius as S_{md} or $S_f < S_* < [S(r_{md,w}) > S_f]$. The calculated saturation distribution and these same conditions show that $S_{gc} < S_{**} < S_{md}$ where S_{gc} is the critical gas saturation on the drainage gas relative permeability curve.

Frontal Development, Second Injection Without Hysteresis

The process of injection after withdrawal (drainage after imbibition when the injected phase is non-wetting) may be deduced by the same reasoning as for the withdrawal after injection case. The conditions to be satisfied are

$$r_+ - r_- = 0 \quad (15)$$

where r_+ and r_- are the radii of the upper and lower saturations at the front during the second injection and for material balance that

$$f'_+ = \frac{1}{(S_+ - S_-)} \left\{ f_+ - f_- + \frac{Q_p}{G_{i,2}} (f_{**} - f_-) + (S_{**} - S_-) \left[\frac{G_{i,1}}{G_{i,2}} (f'_f - f'_*) - \frac{\Delta Q_p}{G_{i,2}} f'_* \right] \right\} \quad (16)$$

An implicit assumption of these two relations is that relative permeability hysteresis is not important.

For the case of injection after withdrawal, further modification of the equation of the front must be made if the gas-water front for the withdrawal cycle broke through into the well-bore. If this situation has occurred then Equation (16) becomes

$$f'_+ = \frac{1}{(S_+ - S_-)} \left\{ f_+ - f_- + \frac{G_{i,1}}{G_{i,2}} f'_f (S_{wb} - S_-) + \frac{Q_p}{G_{i,2}} (f_{wb} - f_-) \right\} \quad (17)$$

Deliberation upon the ranges of S_+ and S_- as was done for S_* and S_{**} shows that $S_{md} < S_+ < S_*$ and $S_{gc} < S_- < S_{**}$ for the conditions implied by Equation (16). S_* and S_{**} are those values existing at the end of withdrawal (beginning of injection). For Equation (17) where breakthrough has occurred, $S_{md} < S_+ < S_{max}$ and $S_{gc} < S_- < S_{wb}$.

Two-Phase Flow With Hysteresis

In the general imbibition case in which relative permeability hysteresis is a factor, Equations (14) and (16) must be modified. This modification is necessitated by the fact that during an imbibition process the fractional flow function, f_i , is no longer a function of saturation only, but is also dependent upon the direction of approach and upon the initial saturation at a given point. Since a saturation gradient exists in the reservoir as a result of two-phase displacement by gas injection, the fractional flow function will then vary from point to point as well as from saturation to saturation during the imbibition process.

These factors lead to a partial differential equation in two dependent and two independent variables as given by Equation (18),

$$\frac{q_t}{2\pi h \phi r} \left(\frac{\partial f}{\partial S} \frac{\partial S}{\partial r} + \frac{\partial f}{\partial S_{gi}} \frac{\partial S_{gi}}{\partial r} \right) + \frac{\partial S}{\partial t} = 0, \quad (18)$$

where

$$f = f_g(S_g, S_{gi}) \quad (19)$$

is the fractional flow of gas and

$$S_{gi} = g(r) \quad (20)$$

is the initial gas saturation at the radius r at the end of the injection period. The solution of Equation (18) would require the use of complex finite difference techniques.

A solution yielding the limiting performance values for the imbibition case with hysteresis can be obtained by modifying Equations (14), (16), and (17) to permit solutions using the two limiting gas relative permeability curves.

Frontal Development, With Hysteresis

When considering hysteresis, the material balance equations [Equations (14), (16), and (17)] for determining the saturation at the front must be modified to use a combination of fractional flow values from both the drainage and imbibition relative curves. Most of these modifications are minor and arise from the fact that all $S < S_f$ were placed on a common radius by material balance.

Several cases must be recognized. First, the trapped or residual gas saturation, S_{gr} , on the imbibition relative permeability curve may be less than ($S_{gr} < S_f$) or greater than ($S_{gr} > S_f$) the saturation at the front during the initial injection. This creates two withdrawal-second injection situations. Also, since the second injection frontal equation is dependent upon whether or not breakthrough occurred during withdrawal, four possible situations exist for the second injection.

Withdrawal

For the case of fluid withdrawal with hysteresis for the condition that $S_{gr} < S_f$, the frontal equation equivalent to Equation (14) is Equation (21).

$$f'_{*2} = \left\{ f_{*2} - f_{**2} + \frac{G_i}{Q_p} [f_{*1} - f_{f1} S_{**} - f'_{*1} (S_* - S_{**})] \right\} \frac{1}{(S_* - S_{**})}, \quad (21)$$

In this equation the subscript "1" indicates values calculated from the drainage relative permeability curve and "2" indicates values from the hysteresis imbibition relative permeability curve. If hysteresis is not to be considered, Equation (21) reduces to Equation (14) upon replacing the subscript "2" with "1" and making algebraic simplifications.

When the trapped gas saturation for withdrawal, S_{gr} , is greater than the initial saturation at the front, S_f , which will generally be the case, Equation (21) will become Equation (22). This condition is depicted by Fig. 3.

$$f'_{*2} = \left\{ f_{*2} - f_{**2} + \frac{G_i}{Q_p} [f_{*1} - f_{**1} - f'_{*1} (S_* - S_{**})] \right\} \frac{1}{(S_* - S_{**})} \quad (22)$$

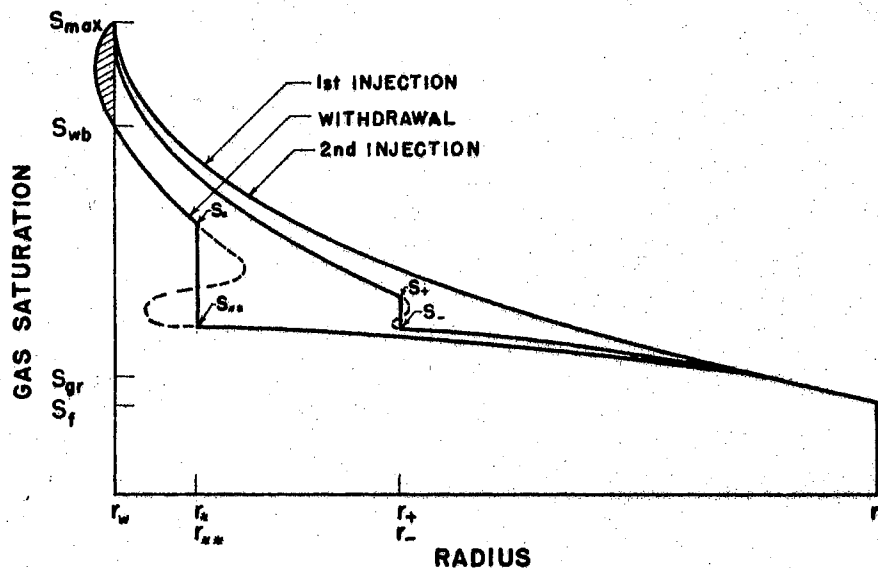


FIG. 3 RADIAL SATURATION DISTRIBUTION WITH HYSTERESIS,
 $S_{gr} > S_f$

Injection

As is shown in Appendix A, Equation (16) for injection after injection-withdrawal may be modified to include hysteresis for the condition that $S_{gr} < S_f$ with the result being Equation (23).

$$f'_{+2} = \left\{ f_{+2} - f_{-2} + \frac{Q_p}{G_{i,2}} (f_{**2} - f_{-2}) + (S_{**} - S_-) \right. \\ \left. \left[\frac{G_{i1}}{G_{i2}} (f'_{f,1} - f'_{*1}) - \frac{Q_p}{G_{i,2}} \right] \right\} / (S_{**} - S_-) \quad (23)$$

For the second injection case where breakthrough has occurred during the withdrawal phase, Equation (17) is valid where all values of f and f' are given a subscript "2".

When considering the case where $S_{gr} > S_f$ then Equation (23) becomes

$$f'_{+2} = \left\{ f_{+2} - f_{-2} + \frac{G_{i1}}{G_{i2}} [f_{**1} - f_{-1} - f'_{*1} (S_{**} - S_-)] \right. \\ \left. + \frac{Q_p}{G_{i2}} [f_{**2} - f_{-2} - f'_{*2} (S_{**} - S_-)] \right\} / (S_+ - S_-) \quad (24a)$$

In the case of breakthrough during withdrawal, Equation (24b) replaces Equation (24a) as the equation giving the saturation of the front.

$$f'_{+2} = \left\{ f_{+2} - f_{-2} + \frac{G_{i1}}{G_{i2}} (f_{wb,1} - f_{-1}) + \frac{Q_p}{G_{i2}} (f_{wb,2} - f_{-2}) \right\} \\ 1 / (S_+ - S_-) \quad (24b)$$

Water Production

As gas is produced the gas-water front (bank) will move toward the well bore. If production is continued, the front will finally reach the well bore and water production will begin. At this time the saturation

distribution will appear as in Fig. 4.

The fraction of gas remaining in the reservoir at or after breakthrough is given by Equation (25a) for the case where hysteresis is neglected.

$$G_{rD} = \frac{G_r}{G_i} = f'_{f,1} S_{wb} + \frac{Q_p}{G_i} f_{wb,1} \quad (25a)$$

The subscript "wb" indicates "at the well bore."

The cumulative water production is given by Equation (25b).

$$W_p = G_i + Q_p - G_r \quad (25b)$$

The produced volume, Q_p , is considered algebraically negative.

In the hysteresis case where the limiting imbibition relative permeability curve is being considered, it is possible for water production to occur before breakthrough. The saturation distribution for

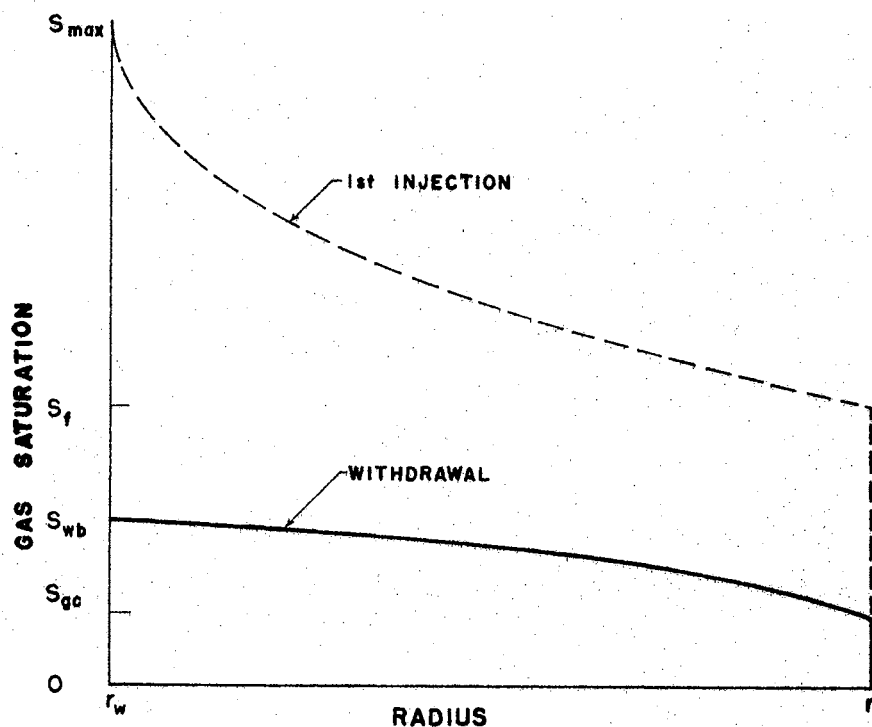


FIG. 4 RADIAL SATURATION DISTRIBUTION AT BREAKTHROUGH
w/o HYSTERESIS

this case as determined from Equation (11) will appear as in Fig. 3. The shaded region in this figure to the left of the well bore, r_w , mathematically represents the volume of water that has been produced as given by Equation (26).

$$W_p = G_i(1 - f_{wb,1}) + Q_p(1 - f_{wb,2}) \quad (26)$$

At or after breakthrough the fraction of gas remaining in the reservoir, for the hysteresis case with the restriction that $S_{gr} > S_f$, is given by Equation (27).

$$G_{rD} = \frac{G_r}{G_i} = f_{wb,1} + \frac{Q_p}{G_i} f_{wb,2} \quad (27)$$

The total water produced will then be

$$W_{p,t} = Q_p + W_{p,bt} + G_i - G_r \quad (28)$$

where $W_{p,bt}$ is the cumulative water produced at breakthrough as given by Equation (26).

The producing water-gas ratio at surface conditions for either withdrawal case is given by

$$R_{wg} = \left(\frac{1}{f_{wb}} - 1 \right) \frac{B_g}{B_w} \quad (29)$$

where "B" is the formation volume factor.

Average Saturation

It is of importance in the underground storage of natural gas in aquifers to develop the maximum possible gas storage volume per unit of pore volume. An expression for the average gas saturation during injection into a linear or single-well radial system can be readily derived and is given by Equation (30). (48)

$$\bar{S}_f = 1/f'_f \quad (30)$$

It is noted that since f'_f is a constant for injection then the average saturation behind the front, \bar{S}_f , is also a constant. Also of interest is the fact that \bar{S}_f can be obtained readily by extending the tangent to the f_g curve, in Fig. 2 up to $f_g = 1$.

It should be pointed out that the average saturation obtained in this manner applies to linear or single well radial systems. This saturation would represent a minimum value in the interior region of a multi-well system and would closely approximate the average saturation in the region beyond the outside wells. The average saturation in the interior region of a multi-well system is very likely dependent upon the initial development program for the field.

Algebraic expressions for the variable average saturation occurring during gas withdrawal and re-injection can be derived. However, they do not have the same simple graphical interpretation and are also of lesser importance.

Two-Phase Gas Zone, Unsteady Aquifer Model

A mathematical model for gas injection into a radial, single-well gas storage reservoir has been presented and discussed by this author and Comer ⁽⁶⁶⁾ in a previous publication. The model consists of a semi-compressible core into which gas is stored and a surrounding compressible aquifer. The geometric configuration for this model is shown in Fig. 5. The equation defining the well-bore pressure of the model at the end of the "n"th time step is given by

$$P_{w,n} = \Delta p_{1,n} + \Delta p_{2,n} + P_{c,n} \quad (30)$$

where the pressure increment in the two-phase zone is

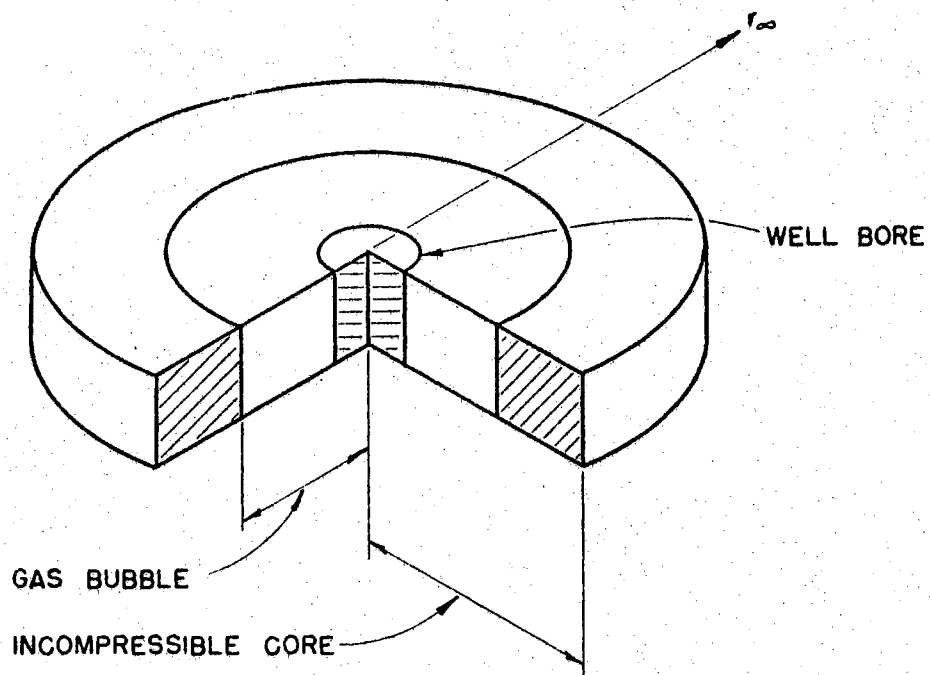


FIG. 5 MATHEMATICAL MODEL.

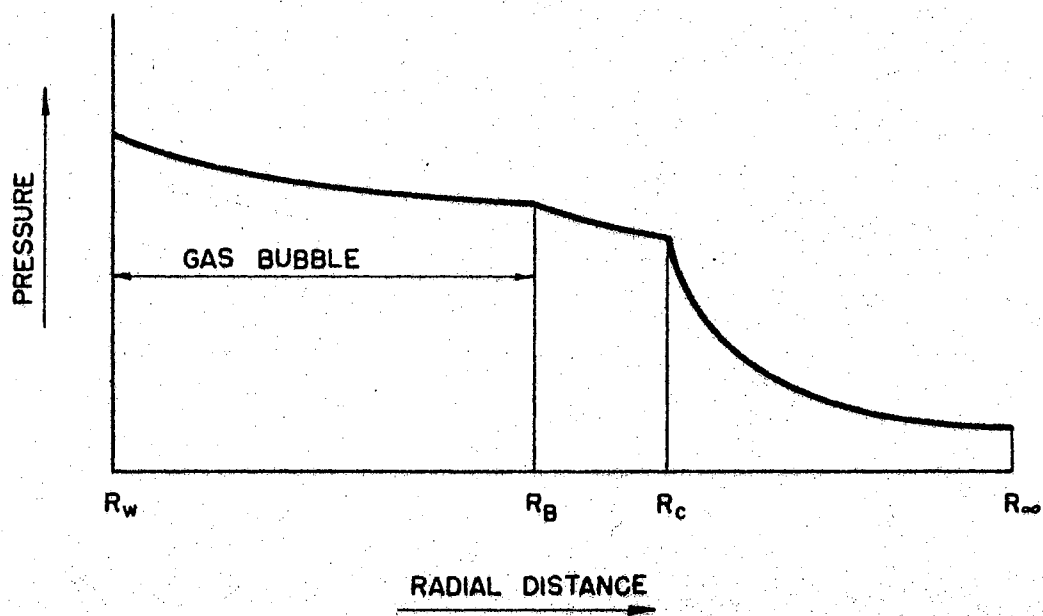


FIG. 6 TYPICAL PRESSURE GRADIENT, INJECTION CASE

$$\Delta p_{1,n} = \frac{i_{g,n}}{.07952\pi hk} \int_{r_w}^{r_f} \frac{dr/r}{\frac{k}{\mu_g} + \frac{k}{\mu_w}} \quad (31)$$

The pressure increment in the incompressible water zone is

$$\Delta p_{2,n} = \frac{\Delta G_{i,n} \mu_w}{.07952\pi hk \Delta t_n} \ln(r_c/r_{f,n}), \quad (32)$$

and the pressure at the inner boundary of the compressible aquifer is

$$p_{c,n} = p_i + \frac{25.1\mu_w}{h k} \sum_{j=1}^n [(\Delta G_i/\Delta t)_j - (\Delta G_i/\Delta t)_{j-1}] P_{t,j} \quad (33)$$

In Equations (32) and (33), $\Delta G_i/\Delta t$ is given by

$$\left(\frac{\Delta G_i}{\Delta t}\right)_j = \left[\frac{z_j^G i_{i,j,sc}}{p_{g,j}(t_j - t_{j-1})} - \frac{z_{j-1}^G i_{i,j-1,sc}}{p_{g,j-1}(t_{j-1} - t_{j-2})} \right] (p_{sc} T_r / z_{sc} T_{sc}) \quad (34)$$

which relates the rate of water flow out of the incompressible core, r_c , to the rate of gas zone growth resulting from gas being injected and/or resulting from change of the gas zone pressure. The pressure distribution for the gas storage model is depicted by Fig. 6.

It is necessary to iterate the solution of Equations (11) and (30) at each time step in order to obtain a pressure solution because of the dependence of gas flow rate, $i_{g,n}$, and gas volume, $G_{i,n}$, upon this pressure.

A new solution of the defining equations of the Two-Phase Gas Zone, Unsteady Aquifer Model is now presented. This new solution has decreased the computation time for the gas storage problem presented by Woods and Comer⁽⁶⁶⁾ by a factor of two. The decrease in solution time has been achieved by increasing the convergence rate of Equation (30). This increase in convergence rate has been accomplished by introducing a

linear approximation of the gas compressibility factor, z , as given by Equation (35),

$$z = a \bar{p}_g + b \quad (35)$$

and by iterating the solution for the average gas zone pressure, \bar{p}_g . The assumption regarding the compressibility factor is valid for the pressure range normally occurring in gas storage reservoirs.

For this situation Equation (30) becomes

$$p_{w,n} = \bar{p}_{g,n} + 0.9 \Delta p_{1,n} - p_{sc} \quad (36)$$

where

$$\bar{p}_g = [\alpha_1 + (\alpha_1^2 + 4\beta_1)^{1/2}] / 2 \quad (37)$$

In Equation (36)

$$\alpha_1 = p_{sc} + p_i + \frac{25.1 \mu_w}{hk_w} \left\{ \sum_{j=1}^{n-1} [\Delta G_i / \Delta t]_j - (\Delta G_i / \Delta t)_{j-1} \right\} P_{tj} - (\Delta G_i / \Delta t)_{n-1} P_{tn} \left. \right\} + \alpha_2 \left\{ \beta_2 [aG'_{i,n} - G_{i,n-1}] + 0.1a \gamma_1 \right\} \quad (38)$$

and

$$\beta_1 = \alpha_2 b (\beta_2 G'_n + 0.1 \gamma_1) \quad (39)$$

where

$$\alpha_2 = \frac{P_{sc} T_{sc} \mu_w}{z_{sc} T_{sc} h k_w \Delta t_n} \quad (40)$$

$$\beta_2 = \frac{1}{0.07952\pi} \ln \frac{r_c}{r_{f,n}} + 25.1 P_{t,n} \quad (41)$$

$$\gamma_1 = \frac{i'_{g,n} k \Delta t_n}{0.07952\pi \mu_w} \int_{r_w}^{r_f} \frac{dr/r}{\frac{k_{rg}(r)}{\mu_g} \frac{k_{rw}(r)}{\mu_w}} \quad (42)$$

and $\Delta t_j = t_j - t_{j-1}$. (43)

P_t is a pressure change function (28, 68) and primed (') values of gas volume, G_i , and rate, i_g , indicate standard conditions.

With the pressure equation in the form of Equation (37), only the β_2 and γ_1 terms are pressure dependent. The radius of the front, r_f , in these terms is related to pressure because of the relation of gas volume in Equation (11) to pressure. However, the pressure dependence of these terms is small, and rapid convergence of the pressure equation is attained.

The pressure distribution in the reservoir follows the trend indicated in Fig. 6.

CHAPTER IV

EXPERIMENTAL APPARATUS

Several experimental methods have been proposed for the measurement of relative permeabilities each of which has its own advantages and disadvantages. An excellent review of the relative merits of the more widely accepted methods is given by Scheidegger⁽⁵⁹⁾, Osaba⁽⁴⁵⁾, and Richardson⁽⁵²⁾. After consideration of the various techniques, the Penn State method^(23, 40) which is a dynamic steady-state method was selected. This method was believed to be the most likely technique to give rapid and accurate results for drainage and imbibition relative permeability curves for a gas-water system.

Core Assembly

The Penn State method was then modified to suit our purposes as experimentation proceeded. The modifications included the use of strain gauge pressure transducers; a constant-rate, positive-displacement liquid pump, and a dispersed-feed gas-water mixing head⁽⁵²⁾. Also, for the core sections mounted in Lucite, o-ring seals were used between the three core sections to maintain a pressure seal, and point-contact, radially opposed electrodes were used to measure the electrical resistance of the core. This modified core assembly is shown in Fig. 7.

Later, the core assembly was further modified by mounting the three core sections in pressurized rubber sleeves as shown in Plate 1.

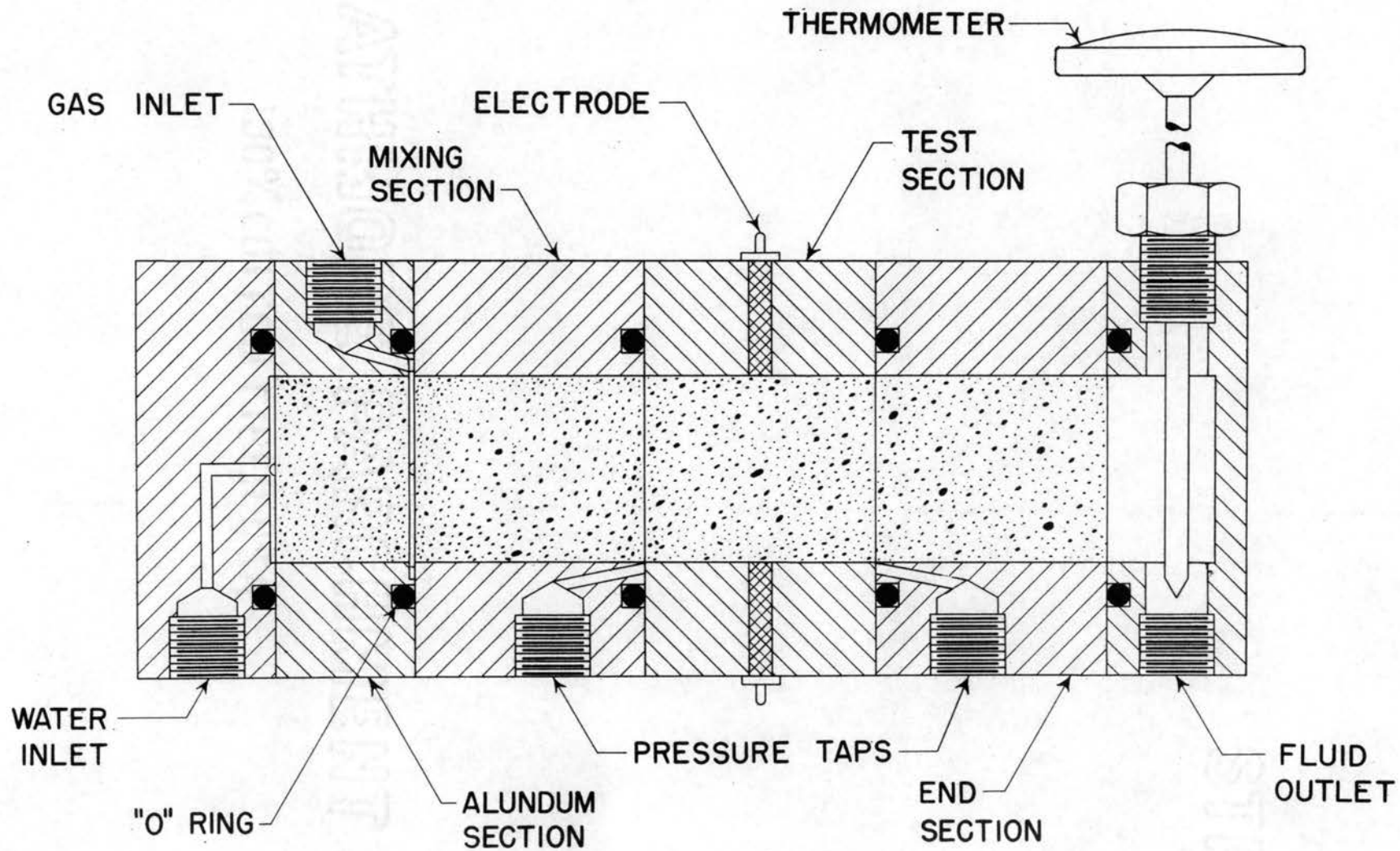
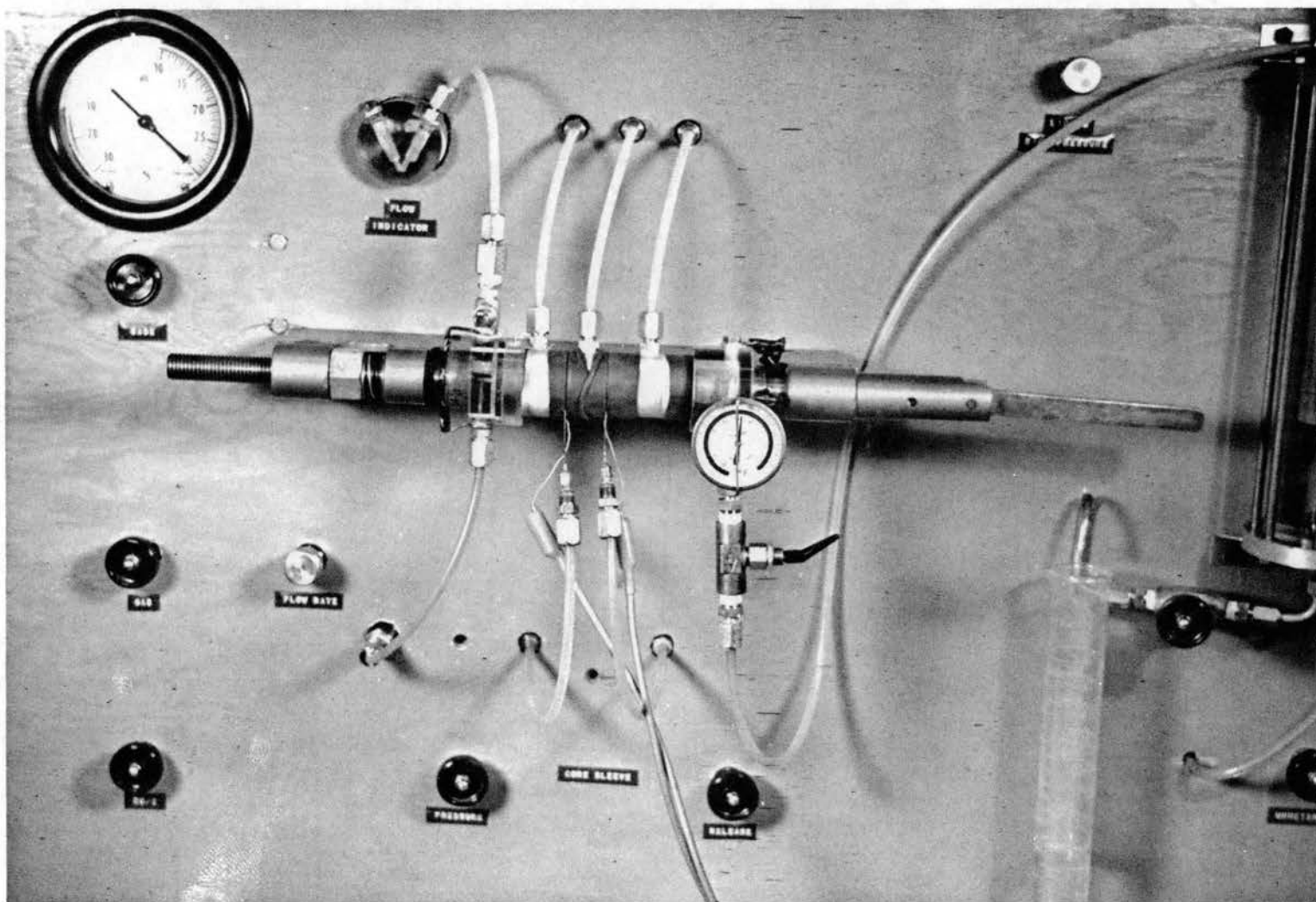


FIG. 7 PLASTIC CORE ASSEMBLY

PLATE I
Rubber Sleeve Core Assembly



The three core sections were placed in rubber sleeves inside of aluminum cylinders. Nitrogen at 300 psi was admitted to the annulus between the aluminum cylinders and the rubber sleeves to cause the sleeves to seal the circumference of the cores. This pressure was found to provide an adequate seal for the internal operating pressures of 0-125 psi. The gas and water were fed into the core assembly through a grooved Lucite dispersing head. The core sections were held in place by a special core clamp designed by the Pan American Research Corporation.

Pressure Measurement

The pressure probes for the rubber sleeve core assembly consisted of two .040 stainless steel tubes which were shaped to fit the test core. Pressure communication was through .020-inch holes in the wall of the tube. One end of each tube was allowed to protrude between the rubber sleeves at each end of the center core section as shown in Plate I. The tubes were then attached to the differential and gauge pressure transducers by high pressure nylon lines.

The transducers consisted of a Dynisco Model PT69-40, 0-50 psi differential pressure transducer with a 0-25 mv output voltage and a Consolidated Electronics Model 4-311-250G, 0-250 psig gauge pressure transducer with an output voltage of 0-25 mv.

The pressure lines from the core to the transducers were $\frac{1}{4}$ -inch, 300-psi test, nylon tubing. These lines permitted electrical isolation of the core which was desirable because of the electrical resistance measurements used to determine the water saturation of the test core.

Fluid Control System

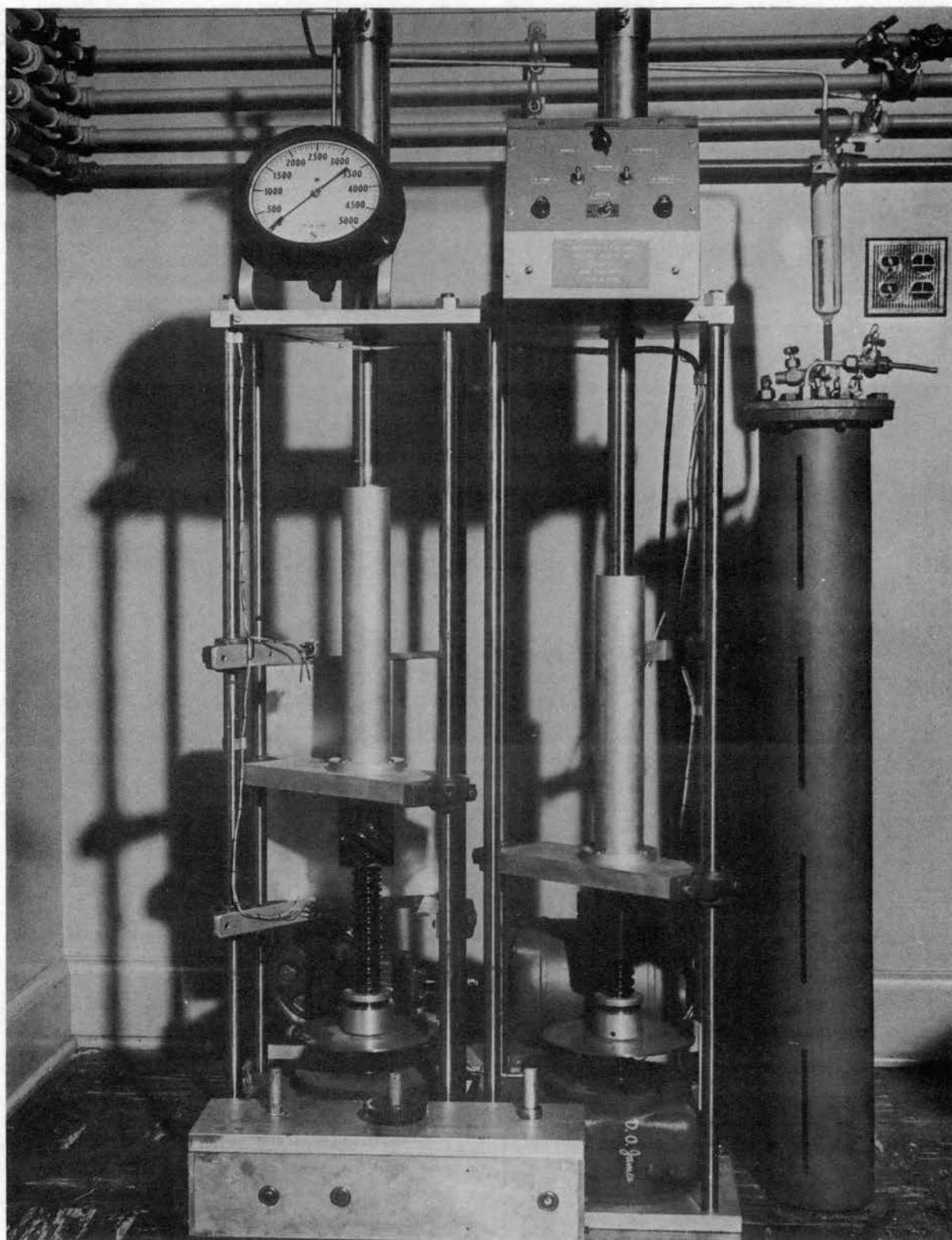
The water phase was controlled by the use of an Exline Model 215 constant rate pump driven by a $\frac{1}{4}$ hp. synchronous motor as shown in Plate II. An auxiliary mechanical transmission was designed and built for the pump to provide water rates of 0.5 to 1000 cc/hr. The transmission consisted of two parallel mechanical gear trains each of which was activated by a separate magnetic clutch. This system permitted a new gear ratio to be set up on the idle gear train while the other train was in operation. Instant shifting from one train to the other was provided by a two-way electrical switch controlling the clutches. The regulation of water rates in this manner prevented the uncontrolled expansion of the gas in the core that occurred when the pump was shut down to change water rates. The transmission and motor unit are shown in Plate III.

The water was stored in a sump constructed of Lucite tubing and was filtered through a fritted glass disk between the sump and pump. The discharge line of the pump contained a 5-micron stainless steel filter and the fluids also circulated through a $1\frac{1}{2}$ -inch long mixing core section before entering into the test core.

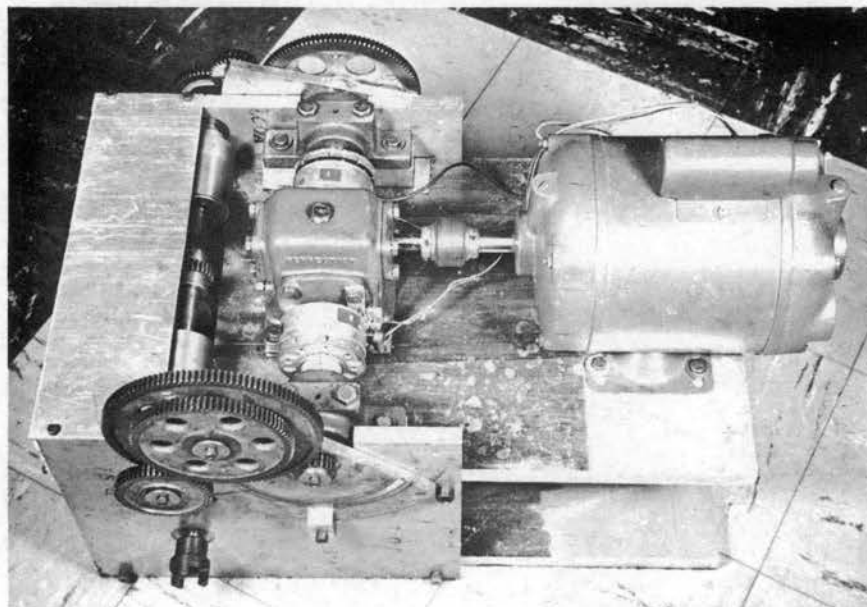
The gas source was a nitrogen bottle with pressure regulation by a Hoke ballast-type constant pressure regulator. The gas was then passed through a 5-micron stainless steel filter before entering the gas flow controller. The gas rate was controlled by a Moore constant upstream pressure flow controller connected across a Hoke vernier-head needle valve. The gas passed from the flow controller to the dispersed feed-type mixing head.

P L A T E I I

Constant Rate Liquid Pump



P L A T E I I I
P u m p T r a n s m i s s i o n a n d M o t o r



The system back pressure was controlled with a Grove 0-300-psi back pressure regulator connected to the gas outlet of the gas-liquid separator.

A flow diagram for the system is shown in Fig. 8.

Fluid Measurement

The gas and water were separated at the outlet of the core assembly by permitting gravity segregation in a thick-walled Lucite tube designed for an internal working pressure of 300 psi. The separator is shown in Fig. 9 and Plate IV.

The gas flow from the gas-liquid separator was measured either by the timed displacement of a soap bubble through a vertically mounted 100-ml. burett or by a 0-20 cfm wet test meter whichever the rate required (Plate IV).

The water flow rate was determined by the displacement rate of the pump when the system had reached a steady state. A number of checks of the calculated displacement rate versus measured rate showed a maximum deviation of two per cent which is within the limits of experimental error.

Electrical System

Electrical power for the strain gage transducer circuits and the potentiometric recorders was supplied through a voltage stabilizing transformer to minimize voltage fluctuations resulting from varying line load within the laboratory.

The 6-volt power source for the strain gage pressure transducers

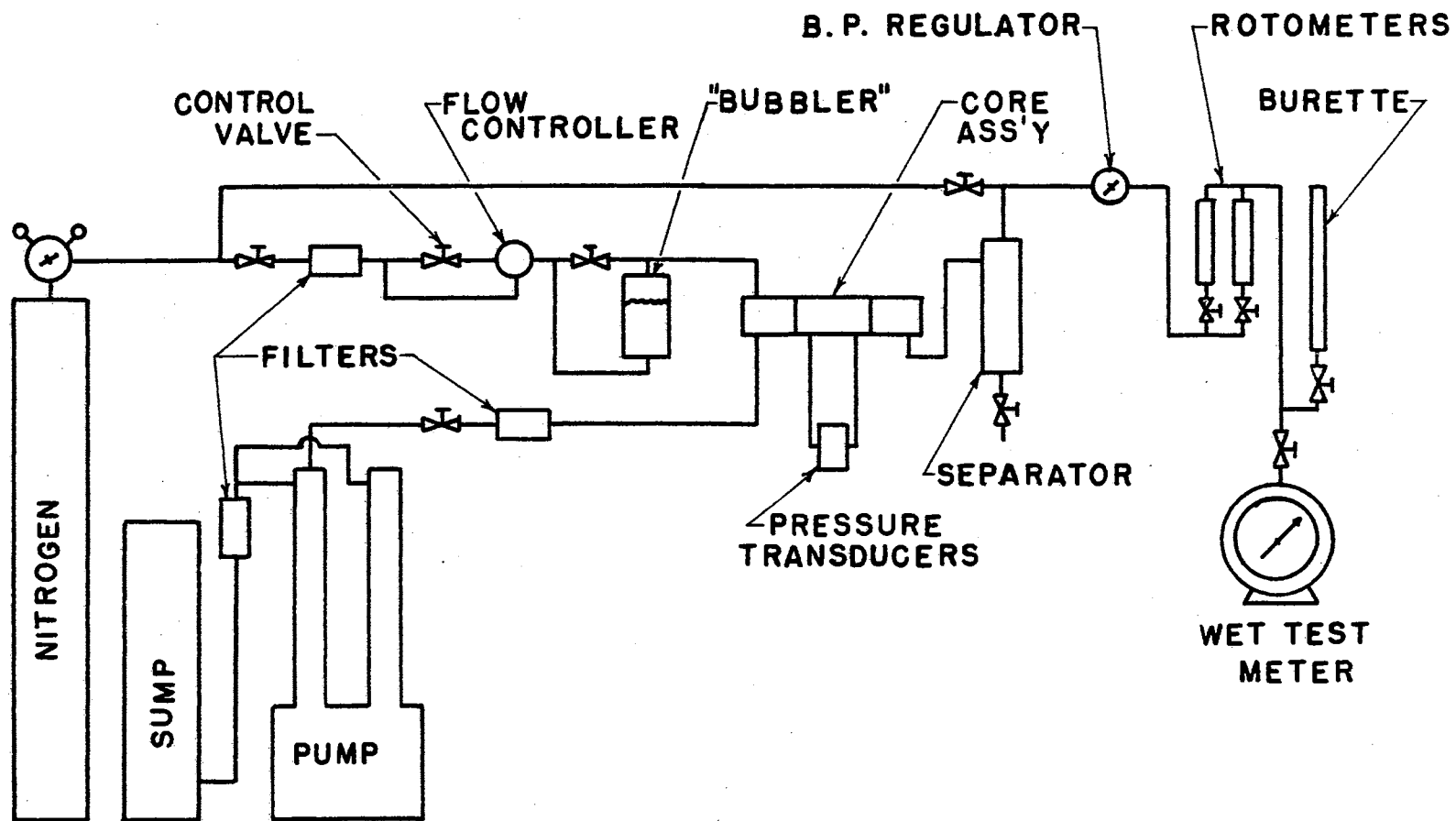


FIG. 8 FLUID FLOW DIAGRAM

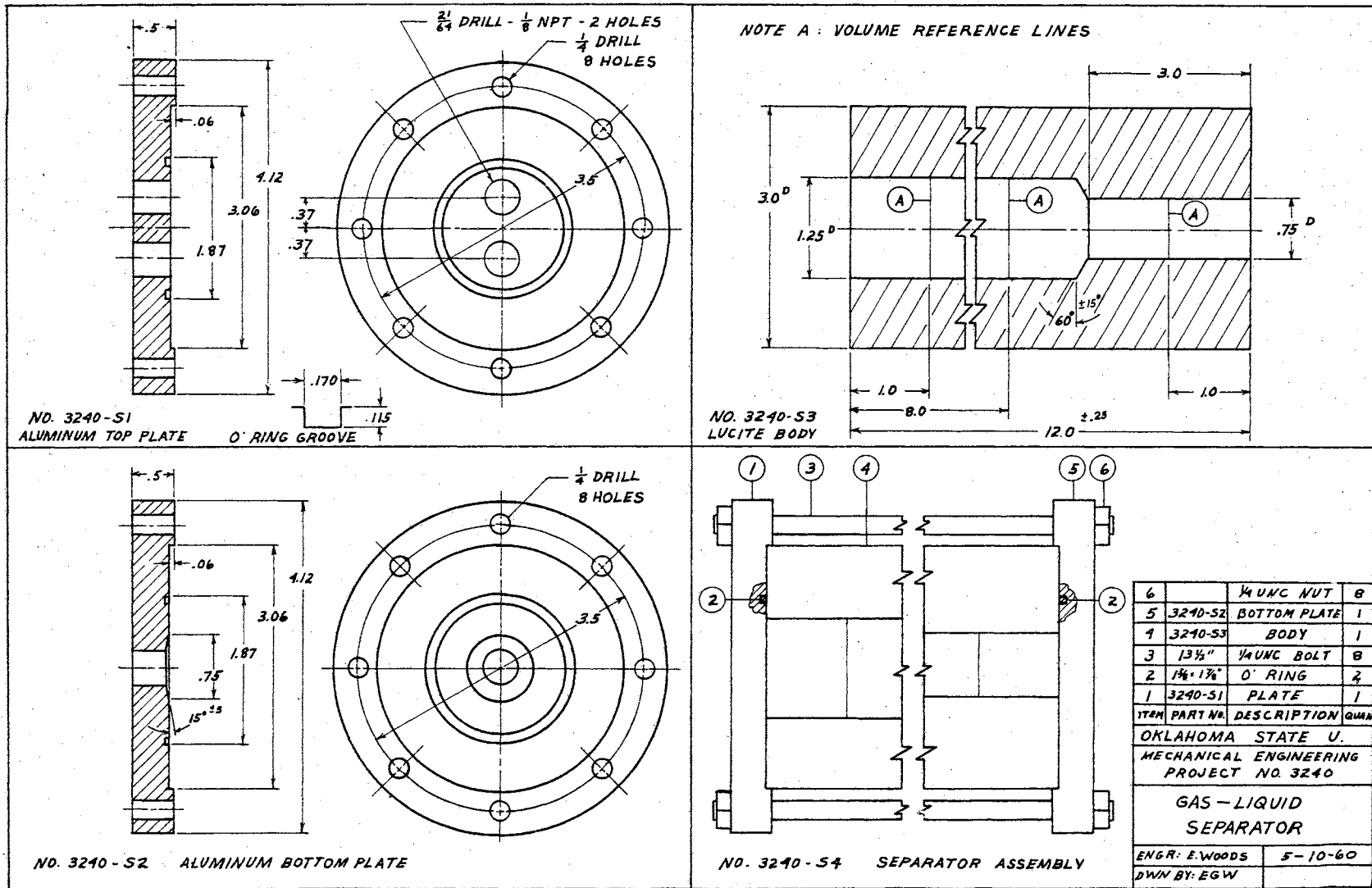


FIG. 9 GAS-LIQUID SEPARATOR

was a 6-12-volt EICO battery eliminator. Its output voltage was continuously monitored with a Keithley electrometer. The transducer circuit also contained precision potentiometers to adjust the zero pressure output voltage to correspond to the recorder zero. The electrical diagram is given in Fig. 10.

Instrument and Control Panel

The complete permeameter and its associated equipment is pictured in Plate IV.

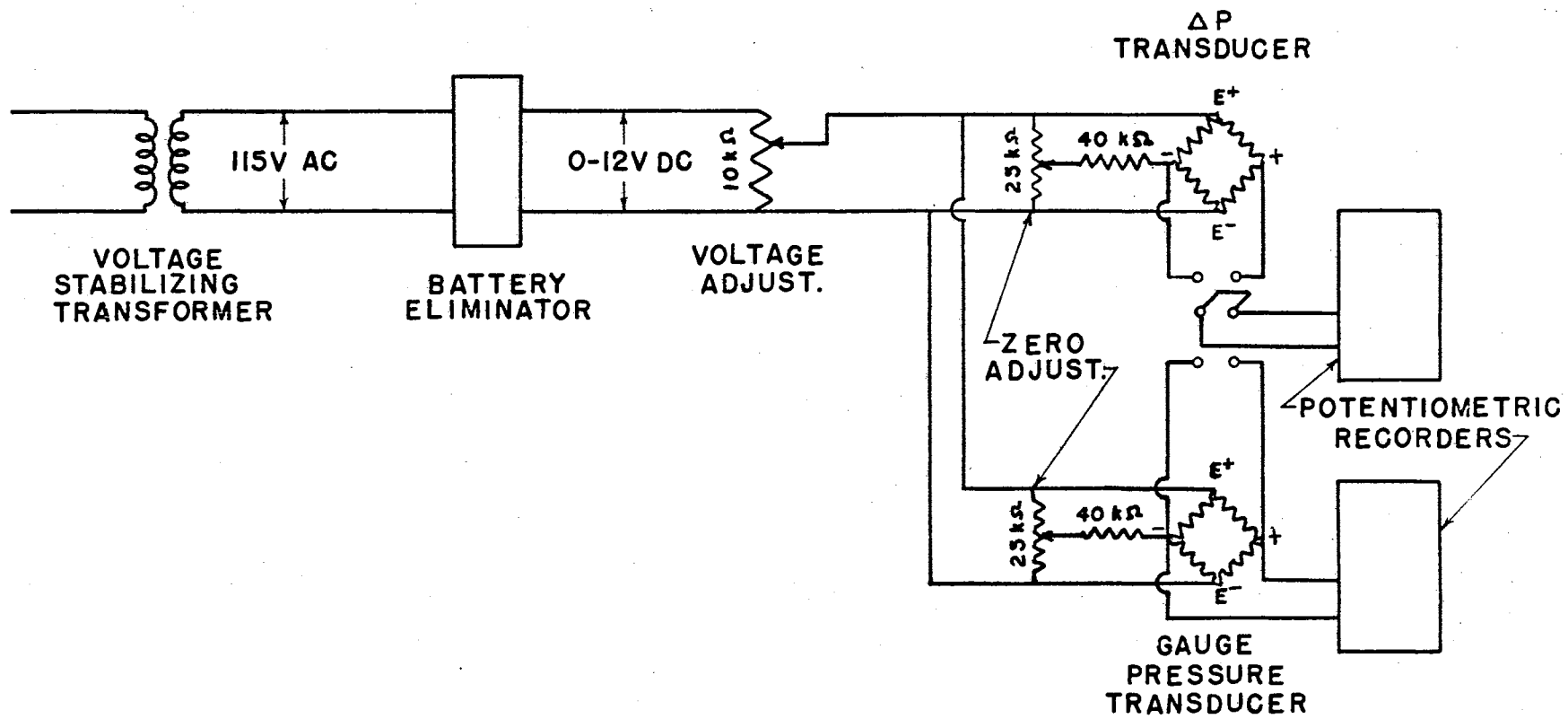
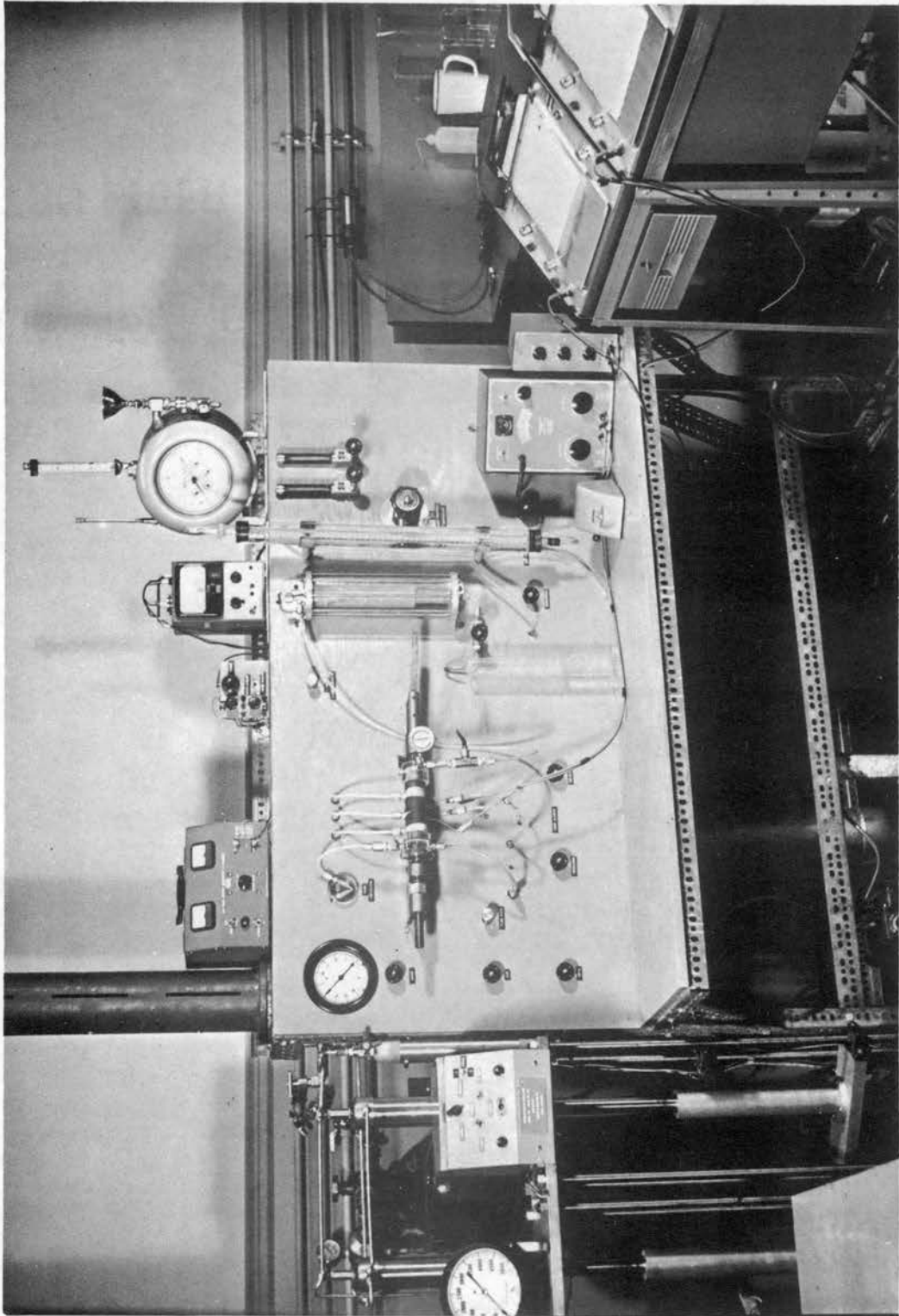


FIG. 10 PRESSURE TRANSDUCER ELECTRICAL CIRCUIT

P L A T E I V
Instrument Panel



CHAPTER V

EXPERIMENTAL PROCEDURE

Once a general experimental method and the experimental apparatus have been selected, it is of equal importance to develop an experimental procedure that will produce consistent, reliable results under known experimental conditions. Sometimes a conflict of interest may develop and a compromise must be made. For example, in measuring the trapped gas saturation during imbibition, S_{gr} , it is desirable to operate at a low mean pressure within the core. Operating at a low pressure permits a weight determination of the saturation of the core without having a significant amount of liquid being expelled from the core by gas expansion as the core is removed from the apparatus. However, experience has shown that the residual gas saturation tends to become a function of the pore volumes of liquid injected when operating near atmospheric pressure. Yet, a rather definite trapped gas saturation is obtained when operating at pressures in the 20-40 psi or higher range. This topic will be discussed further in the section on experimental results.

The general procedure used in the final stages of the experimental testing is given below. The steps reflect experience with numerous experimental difficulties.

1. Dry the core and determine its dry weight.
2. Determine the permeability of the core to dry nitrogen at several different mean pressures in the range of 1 to 8 atmospheres.

3. Evacuate the core sections; then saturate with the test liquid and weigh.
4. Determine the water permeability and electrical resistance of the core while injecting the test liquid at several different back pressures between 1 and 8 atmospheres.
5. Measure the saturated weight of the core.
6. Establish an initial fixed-injection gas-water ratio.
7. Permit the system to reach steady-state conditions and measure the operating variables (differential pressure, mean pressure, flow rates, temperature and electrical resistance).
8. Change the gas-water ratio and repeat Step 7. (Increase the GWR for the drainage cycle; decrease the GWR for the imbibition cycle).
9. When a permeability value has been determined at the lowest pump rate, the pump is stopped and the core is removed for weighing. The core is then returned immediately to the permeameter.
10. Additional mobile water in the core is displaced by gas injection until the residual water saturation is attained. During this latter stage of the testing, the core is removed several times for weighing.
11. After attaining the residual water saturation and weighing the core, repeat Steps 6, 7, and 8 for imbibition.
12. For imbibition, Step 8 is continued until the gas-water ratio becomes zero (gas injection is stopped). Liquid injection is continued for a predetermined number of pore volumes of water to obtain a residual (trapped) gas saturation. During this liquid injection period, a mean core pressure of at least $2\frac{1}{2}$ atmospheres absolute is maintained.
13. Stop the fluid flow; check the core resistance; depressure the system; again check the resistance; and weigh the core.
14. Do not discontinue testing for an extended period of time during either the drainage or imbibition cycles unless the core saturation is very near the residual water saturation.

It is suggested that a different procedure be investigated for determining the saturation-resistance characteristic for the test core. One procedure would be to determine this characteristic curve by

conducting a separate test. The suggested procedure is as follows: The core could be initially saturated with water and displaced with gas at low pressures. During the unsteady-state displacement of the water by gas, the electrical resistance could be measured and the core could be removed periodically for weighing. After the water saturation reached its residual value, the process could be reversed by displacing the gas with water and measuring the core resistance and weight periodically. The saturation-resistance characteristic could then be calculated. A knowledge of the saturation-resistance relationship would greatly facilitate the relative permeability testing since inadequate spacing of the test points could be avoided.

Drying of Cores

The cores which were mounted in plastic were dried by passing air through them for several days. The air first passed through a liquid and solid "knockout," a fiber filter, and a tube filled with a desiccant before passing into the core. The unmounted cores used in the rubber sleeve core assembly were oven-dried at about 200°F.

Klinkenberg Permeability Tests

Klinkenberg permeability tests (7,48) were performed on each of the cores before making a relative permeability test. These gas permeability tests were made with the relative permeability apparatus as shown in Plate IV. Dry nitrogen was used as the test fluid and was allowed to flow through the cores to produce a constant differential pressure. The mean pressure in the core was controlled by the back pressure valve and was varied over a range of approximately 1 to 8

atmospheres absolute pressure. As the mean pressure was varied, the flow rate was also altered to maintain a nearly constant differential pressure. By holding a constant differential pressure, the gas flow rate in the test core was maintained essentially constant. The technique of varying the mean pressure at a constant differential pressure was used in preference to the procedure of controlling the mean pressure by changing the flow rate. This latter method could result in flow rates that were beyond the laminar flow region for which Darcy's equation is valid.

Saturation of Cores

Two methods were used to attain 100 per cent liquid saturation of the test cores.

The first method used was to place the core in the relative permeability test apparatus, to evacuate the system by using a vacuum pump, and then to flush the core with carbon dioxide to remove the remaining air. The core was then re-evacuated and flooded with the test liquid at pressures up to 125 psi in order to dissolve the remaining gas in this liquid and flush it from the core.

The second procedure used was to saturate the cores as follows. First, the cores were placed in a vacuum dessicator or flask which was then evacuated to remove the air. After 30 minutes of evacuation of the vacuum vessel, the test liquid, which also had been de-aerated with a vacuum, was admitted to this container until the cores were completely submerged. The cores and water within this container were then held under vacuum for an additional hour to remove additional air. The method of saturating the cores in a vacuum vessel was adopted as the

more reliable one of the two techniques discussed because the weight gain of the cores was less during the subsequent liquid injection tests.

Water Permeability Tests

The water permeability tests were made with the system under several different pressures between one and nine atmospheres absolute. This procedure permitted a final check for leaks in the test system and also gave an indication of how completely the cores were saturated, since liquid permeability is independent of mean pressure. A significant change of the differential pressure upon changing the back pressure, with the liquid rate being held constant, was an indication of gas saturation within the core.

Saturation Measurement

Liquid saturation determinations under flowing conditions were made with an electrical resistance-saturation correlation. Electrical resistance measurements were made with an A-C resistance bridge operating at 60 or 1000 cps. The choice of frequency remained fixed for any given test run. The resistance measurements were correlated with periodic weight determinations of saturation in order that saturations under flowing conditions could be determined from resistance measurements. Residual water saturation was determined by weight in all cases. The trapped gas saturations, S_{gr} , were determined by resistance correlation in cases where this point was attained at a significant mean core pressure.

Data Observations

The differential pressure and the downstream pressure for the test section of the core were continuously recorded. Periodic observations of gas flow rate, fluid outlet temperature and electrical resistance were made periodically and recorded on the differential pressure chart so that a definite time correlation between the variables would be established. The liquid rate under steady-state conditions was assumed equal to the calculated pump displacement rate as justified in Chapter IV, "Fluid Measurement."

CHAPTER VI

EXPERIMENTAL RESULTS

The experimental results presented here represent drainage-imbibition relative permeability tests of four natural sandstone core samples and two artificial cores composed of aluminum oxide. One of the natural sandstone samples was analyzed twice with an intervening time of approximately fifteen months and with several improvements having been made in the experimental apparatus. The specifications for the cores are presented in Table I.

The experimental results were obtained with the experimental apparatus described in Chapter IV by using the test procedure delineated in Chapter V. The data reduction was accomplished by use of the equations and computer programs presented in Appendix B.

Porosity

The porosity of the test cores was measured by the saturation method as described in Chapter V, "Saturation of Cores." The weight of the test fluid in the core was determined by weighing the core when it was dry and again when it was saturated. The fractional pore space was then obtained from the density of the fluid and the sample dimensions. The experimental values of the porosity of the cores are presented in Table II. The confidence intervals are at the 95 per cent level.

TABLE I

CORE SAMPLE SPECIFICATIONS

Laboratory No.	AL-1-13	AL-1-21	D-1-1
Core Material	Alundum	Alundum	Sandstone
Texture	Fine Grained	Medium Grained	Granular
Orientation	----	----	Horizontal
Type of Mounting	Rubber Sleeve	Rubber Sleeve	Lucite
Type of Electrode	2-Circumferential Steel Wires	2-Circumferential Platinum Bands	4-Radially Opposed Contacts
Dry Weight, gm.	59.487	63.389	130.048
Length, cm.	3.757	4.082	3.49
Diameter, cm.	2.637	2.690	2.54
Porosity, per cent	26.5	27.2	17.3
Permeability, md.			
(water)	87	720	20.8
(nitrogen)	102	759	144 at 7.45 atm

TABLE I (CONTINUED)

Laboratory No.	M-1-1A	M-2-1	N-3-1
Core Material	Sandstone	Sandstone	Sandstone
Texture	Granular	Granular	Fine Grained
Orientation	Horizontal	Horizontal	Horizontal
Type of Mounting	Lucite	Lucite	Lucite
Type of Electrode	4-Radially Opposed Contacts	4-Radially Opposed Contacts	4-Radially Opposed Contacts
Dry Weight, gm.	114.842	136.627	141.753
Length, cm.	2.75	3.68	3.58
Diameter, cm.	2.54	2.54	2.54
Porosity, per cent	16.6	18.5	12.6
Permeability, md.			
(water)	1,130	720	7
(nitrogen)	930--622*	790	60

* See Table IX

TABLE II

POROSITY

Core No.	Weight of Water, gm.	Porosity, per cent
AL-1-13 Upstream Section	4.962	26.14
	4.986	26.27
	4.912	25.88
	4.990	26.29
	4.968	26.17
	4.949	26.07
	4.957	26.12
	4.950	26.08
	4.949	26.07
	4.973	26.20
	4.927	25.96
Confidence Interval	4.957 \pm 0.016	26.11 \pm 0.08
Test Section	5.360	26.16
	5.409	26.40
	5.232	25.54
	5.405	26.38
	5.554	27.11
	5.387	26.29
	5.415	26.43
	5.287	25.81
	5.411	26.41
	5.397	26.34
	5.404	26.38
	5.415	26.43
	5.543	27.05
	5.522	26.95
	5.528	26.98
5.555	27.11	
5.550	27.09	
Confidence Interval	5.434 \pm 0.049	26.52 \pm 0.24
Downstream Section	5.534	26.25
	5.542	26.29
	5.547	26.32
	5.533	26.25
	5.553	26.35
	5.523	26.20
	5.429	25.76

TABLE II (CONTINUED)

Core No.	Weight of Water, gm.	Porosity per cent
AL-1-13		
Downstream	5.542	26.29
Section	5.523	26.20
(Continued)	5.514	26.16
	5.469	25.95
	5.517	26.17
Confidence Interval	5.519 ± 0.079	26.18 ± 0.37
AL-1-21		
Upstream	5.795	28.13
Section		
Test	6.302	27.17
Section	6.302	27.17
	6.352	27.38
Confidence Interval	6.319 ± 0.072	27.24 ± 0.31
Downstream Section	6.265	27.26
D-1-1		
Test	2.919	16.56
Section	3.088	17.52
	3.129	17.75
Confidence Interval	3.045 ± 0.277	17.28 ± 1.57
M-1-1A		
Test	2.275	17.33
Section	2.393	17.17
	2.413	17.32
	2.344	16.82
	2.277	16.34
	2.246	16.11
	2.246	16.11
Confidence Interval	2.313 ± 0.064	16.60 ± 0.46

TABLE II (CONTINUED)

Core No.	Weight of Water, gm.	Porosity, per cent
M-2-1		
Test	3.467	18.59
Section	3.492	18.73
	3.425	18.37
	3.396	18.21
Confidence Interval	3.445 ± 0.068	18.47 ± 0.37
N-3-1		
Test	2.379	12.49
Section	2.474	12.99
	2.160	11.34
	2.455	12.89
	2.418	12.69
	2.537	13.32
Confidence Interval	2.404 ± 0.137	12.62 ± 0.72

Resistance-Saturation Measurements

The saturation of the test cores under flowing conditions was determined from resistance-saturation correlations. These correlations were made by interrupting the fluid flow at intervals, measuring the electrical resistance of the core at atmospheric pressure, and then weighing the core to determine its water content. Since the maximum water content was determined during the porosity measurements, the liquid saturation was readily determined. Each of the measured resistances was corrected to a temperature of 68°F to remove the effects of temperature variation of resistance from the correlation. The saturation-resistance correlations for the test cores are presented in Figs. 11-16 and Tables III-VIII. The data is in floating point form.

Reflection upon the theoretical aspects of the saturation-resistance correlation shows that the resistance ratio, R_R , is an exponential function of water saturation (48).

$$R_R = \frac{R_{i,68}}{R_{100,68}} = S_w^{-2} \quad (44)$$

In this equation, $R_{100,68}$ is the core resistance at 100 per cent water saturation as corrected to 68°F. This theory is based upon the assumptions that the core material is non-conducting, the water within the pores is the only electrical conductive material, the electrical current field is linear (end electrodes are used), and a unique distribution of water in the pores exists for each saturation.

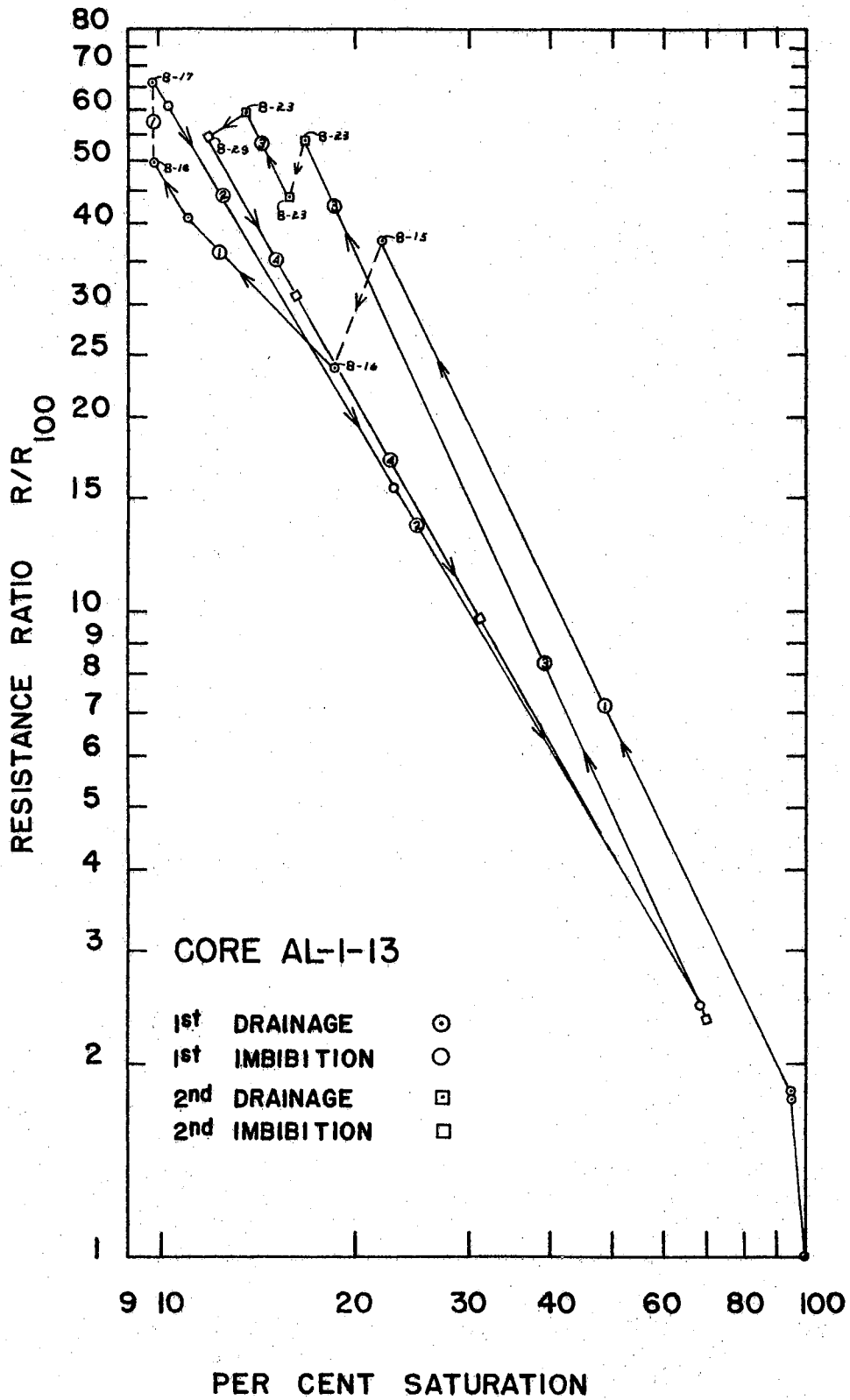


FIG. II SATURATION-RESISTANCE, CORE AL-1-13

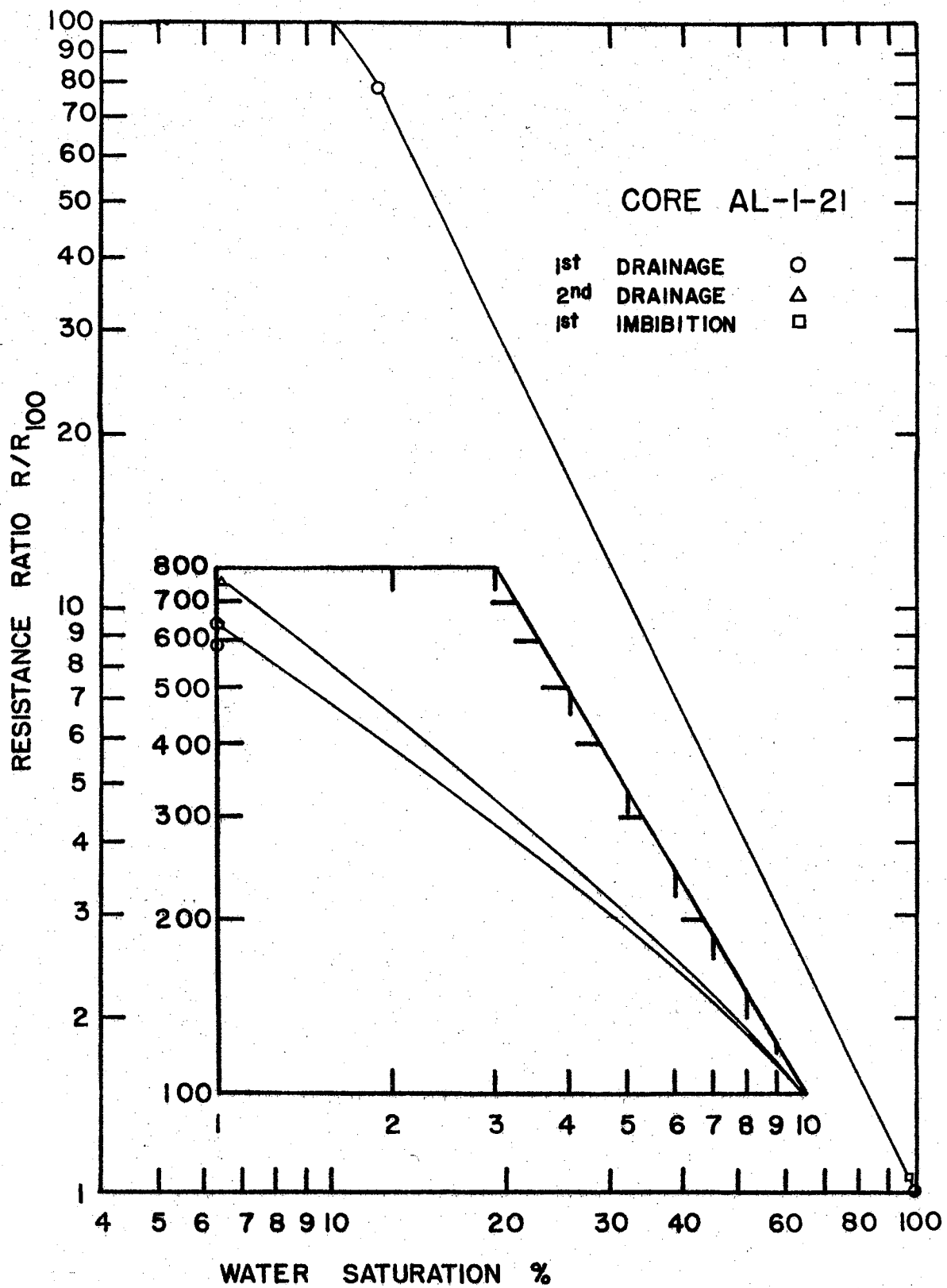


FIG. 12 SATURATION-RESISTANCE, CORE AL-1-21

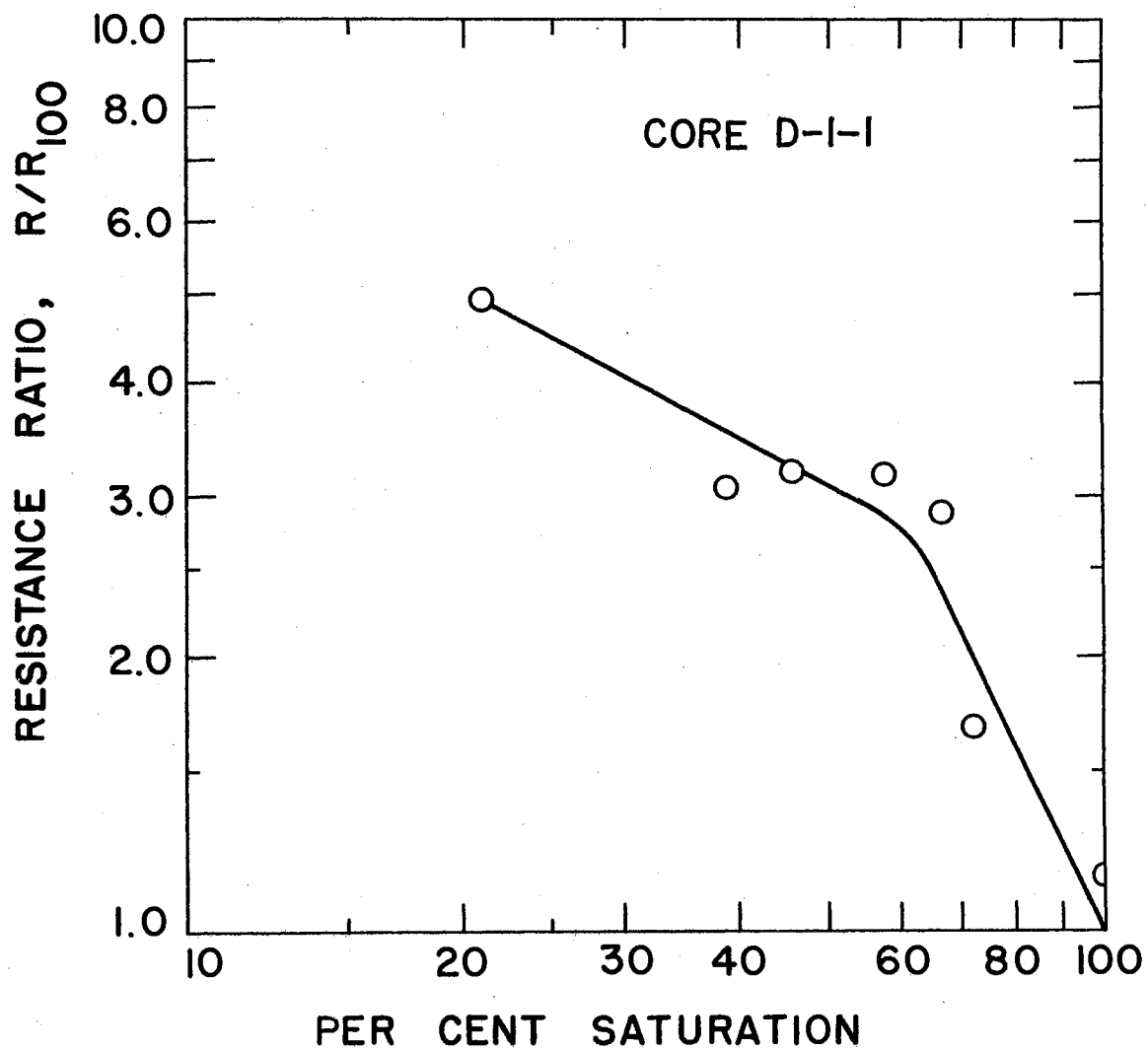


FIG. 13 SATURATION-RESISTANCE, CORE D-1-1

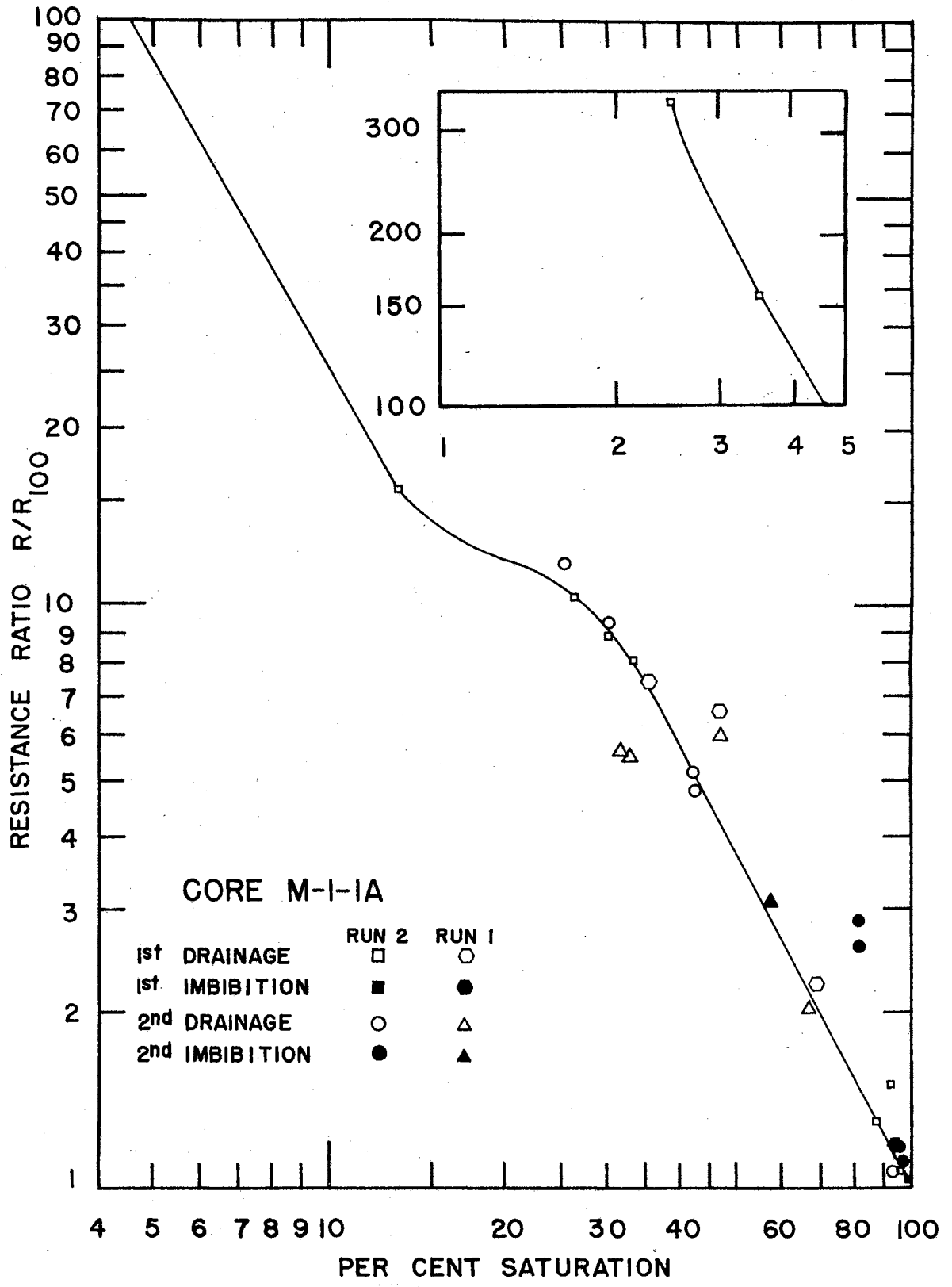


FIG. 14 SATURATION-RESISTANCE, CORE M-1-1A

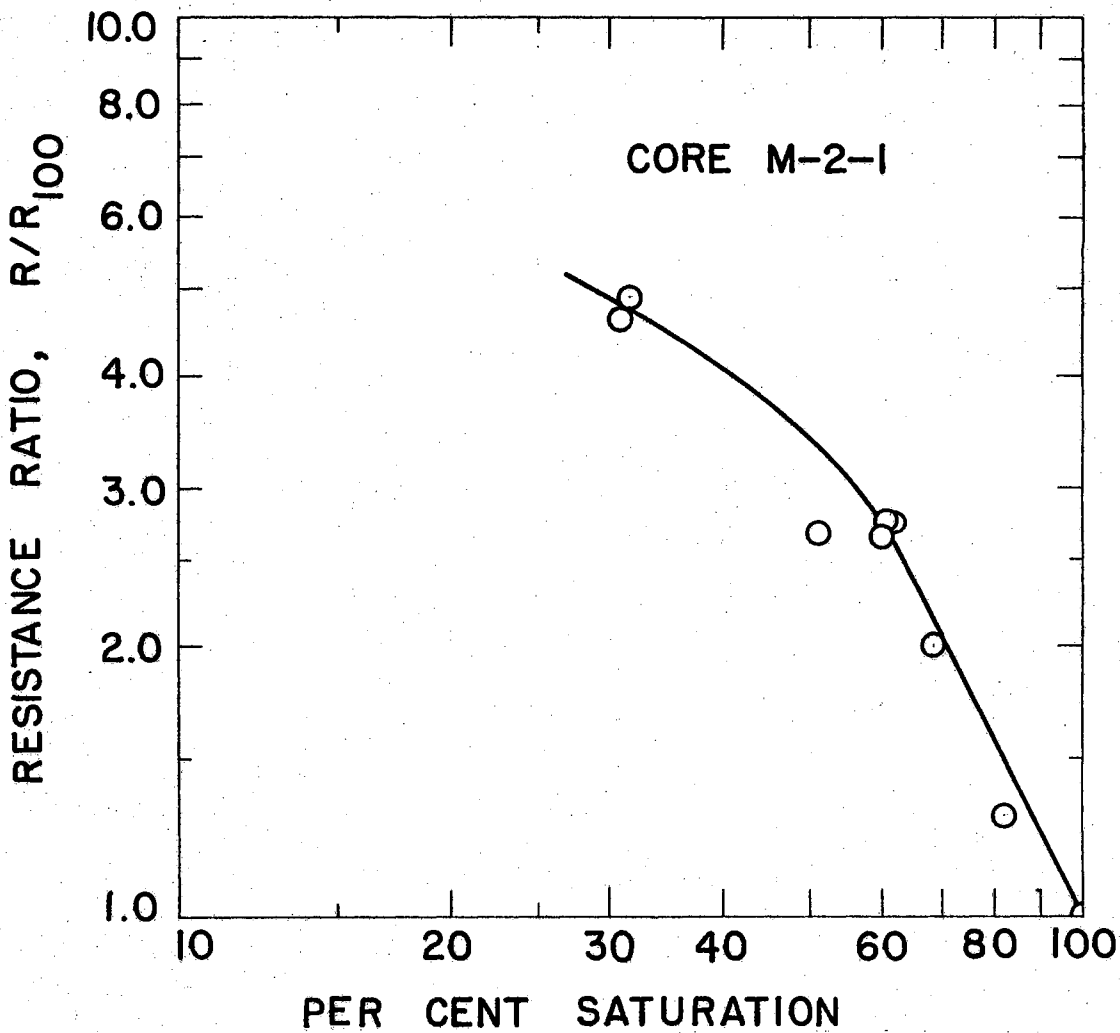


FIG. 15 SATURATION-RESISTANCE, CORE M-2-1

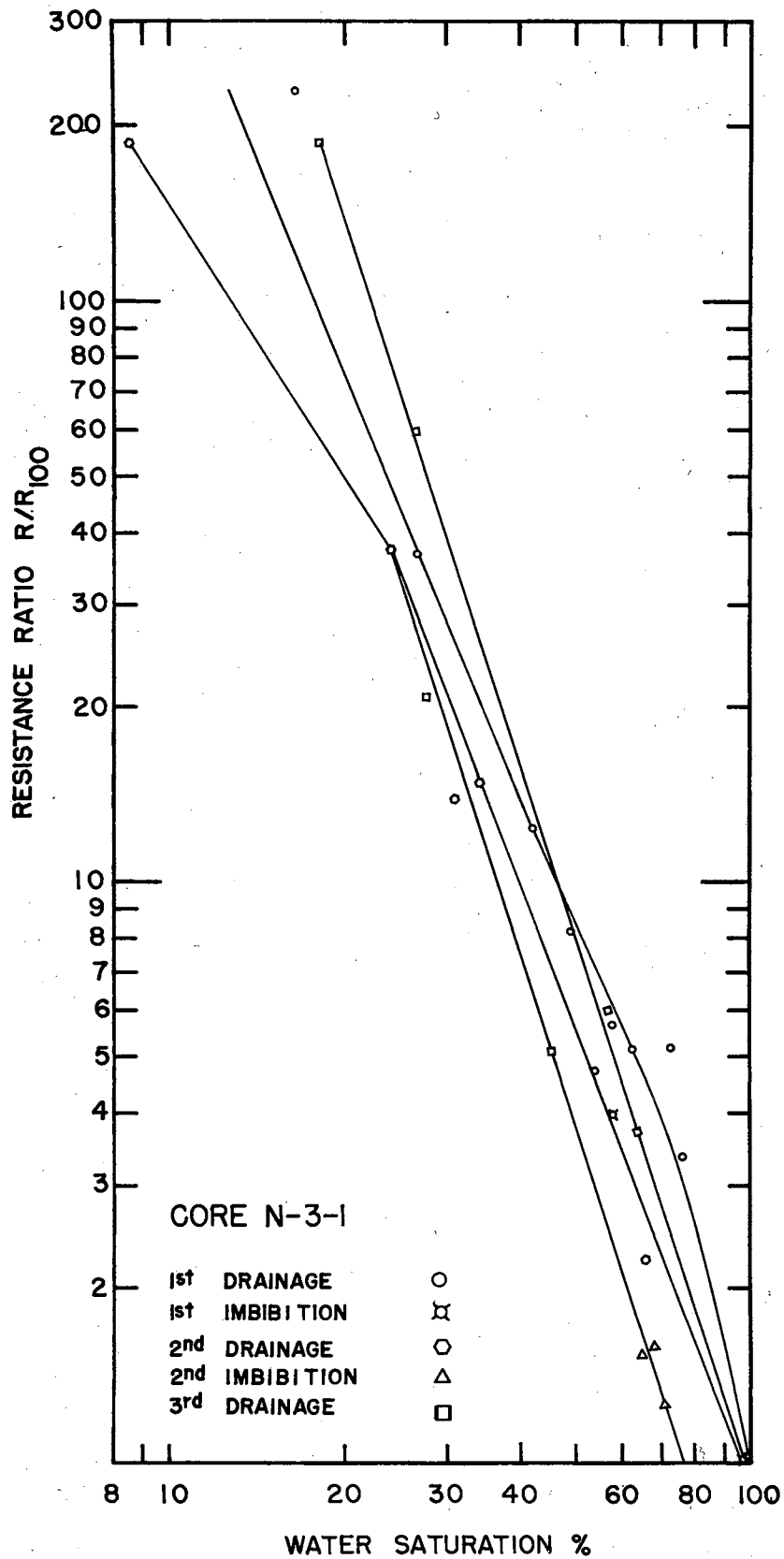


FIG. 16 SATURATION-RESISTANCE, CORE N-3-1

TABLE III
SATURATION-RESISTANCE, CORE AL-I-13

IDENTIFICATION	RMIN RESISTANCE SW=100 KILOHMS	WMAX MAXIMUM WEIGHT OF WATER GRAMS	POR FRAC-TIONAL POROSITY	CARD NO.
8140001001+	2179264751+	5405000051+	2634063050+	690000+

IDENTIFICATION	WS WEIGHT AT SAT. GRAMS	WD DRY WEIGHT GRAMS	RESISTANCE AT SAT. AND TEMP, OHMS	TR TEMPERATURE F	RR RESISTANCE RATIO	SW WATER SATURATION	CARD NO.
8140001001+	6411500052+	5871000052+	2030000051+	7300000052+	1000000051+	1000000051+	700000+
8140001001+	6411500052+	5871000052+	1800000051+	7300000052+	8866994950+	1000000051+	710000+
8150001001+	6390400052+	5871000052+	4050000051+	6400000052+	1749105951+	9609620750+	720000+
8150001002+	6480400052+	5961000052+	4200000051+	6400000052+	1813887651+	9609620750+	730000+
8150001003+	6080000052+	5961000052+	7700000052+	7100000052+	3689182852+	2201665150+	740000+
8150001031+	6080000052+	5961000052+	8050000052+	7100000052+	3856873052+	2201665150+	750000+
8160001001+	6061000052+	5961000052+	5000000052+	7080000052+	2388825252+	1850138850+	760000+
8160001002+	6020500052+	5961000052+	8300000052+	7350000052+	4116674552+	1100832650+	770000+
8160001003+	6014200052+	5961000052+	1200000053+	5900000052+	4777650552+	9842738249+	780000+
8160001003+	6014200052+	5961000052+	1270000053+	5900000052+	5056346852+	9842738249+	790000+
8170001001+	6001900052+	5948700052+	1600000053+	6100000052+	6586139452+	9842738249+	800000+
8170002001+	6001900052+	5948700052+	1600000053+	6100000052+	6586139452+	9842738249+	810000+
8170002002+	6270600052+	5948700052+	6800000051+	7050000052+	3235036151+	5955596750+	820000+
8220002001+	6327400052+	5948700052+	5180000051+	6610000052+	2310533851+	7006475550+	830000+
8220003001+	6327400052+	5948700052+	5180000051+	6610000052+	2310533851+	7006475550+	840000+
8220003002+	6031900052+	5948700052+	1030000053+	7080000052+	4920980052+	1539315450+	850000+
8220003002+	6031900052+	5948700052+	1240000053+	7080000052+	5924286352+	1539315450+	860000+
8231003001+	6032200052+	5948700052+	9000000052+	6700000052+	4069100552+	1544865950+	870000+
8231003001+	6032200052+	5948700052+	1050000053+	6700000052+	4747283852+	1544865950+	880000+
8231003002+	6022000052+	5948700052+	1180000053+	7250000052+	5772994052+	1356151750+	890000+
8231003002+	6022000052+	5948700052+	1280000053+	7250000052+	6262231052+	1356151750+	900000+
8291003001+	6017400052+	5948700052+	1210000053+	6500000052+	5307375552+	1271045350+	910000+
8291004001+	6017400052+	5948700052+	1210000053+	6500000052+	5307375552+	1271045350+	920000+
8291004002+	6319600052+	5948700052+	4950000051+	7200000052+	2405020651+	6862164750+	930000+
8290004002+	6319600052+	5948700052+	5050000051+	7200000052+	2453606951+	6862164750+	940000+

TABLE IV
SATURATION-RESISTANCE, CORE AL-I-2I

IDENTI- FICATION	RMIN RESIST- ANCE SW=100 KILOHMS	WMAX MAXIMUM WEIGHT OF WATER GRAMS	POR FRAC- TIONAL POROSITY	CARD NO.
9250001001+	2095220651+	6365000051+	2744404450+	950000+

IDENTI- FICATION	WS WEIGHT AT SAT. GRAMS	WD DRY WEIGHT GRAMS	RESIST- ANCE AT SAT. AND TEMP, OHMS	TR TEMPER- ATURE F	RR RESIST- ANCE RATIO	SW WATER SATURA- TION	CARD NO.
9250001001+	6970400052+	6338900052+	1620000051+	7050000052+	8016143050+	9921445450+	960000+
9250001002+	6970400052+	6338900052+	1900000051+	7050000052+	9401649250+	9921445450+	970000+
9260001001+	6975400052+	6338900052+	2050000051+	6950000052+	1000000051+	1000000051+	980000+
9250001002+	6416400052+	6338900052+	1640000053+	6750000052+	7769784252+	1217596250+	990000+
9260001003+	6339300052+	6338900052+	1270000054+	6600000052+	5883137653+	6284367647+	1000000+
1001001003+	6339300052+	6338900052+	7600000053+	6600000052+	3520617653+	6284367647+	1010000+
1001001002+	6338900052+	6338700052+	1350000054+	6650000052+	6301105553+	3142183847+	1020000+
1001002002+	6338900052+	6338700052+	1350000054+	6650000052+	6301105553+	3142183847+	1030000+
1001002003+	6958800052+	6338900052+	2080000051+	7300000052+	1065730851+	9739198750+	1040000+
1001003003+	6958800052+	6338900052+	2080000051+	7300000052+	1065730851+	9739198750+	1050000+
1001003004+	6339100052+	6338900052+	1480000054+	7400000052+	7686962453+	3142183847+	1060000+
1001003004+	6339100052+	6338900052+	2500000054+	7400000052+	1298473454+	3142183847+	1070000+

TABLE V

SATURATION-RESISTANCE, CORE D-1-1

Weight of Core and Water, g	Resistance, ohms	Temperature, °F	Correction to 68°F for Resistance	Saturation, per cent	Resistance Ratio, R/R ₁₀₀
133.177	21,500	83.0	1.205	100.0	1.00
132.330	32,500	93.0	1.342	72.0	1.68
132.166	55,800	92.5	1.335	66.5	2.68
131.895	61,500	93.0	1.342	57.6	3.19
131.540	62,500	92.0	1.329	45.8	3.21
131.328	60,500	91.5	1.322	38.8	3.09
130.796	355,000	93.5	1.349	21.1	18.50
130.790	102,000	86.0	1.247	20.9	4.92
132.129	34,000	95.5	1.373	65.4	1.81

TABLE VI
SATURATION-RESISTANCE, CORE M-1-1A

IDENTI- FICATION	RMIN RESIST- ANCE SW=100 KILOHMS	WMAX MAXIMUM WEIGHT OF WATER GRAMS	POR FRAC- TIONAL POROSITY	CARD NO.
1017001001+	8058823551+	2339000051+	1678569050+	10000+

IDENTI- FICATION	WS WEIGHT AT SAT. GRAMS	WD DRY WEIGHT GRAMS	RESIST- ANCE AT SAT. AND TEMP, OHMS	TR TEMPER- ATURE F	RR RESIST- ANCE RATIO	SW WATER SATURA- TION	CARD NO.
1017001001+	1171810053+	1148420053+	8000000051+	6850000052+	1000000051+	1000000051+	20000+
9050001001+	1170880053+	1148420053+	8000000051+	6850000052+	1000000051+	9602394250+	30000+
9050001001+	1170880053+	1148420053+	8300000051+	6850000052+	1037500051+	9602394250+	40000+
9060001001+	1156160053+	1148420053+	5900000052+	7150000052+	7697992851+	3309106550+	50000+
9070001001+	1155480053+	1148420053+	6200000052+	7400000052+	8372262851+	3018383950+	60000+
9070001002+	1154600053+	1148420053+	7100000052+	7450000052+	9652372351+	2642154850+	70000+
9050001002+	1169950053+	1148420053+	1140000052+	6850000052+	1425000151+	9204788450+	80000+
9060001001+	1169010053+	1148420053+	9600000051+	7000000052+	1226277451+	8802907250+	90000+
9120001001+	1151520053+	1148420053+	1210000053+	6700000052+	1479379652+	1325352750+	100000+
9120001002+	1149240053+	1148420053+	1210000054+	6650000052+	1468339453+	3505771749+	110000+
9120001002+	1149240053+	1148420053+	1090000054+	6650000052+	1322719053+	3505771749+	120000+
9120001003+	1149000053+	1148420053+	2500000054+	6900000052+	3147810253+	2479692249+	130000+
9120001003+	1149000053+	1148420053+	2000000054+	6900000052+	2518248253+	2479692249+	140000+
9120002003+	1149000053+	1148420053+	2500000054+	6900000052+	3147810253+	2479692249+	150000+
9130002003+	1171680053+	1148420053+	8000000051+	7100000052+	1036496451+	9944420750+	160000+
9130002003+	1171680053+	1148420053+	8100000051+	7100000052+	1049452651+	9944420750+	170000+
9170003003+	1171680053+	1148420053+	8100000051+	7100000052+	1049452651+	9944420750+	180000+
9170003001+	1170270053+	1148420053+	8500000051+	7600000052+	1178832151+	9341599050+	190000+
9170003002+	1159420053+	1148420053+	4000000052+	6550000052+	4781021951+	4702864550+	200000+
9170003002+	1159420053+	1148420053+	3900000052+	6550000052+	4661496351+	4702864550+	210000+
9170003003+	1155520053+	1148420053+	7100000052+	6850000052+	8875000151+	3035485350+	220000+
9180003001+	1154350053+	1148420053+	8900000052+	6800000052+	1104379652+	2535271550+	230000+
9190004001+	1167270053+	1148420053+	2380000052+	6580000052+	2857737251+	8058999650+	240000+
9190004001+	1167270053+	1148420053+	2130000052+	6580000052+	2557554751+	8058999650+	250000+
9200004001+	1167420053+	1148420053+	2070000052+	6850000052+	2587500051+	8123129550+	260000+
9200004001+	1167420053+	1148420053+	1770000052+	6850000052+	2212500051+	8123129550+	270000+
9200004002+	1170710053+	1148420053+	9200000051+	6800000052+	1141605851+	9529713650+	280000+
9200004002+	1170710053+	1148420053+	1300000051+	6800000052+	1613138750+	9529713650+	290000+
9210004001+	1170900053+	1148420053+	9000000051+	6650000052+	1092153351+	9610944850+	300000+

TABLE VI (CONTINUED)

RUN 1

Weight of Core and Water, g	Resistance, ohms	Temperature, °F	Correction to 68°F for Resistance	Saturation, per cent	Resistance Ratio, R/R_{100}
108.655	16,000	80.0	1.163	100.0	1.00
107.938	35,500	81.5	1.183	69.0	2.26
107.399	108,000	78.0	1.135	46.8	6.60
107.123	122,000	77.5	1.127	35.2	7.43
108.567	19,000	80.0	1.163	95.0	1.19
107.892	35,000	75.3	1.080	67.2	2.04
107.398	103,000	74.5	1.085	46.5	6.00
107.062	86,000	82.8	1.200	32.5	5.55
107.020	92,000	77.5	1.150	30.8	5.68
107.642	47,000	86.0	1.245	56.8	3.15

TABLE VII

SATURATION-RESISTANCE; CORE M-2-1

Weight of Core and Water, g	Resistance, ohms	Temperature, °F	Correction to 68°F for Resistance	Saturation, per cent	Resistance Ratio, R/R_{100}
140.052	26,000	76.5	1.115	100.0	1.00
140.053	25,000	82.0	1.190	100.0	1.03
139.435	29,800	87.0	1.260	82.1	1.30
138.958	45,000	88.0	1.275	68.4	1.98
138.741	62,000	88.5	1.282	62.0	2.74
137.674	114,000	86.0	1.247	31.4	4.92
137.649	108,000	86.0	1.247	30.7	4.65
138,350	62,000	87.0	1.260	51.0	2.69
138,660	60,000	88.5	1.282	60.0	2.65
138,678	63,000	89.0	1.290	60.3	2.78

TABLE VIII
SATURATION-RESISTANCE, CORE N-3-1

IDENTIFICATION	RMIN RESISTANCE SW=100 KILOHMS	WMAX MAXIMUM WEIGHT OF WATER GRAMS	POR FRAC-TIONAL POROSITY	CARD NO.
3226201002+	1327941252+	2537000051+	1331982250+	10000+

IDENTIFICATION	WS WEIGHT AT SAT. GRAMS	WD DRY WEIGHT GRAMS	RESISTANCE AT SAT. AND TEMP. OHMS	TR TEMPERATURE F	RR RESISTANCE RATIO	SW WATER SATURATION	CARD NO.
3226201002+	1439850053+	1417530053+	8700000051+	8000000052+	7707641050+	8797792750+	20000+
3226201003+	1439130053+	1417530053+	9400000051+	8200000052+	8535990950+	8513992950+	30000+
3236201004+	1442060053+	1417530053+	1050000052+	8300000052+	9651162350+	9668900350+	40000+
3236201005+	1441710053+	1417530053+	1280000052+	7900000052+	1119822851+	9530942150+	50000+
3286101006+	1442900053+	1417530053+	1050000052+	8600000052+	1000000051+	1000000051+	60000+
3286201007+	1436110053+	1417530053+	5360000052+	8700000052+	5164119551+	7323610650+	70000+
3286201008+	1437100053+	1417530053+	3800000052+	8050000052+	3387596851+	7713835250+	80000+
3286201009+	1433530053+	1417530053+	5850000052+	8000000052+	5182724151+	6306661450+	90000+
3286201010+	1432310053+	1417530053+	6300000052+	8100000052+	5651162751+	5825778550+	100000+
3286201011+	1431320053+	1417530053+	5450000052+	7800000052+	4707641151+	5435553850+	110000+
3306101012+	1430140053+	1417530053+	7700000052+	7350000052+	6267441751+	4970437550+	120000+
3306101013+	1428290053+	1417530053+	1220000053+	6900000052+	9322259151+	4241229850+	130000+
3306101014+	1424360053+	1417530053+	3600000053+	7000000052+	2790697752+	2692156150+	140000+
3306101015+	1421500053+	1417530053+	2500000054+	7000000052+	1937984553+	1564840450+	150000+
3306101016+	1419220053+	1417530053+	2500000054+	7000000052+	1937984553+	6661411149+	160000+
4026102017+	1432310053+	1417530053+	4600000052+	7700000052+	3922480551+	5825778550+	170000+
4036102018+	1422400053+	1417530053+	3550000052+	7600000052+	2987818451+	1919590150+	180000+
4036102019+	1442290053+	1417530053+	1120000052+	8300000052+	1029457351+	9759558550+	190000+
4046102020+	1441860053+	1417530053+	1250000052+	7850000052+	1086655651+	9590067050+	200000+
4056103020+	1434500053+	1417530053+	2530000052+	7850000052+	2199390951+	6689002850+	210000+
4066103021+	1426220053+	1417530053+	1730000053+	7750000052+	1484773052+	3425305550+	220000+
4066103022+	1425410053+	1417530053+	1610000053+	7700000052+	1372868252+	3106030750+	230000+
4066103023+	1423680053+	1417530053+	4580000053+	7250000052+	3677187152+	2424123050+	240000+
4066103024+	1419740053+	1417530053+	2400000054+	6900000052+	1833887053+	8711076149+	250000+
4066103025+	1418440053+	1417530053+	2500000054+	8200000052+	2270210453+	3586913749+	260000+
4066103026+	1418860053+	1417530053+	2500000054+	6900000052+	1910299053+	5242412349+	270000+
4096104027+	1434060053+	1417530053+	1700000052+	8100000052+	1524916951+	6515569650+	280000+
4106104028+	1435050053+	1417530053+	1980000052+	7550000052+	1655481751+	6905794250+	290000+
4106104029+	1435640053+	1417530053+	1480000052+	7600000052+	1245625651+	7138352450+	300000+
4116105030+	1433860053+	1417530053+	4450000052+	7450000052+	3671373151+	6436736350+	310000+
4116105031+	1432300053+	1417530053+	7000000052+	7700000052+	5968992251+	5821836850+	320000+
4126105032+	1429110053+	1417530053+	6300000052+	7200000052+	5023255751+	4564446250+	330000+
4126105033+	1424610053+	1417530053+	2500000053+	7450000052+	2062569252+	2790697750+	340000+
4166105034+	1424300053+	1417530053+	7000000053+	7700000052+	5968992252+	2668506150+	350000+
4166105035+	1422160053+	1417530053+	2110000054+	8050000052+	1881007753+	1824990150+	360000+
4166105036+	1418240053+	1417530053+	2500000054+	7650000052+	2117940253+	2798581049+	370000+
4166105037+	1418260053+	1417530053+	2500000054+	8350000052+	2311738653+	2877414349+	380000+

The relationship implied by Equation (44) suggests a log-log plot of the experimental data thereby yielding a straight line with a slope of two. Actually the assumption that the water is the only conducting material is not always valid. For example, the core may contain natural clays or bentonite from drilling fluids which become electrical conductors when water saturated ⁽⁴⁷⁾. This clay then acts as a conductor in parallel with the water contained in the pores. As a result the resistance ratio for the core becomes

$$R_{R,i} = \frac{R_i}{R_{100}} \left(\frac{1 + R_{100}/R_{c,100}}{1 + R_i/R_{c,i}} \right) \quad (45)$$

where R_i is the electrical resistance of the water in the core at a fractional saturation "i", R_{100} is the resistance of the water at 100 per cent core saturation, and R_c is the resistance of conducting solids within the core. The resistance of the conducting solids can be considered virtually independent of water saturation when compared with the change of the resistance of the water with changing water saturation. Therefore, at high water saturations the experimental resistance ratio R_R approaches ratio of the water resistances, R_i/R_{100} , which is the same as Equation (44) for the case without conducting solids. However, as the water saturation decreases with a concurrent increase in water resistance, R_i , and R_i becomes large compared to $R_{c,i}$, the resistance ratio, R_R , begins to approach a finite limit instead of infinity as predicted by Equation (44). This offers a possible explanation of the saturation-resistance relationships exhibited by Cores D-1-1 and M-2-1 (Figs. 13 and 15) respectively.

The resistance of the cores tested would also be expected to deviate from Equation (44) because of the complex geometry of the current field when using radial and band-type electrodes instead of end electrodes.

Naar and Henderson (42) state that the exponent in Equation (44) becomes $-(1+\epsilon)$ with $\epsilon \leq 1$ for the imbibition case where ϵ is a function of the imbibition saturation [$\epsilon = \epsilon(S_{imb})$]. There was some shifting of the curve for Core AL-1-13 (Fig. 11); however, it should be pointed out that most of this change can be attributed to the changes that accompanied the repair of the wire band-type electrodes. These changes are shown by the dashed portions of the curve. Core N-3-1 (Fig. 16), which had radial electrodes, exhibited shifting of the saturation resistance curve, but a definite pattern was not established.

It is of interest to note that the slopes of the saturation-resistance correlation for Core M-1-1A (Fig. 14) for Runs 1 and 2 are essentially the same for the saturation range covered by Run 1 even though these experimental runs were separated by 15 months during which a significant change occurred in the measured permeability.

Single-Phase Permeability

The single-phase permeability of each core to nitrogen and to water was measured. The water permeability of Cores D-1-1, M-1-1A (Run 1), and M-2-1 were measured with distilled water containing 1250 ppm sodium chloride and 50 ppm formaldehyde. St. Peter formation water containing 50 ppm formaldehyde was used for this test for Cores AL-1-13, AL-1-21 and N-3-1. Dry nitrogen was used for the Klinkenberg gas permeability tests. The results of these tests are shown in Table IX.

Those gas permeabilities with an indicated infinite mean pressure have been obtained by the Klinkenberg method of extrapolating to $1/\bar{p} = 0$ on a k_g versus $1/\bar{p}$ plot. Most of the Klinkenberg values were calculated by the least squares method using the computer program described in Appendix B. The computer-calculated values include the 95 per cent confidence interval for the Klinkenberg permeability as determined from Student's "t" distribution ⁽⁶²⁾. An example of this method of obtaining the equivalent non-reactive liquid permeability (Klinkenberg permeability) for Core AL-1-21 is shown in Fig. 17.

An observation of the water permeability of the test cores indicates that flow rate sensitivity is present to a small degree. Scheiddegger ⁽⁵⁹⁾ has discussed this effect, and it is thought that the increase in permeability with increasing water flow rate can be attributed to the destruction of the ionic double-layer that exists at solid-liquid interfaces. This effect is best demonstrated by the behavior of Core D-1-1, as given in Table IX, when it was subjected to a two-fold increase in water rate. Core M-1-1A (Run 1) exhibited the same effect for a nine-fold increase in water rate. Yet, one should be cognizant of the fact that with the equipment and procedure available at the time of the initial test on Core M-1-1A, the lower water rate represents a very small recorded differential pressure which, thereby, decreased the sensitivity of the measurement. The water permeability of Core M-2-1 exhibited the opposite of this effect for reasons that are not presently known.

Also of interest are the differences between the Klinkenberg and water permeabilities of the cores, since the Klinkenberg gas permea-

bility is theoretically equivalent to the permeability to a non-reactive liquid. The fact that the liquid permeability is sometimes significantly lower than the Klinkenberg permeability, such as that exhibited by Core N-3-1 in Table IX, is generally attributed to a reaction between the test liquid and some of materials contained in the core such as clays or bentonite from drilling fluids. This phenomenon was not overcome even by using in situ fluid from the same formation as Core N-3-1.

TABLE IX

SINGLE-PHASE PERMEABILITY

Core No.	Water Flow Rate, cc/sec.	Water Permeability md.	Mean Pressure atm.	Gas Permeability md.
AL-1-13	0.0475	87.4	∞	102 \pm 5
AL-1-21	0.1344	720	∞	759 \pm 14
D-1-1	0.0115 0.0183 0.0309	18.0 19.0 20.8	7.45	144
M-1-1A (Run 1)	0.0309 0.297	846 1,130	∞	930
(Run 2)	-----	-----	∞	622 \pm 38
M-2-1	0.188 0.297	720 614	∞	790
N-3-1	0.00300	7	∞	60 \pm 5

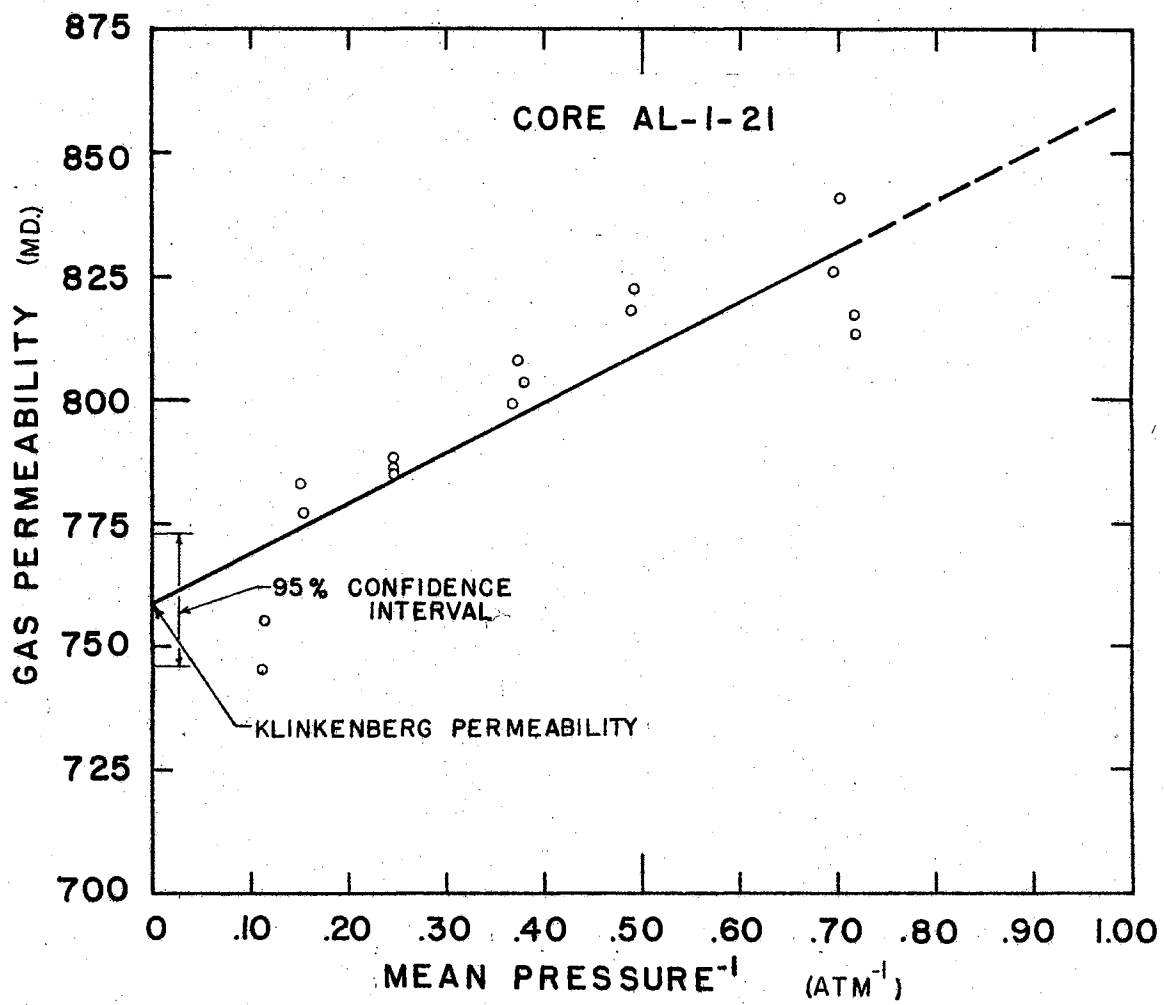



FIG. 17 KLINKENBERG PERMEABILITY, CORE AL-1-21

Relative Permeability

Gas-water relative permeability curves have been determined experimentally for the cores that are identified in Table I. The equipment and procedures that were used have been described in Chapters IV and V. Two liquid solutions were used, both containing formaldehyde to retard bacterial growth.

The relative permeability characteristics of Core AL-1-13, an Alundum core, were measured with nitrogen and St. Peter formation water, and it was found that the curves exhibited the imbibition hysteresis phenomenon that is normally expected when a consolidated porous media is subjected to two-phase flow. Experimental difficulties in the measurement of the gas permeability were encountered near the end of the first and second drainage curves, but the final saturations were determined from weight measurements at the residual water saturation. The dashed portions of these relative permeability curves for Core AL-1-13 represent extrapolations based on weight determined residual saturations and on relative permeability theory.

The gas and water imbibition curves exhibited instability near the trapped gas saturation. It is noted that this value changed from an apparent value of 45 per cent gas (55 per cent water) to about 35 per cent after several hundred pore volumes of water had been injected into the core after ceasing gas injection. A reason for this change in trapped gas saturation was not known at the time of the test. After analyzing the other cores and finding this same condition to be even more pronounced it was decided that the change in trapped gas saturation was probably due to low pressure gas diffusion



as was observed by Gardner, et al (22) and discussed by Naar and Henderson (42). Difficulty in measuring the trapped gas saturation is also mentioned by Geffen, et al (24).

It is interesting to compare the trapped gas saturations with the theoretical prediction of 50 per cent of the initial gas in place (42). For the first imbibition, originating at a gas saturation of 91 per cent, the trapped gas saturation of 45 per cent is essentially 50 per cent of the initial gas in place as is predicted by the theory. For the second imbibition, which began at 87 per cent gas saturation, the trapped gas value was 38 per cent which is 44 per cent of the initial gas in place and is less than the theoretical maximum.

The base permeability for the relative permeability curves for Core AL-1-13 (Fig. 18 and Table X) is the Klinkenberg permeability given in Table IX.

Relative permeability curves for Core AL-1-21, based on its Klinkenberg permeability, are presented in Fig. 19 and Table XI. This permeability test yielded essentially no indication of reaction between the St. Peter formation water and the core as would be expected of an Alundum core. The hysteresis phenomenon was again present as illustrated in Fig. 19.

The imbibition curve for Core AL-1-21 is of particular interest because actually it cannot be considered different from the drainage curve for water saturations greater than 60 per cent, and also, the trapped gas saturation is very low (approximately 2.5 per cent). Also of interest is the fact that the imbibition water permeability curve falls below the drainage water permeability curve at water saturations

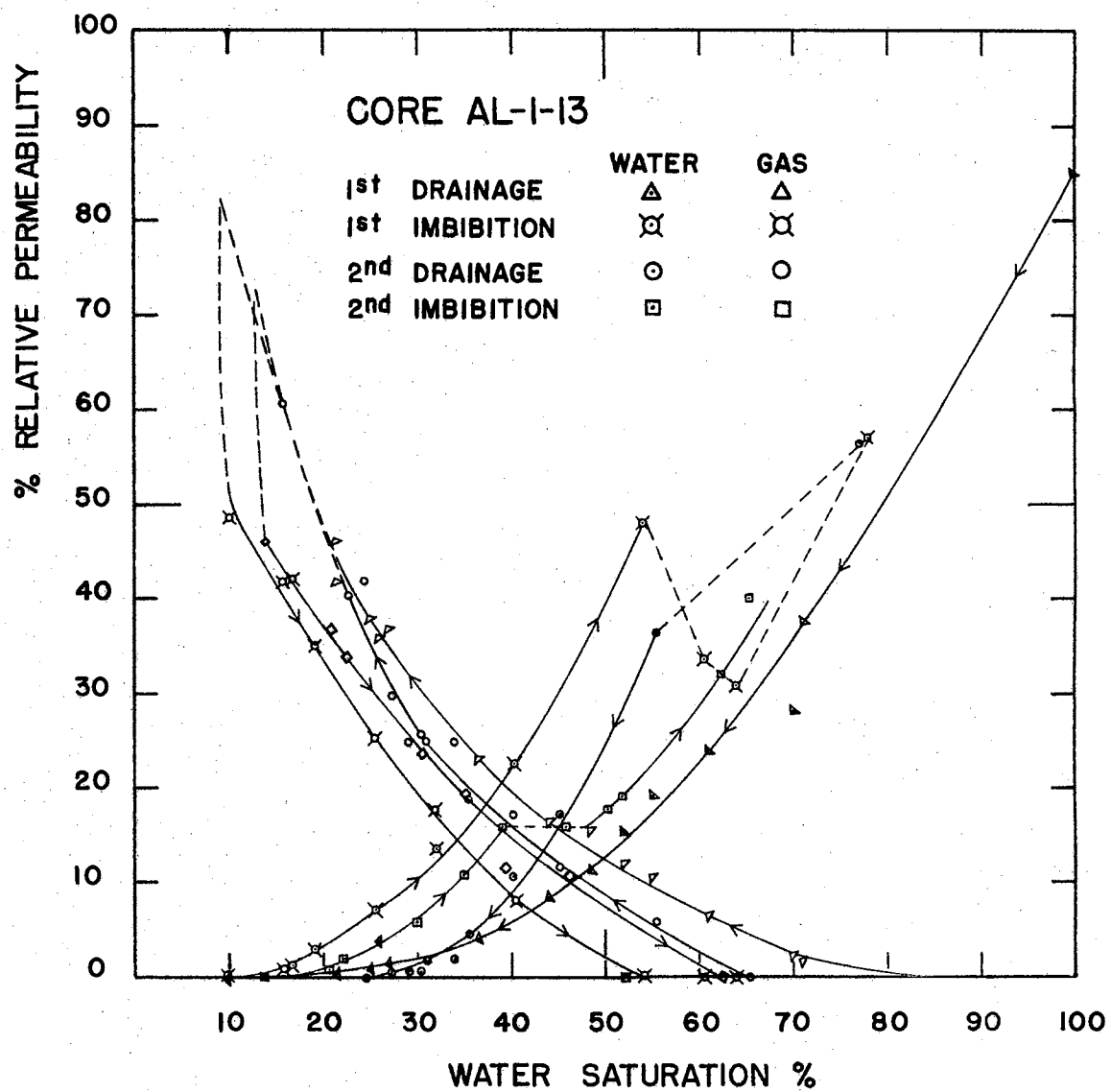


FIG. 18 RELATIVE PERMEABILITY, CORE AL-1-13

TABLE X
RELATIVE PERMEABILITY, CORE AL-1-13

IDENTIFICATION	WATER FLOW RATE CC/SEC	GAS FLOW RATE CC/SEC	DIFF. PRESSURE ATM	MEAN PRESSURE ATM	RESISTANCE AT SAT. AND TEMP. KILOHOMS	TEMPERATURE F	CARD NO.
8140000018+	4746944449+		2334375050+	1422935951+	3100000051+	7600000052+	A0590000+
8150000002+	4746944449+	1197090450+	5878125050+	2268232651+	7100000051+	6800000052+	A0630000+
81500000011+	2813055649+	1332391450+	4584375050+	2005920151+	7150000051+	6950000052+	A0810000+
81500000017+	1796388949+	2721723750+	3346875050+	2260508351+	9400000051+	7100000052+	A0930000+
81500000021+	1120277849+	3250051150+	2615625050+	2013145851+	1130000052+	7150000052+	A1010000+
81500000027+	8336111148+	3662787250+	2460937550+	1913186451+	1280000052+	7200000052+	A1130000+
81500000033+	5991666748+	3990558150+	2123437550+	1751386451+	1461000052+	7400000052+	A1250000+
81500000038+	4305555648+	4211627150+	2137500050+	2463539551+	1670000052+	7500000052+	A1350000+
81500000042+	2994444448+	4307842350+	2039062550+	2438855151+	1780000052+	7500000052+	A1430000+
81500000047+	1775000048+	5287443250+	1898437550+	2378860751+	2570000052+	7350000052+	A1530000+
81500000050+	1114722248+	5941529950+	1364062550+	2226979451+	5250000052+	7300000052+	A1590000+
81500000054+	6827777847+	9301546350+	2123437550+	2370348251+	4900000052+	7200000052+	A1670000+
81500000059+	3780555647+	9296127550+	2010937550+	2377898251+	5850000052+	7200000052+	A1770000+
81500000064+	1610555647+	9329500350+	1828125050+	2375345151+	7950000052+	7150000052+	A1870000+
81600000015+		7365215752+	1870312550+	2242538051+	8000000052+	7400000052+	A2210000+
81700000002+	1610555647+	1119449251+	1926562550+	1539830151+	1500000053+	6300000052+	A2290000+
81700000010+	3780555647+	1140343351+	2235937550+	1555298951+	6200000052+	7100000052+	A2450000+
81700000017+	6827777847+	1180752951+	2306250050+	1512702051+	5800000052+	7350000052+	A2590000+
81700000022+	1775000048+	1109198651+	2615625050+	1594045851+	4120000052+	7450000052+	A2690000+
81700000029+	4305555648+	8023268150+	2601562550+	1606517651+	2620000052+	7400000052+	A2830000+
81700000040+	1796388949+	3454088850+	3501562550+	1651517651+	1240000052+	7250000052+	A3050000+
81700000055+	2813055649+		3740625050+	2019195851+	6410000051+	7100000052+	A3350000+
81700000068+	2813055649+		4106250050+	1965014551+	5850000051+	7050000052+	A3610000+
82200000004+	1796388949+	1589756050+	2221875050+	1941819551+	8520000051+	6700000052+	A3690000+
82200000010+	1796388949+	1630552350+	2264062550+	1878053851+	8450000051+	6900000052+	A3810000+
82200000017+	8336111148+	3028331350+	2137500050+	1884900751+	1270000052+	7150000052+	A3950000+
82200000020+	4305555648+	3653329350+	1800000050+	1558413251+	1600000052+	7250000052+	A4010000+
82200000025+	1775000048+	3887203350+	1673437550+	1646447651+	2090000052+	7280000052+	A4110000+
82200000032+	6827777847+	4184084050+	1392187550+	1353572651+	2820000052+	7280000052+	A4250000+
82200000044+	2717777847+	3955743950+	1307812550+	2357241351+	3420000052+	7300000052+	A4490000+
82300000008+		1452720951+	2770312550+	2476478851+	1120000053+	7080000052+	A4870000+
82900000006+	2717777847+	7300390850+	1631253050+	2375386851+	4310000052+	6800000052+	A5030000+
82900000012+	6827777847+	6792485450+	1659375050+	2574418151+	3680000052+	7000000052+	A5153000+
82900000014+	1775000048+	3878628150+	1350020050+	2084649351+	2150000052+	7100000052+	A5190000+
82900000019+	4305555648+	4004340650+	1715625050+	2030468151+	1620000052+	7250000052+	A5290000+
82900000026+	8336111148+	3149681250+	2278125050+	2565830651+	1310000052+	7400000052+	A5430000+
82900000033+	1796388949+	6000043749+	4921875050+	1887755651+	9990000051+	7400000052+	A5570000+
82900000047+	2813055649+		3276562550+	1304839951+	5700000051+	7200000052+	A5850000+
82900000049+	2813055649+		3023437550+	1325121251+	5600000051+	7200000052+	A5890000+

IDENTIFICATION	WATER VISCOSITY CP	GAS VISCOSITY CP	WATER RELATIVE PERM EABILITY	GAS RELATIVE PERM EABILITY	RESISTANCE RATIO	AREA CM	SATURATION, PER CENT
8140000018+	9017007650+	1780799349+	8529101950+		1589314651+	545320895	100.0+
81500000002+	1002000051+	1761498849+	3763920050+	1668659949+	3256880851+	545320895	71.0+
81500000011+	9818645450+	1765026449+	2802509650+	2386163649+	352165451+	545320895	70.0+
81500000017+	9623720150+	1769062449+	2402709250+	6691832249+	4502158751+	545320895	61.0+
81500000021+	9560126250+	1770075049+	1904632650+	1023066150+	5450283351+	545320895	55.0+
81500000027+	9497206650+	1771236849+	1496429250+	1226267150+	6216945551+	545320895	52.0+
81500000033+	9252081350+	1776102749+	1214353150+	1552600050+	7293173251+	545320895	46.2+
81500000038+	9133323150+	1779326949+	8557546349+	1630785750+	8449136551+	545320895	44.5+
81500000042+	9133323150+	1779302349+	6238955349+	1748543150+	9005666551+	545320895	43.0+
81500000047+	9312398150+	1775473749+	4050055249+	2300175750+	1274251252+	545320895	36.5+
81500000050+	9373351950+	1774067049+	3563072449+	3594441250+	2585334652+	545320895	26.0+
81500000054+	9497206650+	1771693949+	1420473649+	3609954450+	2379924552+	545320895	27.0+
81500000059+	9497206650+	1771701549+	8305204048+	3809705750+	2841338452+	545320895	25.0+
81500000064+	9560126250+	1770437249+	3917696748+	4202719350+	3834491452+	545320895	21.5+
81600000015+	9252081350+	1776593849+		3254294052+	3993524052+	545320895	12.0+
81700000002+	1074143051+	1748101949+	4176880648+	4724821250+	6374797752+	545320895	10.0+
81700000010+	9623720150+	1768357249+	7568961848+	4195109750+	2969508952+	545320895	15.7+
81700000017+	9312398150+	1774607549+	1282424749+	4226221950+	2875742052+	545320895	16.8+
81700000022+	9192392650+	1777203649+	2901675049+	3505648450+	2070561252+	545320895	19.2+
81700000029+	9252081350+	1775957849+	7122488049+	2547692650+	1307879152+	545320895	25.5+
81700000040+	9434951550+	1772232449+	2251518450+	8131855349+	6064490151+	545320895	40.2+
81700000055+	9623720150+	1768821149+	3366467750+		3070089151+	545320895	60.5+
81700000068+	9687998050+	1767508749+	3087196950+		2782143851+	545320895	64.0+
82200000004+	1015794951+	1758642649+	3820182350+	5853097549+	3850782551+	545320895	78.0+
82200000010+	9885035350+	1763633549+	3648274650+	5908156849+	3933148951+	545320895	55.5+
82200000017+	9560126250+	1769946849+	1734276650+	1166419650+	6125539751+	545320895	45.2+
82200000020+	9434951550+	1772139349+	1049769050+	1673060050+	7825148551+	545320895	40.3+
82200000025+	9397913750+	1772803849+	4636792649+	1915516150+	1026389652+	545320895	35.5+
82200000032+	9397913750+	1772691049+	2143929349+	2478181250+	1384889452+	545320895	31.0+
82200000044+	9373351950+	1774197249+	9060678648+	2496214650+	1684160852+	545320895	28.2+
82300000008+	9649348750+	1768772549+		4314423250+	5349163652+	545320895	13.9+
82900000006+	1002000051+	1761606049+	7765304548+	3667175650+	1977064252+	545320895	20.7+
82900000012+	9752969750+	1766855749+	1866676449+	3364206150+	1737722652+	545320895	22.4+
82900000014+	9623720150+	1768886549+	5885792149+	2363968650+	1092749152+	545320895	30.3+
82900000019+	9434951550+	1772611449+	1101397050+	1924507150+	7222962851+	545320895	35.2+
82900000026+	9252081350+	1776917149+	1574790250+	1142756150+	6539395651+	545320895	39.3+
82900000033+	9252081350+	1776239149+	1570748150+	1007216049+	4986913151+	545320895	46.0+
82900000049+	9497206650+	1770648749+	4110272150+		2719913751+	545320895	65.5+

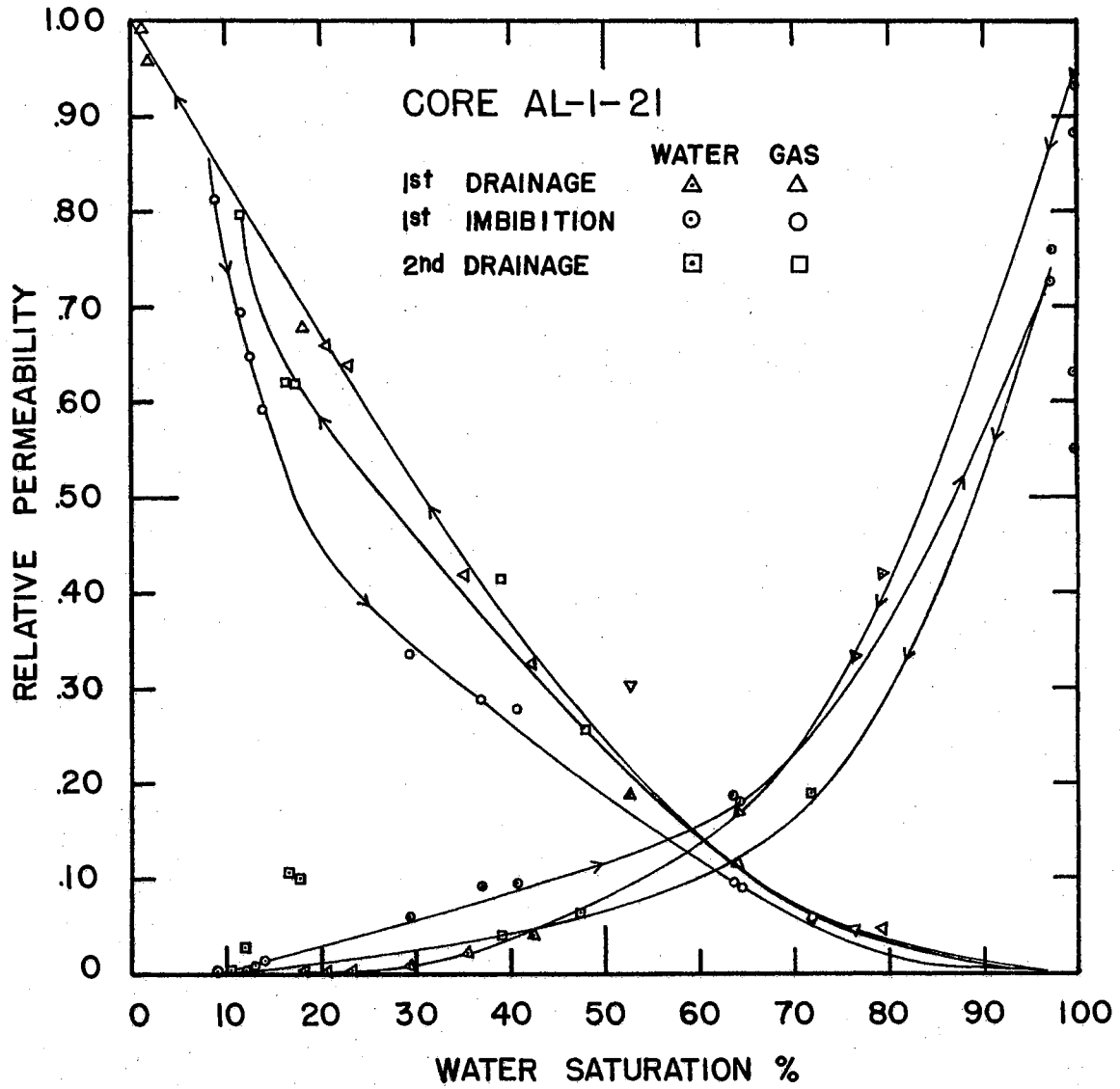


FIG. 19 RELATIVE PERMEABILITY, CORE AL-1-21

TABLE XI
RELATIVE PERMEABILITY, CORE AL-1-21

IDENTIFICATION	WATER FLOW RATE CC/SEC	GAS FLOW RATE CC/SEC	DIFF. PRESSURE ATM	MEAN PRESSURE ATM	RESISTANCE AT SAT. AND TEMP. KILOHOMS	TEMPERATURE F	CARD NO.
9270000003+	1344027850+		8437500049+	1149463851+	1910000051+	6950000052+	590000+
9270000006+	9818645450+	1764122049+	6860161050+		9291443850+	5704379851+	660000+
9260000010+	9752969750+	1765845349+	4193399650+	4994512149+	1585983751+	5704379851+	740000+
9260000018+	9726897250+	1766314849+	1673448650+	1144461050+	2494441351+	5704379851+	900000+
9260000025+	9752969750+	1765729949+	1878556750+	3010651250+	3856600051+	5704379851+	1040000+
9260000033+	9752969750+	1765802849+	3959853249+	3235769250+	5811989851+	5704379851+	1200000+
9260000039+	9726897250+	1766226849+	1995742249+	4180680250+	8397129351+	5704379851+	1320000+
9260000046+	9752969750+	1765677249+	9085083448+	5323390650+	1231353852+	5704379851+	1460000+
9260000048+	9752969750+	1765704749+	3097579848+	6392011350+	2093301452+	5704379851+	1500000+
9260000050+	9752969750+	1768904849+	3145604548+	1983530650+	2068674352+	5704379851+	1540000+
9260000056+	1015794951+	1758537549+	1984190548+	6600335550+	2644736852+	5704379851+	1660000+
9260000064+	1089570951+	1746586049+	1325520048+	6790326450+	3162820252+	5704379851+	1820000+
9260000072+	1089570951+	1746131249+		9578245550+	4537011053+	5704379851+	1980000+
9260000082+	9560126250+	1770891349+		9925052150+	6640866953+	5704379851+	2180000+
1010000005+	1029897351+	1756582449+		2257134151+	6315789453+	5704379851+	2280000+
1010000007+	1022807151+	1758103449+		6458047651+	6316844953+	5704379851+	2320000+
1010000018+	1141396551+	1738547049+	1439062148+		8219438850+	1117084153+	2540000+
1010000023+	1138043251+	1739285849+	3533698848+	6947709550+	8095271552+	5704379851+	2640000+
1010000027+	1138043251+	1739304049+	6593682348+	6461552550+	6974387852+	5704379851+	2720000+
1010000031+	1113386151+	1743214249+	1119156949+	5921546850+	5704334352+	5704379851+	2800000+
1010000038+	1066559651+	1751586249+	6083195549+	3349798750+	1206374952+	5704379851+	2940000+
1010000042+	1002000051+	1761617349+	9231883349+	2894742050+	7751196251+	5704379851+	3020000+
1010000045+	1015794951+	1759139249+	9157713449+	2774918950+	6364340051+	5704379851+	3080000+
1010000047+	9752969750+	1766324149+	1844340850+	9541943349+	2511961751+	5704379851+	3120000+
1010000051+	9687998050+	1767737549+	1730273550+	8620456849+	2455495451+	5704379851+	3200000+
1010000054+	9497206650+	1770574349+	9159470350+		9777652750+	5704379851+	3260000+
1010000055+	9497206650+	1770575749+	8864003850+		9777652750+	5704379851+	3280000+
1010000059+	9312398150+	1774225849+	5555402650+		9929636950+	5704379851+	3360000+
1010000060+	9312398150+	1774217349+	6339694850+		9671052650+	5704379851+	3380000+
1010000067+	9312398150+	1774539249+	1858986650+	5831529049+	1970412351+	5704379851+	3520000+
1010000071+	9373351950+	1773017349+	1887502450+	4100693450+	1756684552+	5704379851+	3600000+
1010000074+	9687998050+	1767555349+	6311613649+	3017691850+	4514143051+	5704379851+	3660000+
1010000078+	9687998050+	1767138249+	1034192150+	6211901750+	3621235652+	5704379851+	3740000+
1010000087+	9687998050+	1767188849+	1053226350+	6219833250+	3963516852+	5704379851+	3920000+
1010000100+	9560126250+	1769877149+	3779346049+	4138836150+	6842105351+	5704379851+	4180000+
1010000108+	9348893450+	1773947249+	2911058549+	7993535250+	7983394452+	5704379851+	4340000+
1010000116+	9623720150+	1768676449+		1102975351+	2397973553+	5704379851+	4500000+
1010000123+	9312398150+	1775572649+		1105241351+	7654095153+	5704379851+	4640000+

IDENTIFICATION	WATER VISCOSITY CP	GAS VISCOSITY CP	WATER RELATIVE PERM EABILITY	GAS RELATIVE PERM EABILITY	RESISTANCE RATIO	AREA CM	SATURATION PER CENT
9270000003+	9818645450+	1764170049+	9464478250+		9340346250+	570437985	100.0+
9270000006+	7789444449+		6752000049+	1101501351+	1900000051+	695000005	100.0+
9260000010+	7789444449+	5124099450+	1097875050+	1563957651+	3220000051+	700000005	79.5+
9260000018+	4115833349+	1550074851+	1442437550+	1528835751+	5050000051+	702000005	64.3+
9260000025+	4115833349+	3643397051+	1294750050+	1448638851+	7830000051+	700000005	52.6+
9260000033+	9618888948+	4341282351+	1435375050+	1521545151+	1180000052+	700000005	42.5+
9260000039+	5194444448+	5992520251+	1539812550+	1440829451+	1700000052+	702000005	39.5+
9260000046+	2596305648+	8403124451+	1681500050+	1395863851+	2500000052+	700000005	29.5+
9260000048+	9663611147+	1101471552+	1842187550+	1423360751+	4250000052+	700000005	23.2+
9260000050+	9663611147+	3359747651+	1815062550+	4623479451+	4200000052+	700000005	23.0+
9260000056+	9663611147+	1856848652+	2998312550+	1836741951+	5610000052+	670000005	20.7+
9260000064+	9663611147+	3088227752+	4800375050+	2566432651+	7250000052+	620000005	18.3+
9260000072+		3516419552+	3882250050+	2111601351+	1040000054+	620000005	1.9+
9260000082+		4686254952+	5068500050+	2829413851+	1320000054+	715000005	1.2+
1010000005+		4596127652+	2163625050+	2410272151+	1360000054+	660000005	1.3+
1010000007+		8787727352+	1448437550+	2670850251+	1350000054+	665000005	1.3+
1010000018+	9663611147+	3623699752+	4648625050+	2672359651+	2700000053+	588000005	9.0+
1010000023+	2596305648+	3340071152+	5061500050+	2904253351+	1950000053+	590000005	11.7+
1010000027+	5194444448+	3330666952+	5423125050+	2922534651+	1680000053+	590000005	12.7+
1010000031+	9618888948+	3250604552+	5796750050+	3006690851+	1340000053+	605000005	14.0+
1010000038+	7789444449+	2611842852+	8267750050+	3756253351+	2700000052+	635000005	29.5+
1010000042+	7789444449+	1389255752+	5118750050+	2386653351+	1620000052+	680000005	37.0+
1010000045+	7789444449+	1362936352+	5234250050+	2438390851+	1350000052+	670000005	40.8+
1010000047+	1344027850+	3839462151+	4305125050+	2042847151+	5100000051+	705000005	66.0+
1010000051+	1344027850+	3669780051+	4452250050+	2193840851+	4950000051+	705000005	64.5+
1010000054+	1344027850+		8437500049+	1250653351+	1930000051+	720000005	100.0+
1010000055+	1344027850+		8715750049+	1252059651+	1930000051+	720000005	100.0+
1010000059+	1344027850+		1364062550+	1130954451+	1920000051+	735000005	100.0+
1010000060+	1344027850+		1192312550+	1122516951+	1870000051+	735000005	100.0+
1010000067+	7789444449+	1282297051+	2360500050+	1444376351+	3810000051+	735000005	72.0+
1010000071+	4115833349+	4727260151+	1237500050+	1177326351+	3470000052+	730000005	76.0+
1010000074+	4115833349+	1078582352+	3825000050+	2011563851+	9100000051+	705000005	48.0+
1010000078+	4115833349+	1355328852+	2334375050+	1594482651+	7300000052+	705000005	17.5+
1010000087+	9687998050+	1767188849+	1053226350+	6219833250+	3963516852+	5704379851+	16.7+
1010000100+	2084305649+	1232944452+	3192187550+	1815235751+	1360000052+	715000005	39.4+
1010000108+	9618888948+	1391978052+	1870312550+	1604216951+	1550000053+	732000005	11.8+
1010000116+		2201625852+	2137500050+	1874488851+	4800000053+	710000005	3.8+
1010000123+		3224082052+	3135937550+	2477760751+	1480000054+	735000005	1.0+

greater than 70 per cent. This behavior of the imbibition water permeability curve is contrary to the experience with Core AL-1-13, and it is also contrary to the imbibition theory of Naar and Henderson (42).

As expressed under the discussion of Core AL-1-13, the behavior of the imbibition gas permeability curve at high water saturations is believed to be due to low pressure gas diffusion. This diffusion effect would be expected to be more significant in this core because its permeability is greater than that of Core AL-1-13 by a factor of about seven and one-half. This higher permeability implies that the average pore diameter is greater, and therefore, the interfacial tension between the bubbles of trapped gas and the surrounding liquid would be less. It is not known whether the abnormal behavior of the imbibition water curve is related to this phenomenon.

The relative permeability characteristics that were measured for Core D-1-1 are given in Fig. 20 and Table XIII with the maximum water permeability being used for a relative permeability base. The test fluid for this core was distilled water containing 1250 ppm sodium chloride and 50 ppm formaldehyde.

Cores D-1-1, M-1-1A (Run 1) and M-2-1 were the first cores tested. At the time of these tests it was not possible to obtain intermediate points on the imbibition curves because the pump transmission described in Chapter IV had not yet been developed. Nevertheless, it was possible to determine the end points of the imbibition relative permeability curves.

Observation of Fig. 20 indicates that Core D-1-1 had a high sensitivity to the test liquid with the absolute water permeability

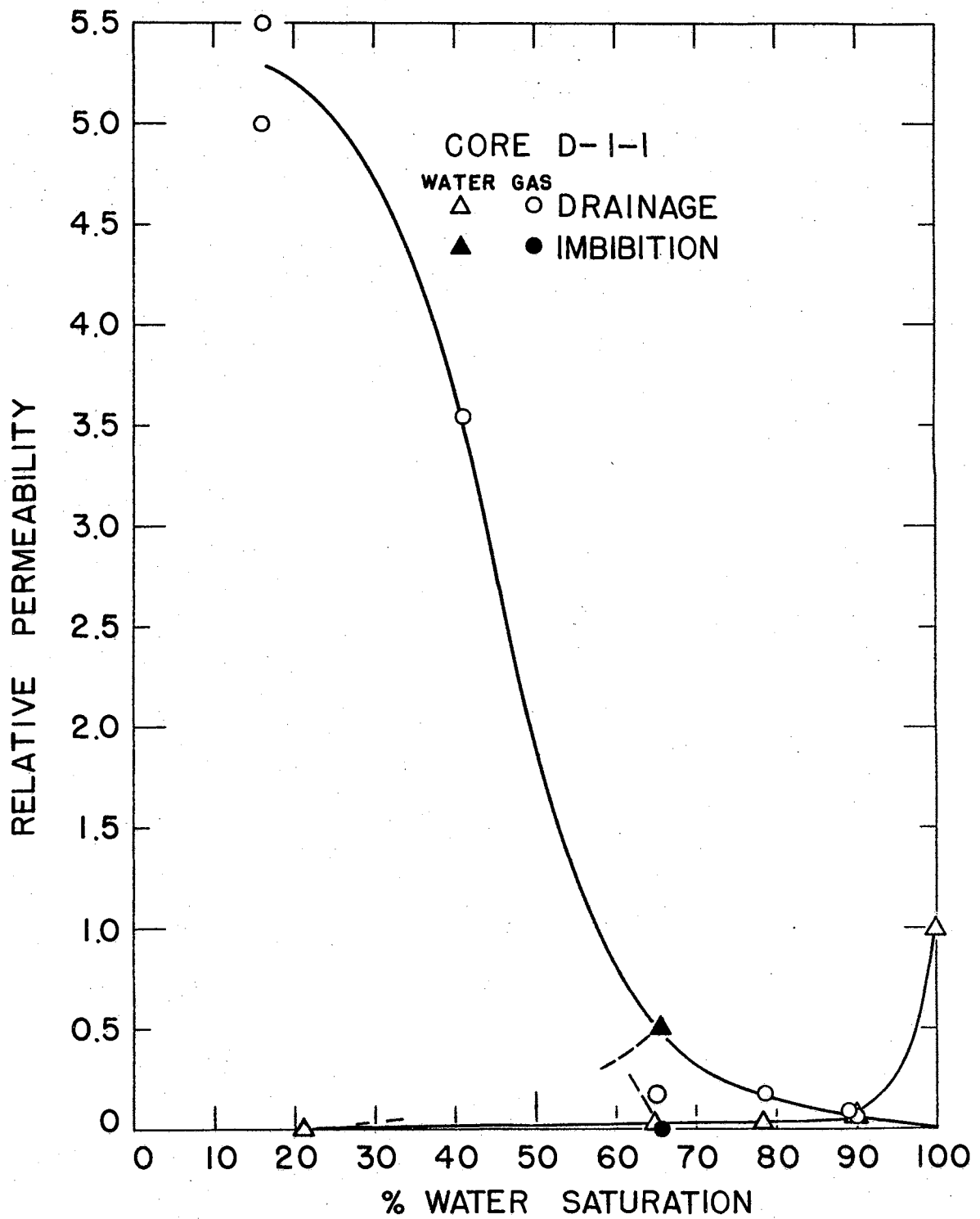


FIG. 20 RELATIVE PERMEABILITY, CORE D-1-1

TABLE XII

RELATIVE PERMEABILITY, CORE D-1-1

Water Flow Rate cc/sec	Gas Flow Rate cc/sec	Flowing Temp., °F	Resistance at Temp., ohms	Pressure Drop, atm	Barom. Pressure, atm	Average Pressure, atm
0.0027	0.611	93.0	24,000	1.250	0.976	8.18
0.0027	0.601	93.0	24,000	1.265	0.976	8.19
0.0027	0.603	93.0	24,200	1.358	0.976	8.10
0.0027	0.605	93.0	24,300	1.380	0.976	8.14
0.0027	1.537	87.0	26,200	1.370	0.980	8.05
0.0027	1.494	87.5	26,100	1.360	0.980	8.26
0.0027	4.180	87.5	33,500	1.890	0.980	8.20
0.0027	4.200	89.0	50,100	1.960	0.980	8.54
-----	9.330	91.0	67,500	0.279	0.980	6.26
-----	15.900	93.0	-----	0.312	0.976	6.31
0.0000	41.700	86.0	102,000	0.825	0.980	7.01
0.0027	0.000	95.0	27,000	0.142	0.976	2.39
0.0000	12.800	77.5	-----	0.142	0.980	7.45

Water Viscosity, cp	Gas Viscosity cp	Relative Gas Perm.	Relative Water Perm.	R/R ₁₀₀	Water Saturation, %
0.736	0.01829	0.0410	0.0610	1.24	90.0
0.736	0.01829	0.0398	0.0604	1.24	90.0
0.736	0.01829	0.0375	0.0568	1.26	89.5
0.736	0.01829	0.0370	0.0555	1.26	89.5
0.788	0.01812	0.0949	0.0596	1.28	89.0
0.784	0.01813	0.0908	0.0596	1.28	89.0
0.784	0.01811	0.1840	0.0430	1.66	78.5
0.770	0.01816	0.1710	0.0406	2.50	65.0
0.752	0.01820	3.5500	-----	3.43	41.0
0.736	0.01825	5.5100	-----	----	21.1
0.797	0.01808	5.0000	-----	----	20.9
0.719	-----	0.0000	0.5240	----	65.4
-----	0.01787	8.0000	0.0000	----	0.0

being only one-fifth of the value of gas permeability at residual water saturation. Also, the shape of the water permeability is unusual when compared with non-reactive cores such as Core AL-1-13 or Core AL-1-21. It is noted that a very rapid change in water permeability, to about 5 per cent of its initial value, occurred between 90 and 100 per cent saturation; then the permeability decreased very slowly as the saturation continued to decrease. It is not known if this particular permeability behavior is typical of reactive cores, or if it is only a function of the pore configuration of this test sample. In spite of the reactivity of Core D-1-1, its trapped gas saturation of 35 per cent compared well with the value obtained for Cores M-1-1A and M-2-1 which also were cut from the Mount Simon formation, but from another well. The end point of the imbibition water permeability curve fell above the drainage curve as predicted by imbibition theory (42), but to an extreme degree as compared with other test cores. Possibly, equilibrium had been reached between the test liquid and materials in the core at this stage of the testing, or possibly contaminants from the drilling fluid were flushed from the core as water injection continued. Since other points on the imbibition curve were not obtained, it is impossible to establish a hypothesis regarding the behavior that was observed.

Two different experimental tests of the relative permeability of Core M-1-1A were made which were separated by an interim period of 15 months. Run No. 1 was made with a prepared liquid solution of distilled water, 1250 ppm sodium chloride and 50 ppm formaldehyde, and St. Peter formation water with 50 ppm formaldehyde was used in

Run No. 2. The data for these two tests are represented by Figs. 21 and 22 and Tables XIII and XIV respectively. The water permeability was used as a base permeability for Run 1 and the Klinkenberg permeability was used as a base permeability for Run 2.

It is of interest that the relative permeability curves for the two tests at Core M-1-1A are very similar; however, the gas permeability increased more rapidly at high water saturations in Run 1 than it did in Run 2. Also, there was a change in the trapped gas saturation from 38 to 27 per cent. This occurrence may be partially the result of the lower pressure and higher water rate used to determine the trapped gas-saturation for Run 2. Of significance is the apparent change in single-phase permeability between the two tests. The water permeability of Run 1 was 1,130 md. The water permeability for Run 2 is not considered reliable because of experimental difficulties, but the Klinkenberg permeability was 622 md. This is a remarkable change in single-phase permeability but no definite conclusions can be drawn because the effects of the interim period, of the change of test liquid, and of previous testing are not known. It is significant that the drainage relative permeability curves were very similar in spite of this apparent permeability change.

It is noted that the gas relative permeability curve for the second drainage cuts across the hysteresis loop. Scrutiny of the original experimental data showed that the fluid outlet temperature dropped markedly between the water saturations of 41 and 29 per cent. This occurrence and the fact that a lower residual water saturation was obtained during Run 2 infer that evaporation of the water in the core

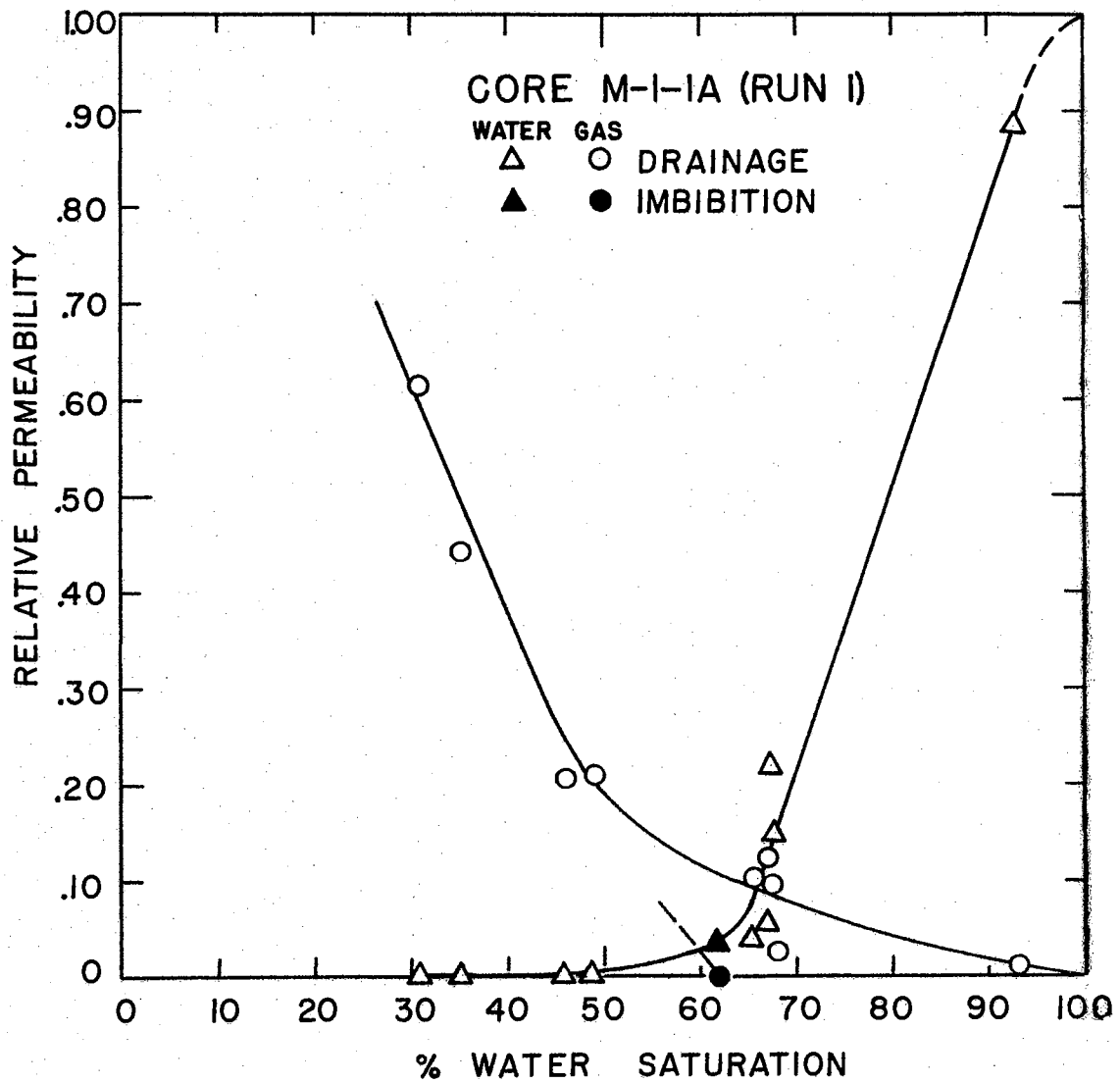


**FIG. 21 RELATIVE PERMEABILITY, CORE M-1-1A
(RUN 1)**

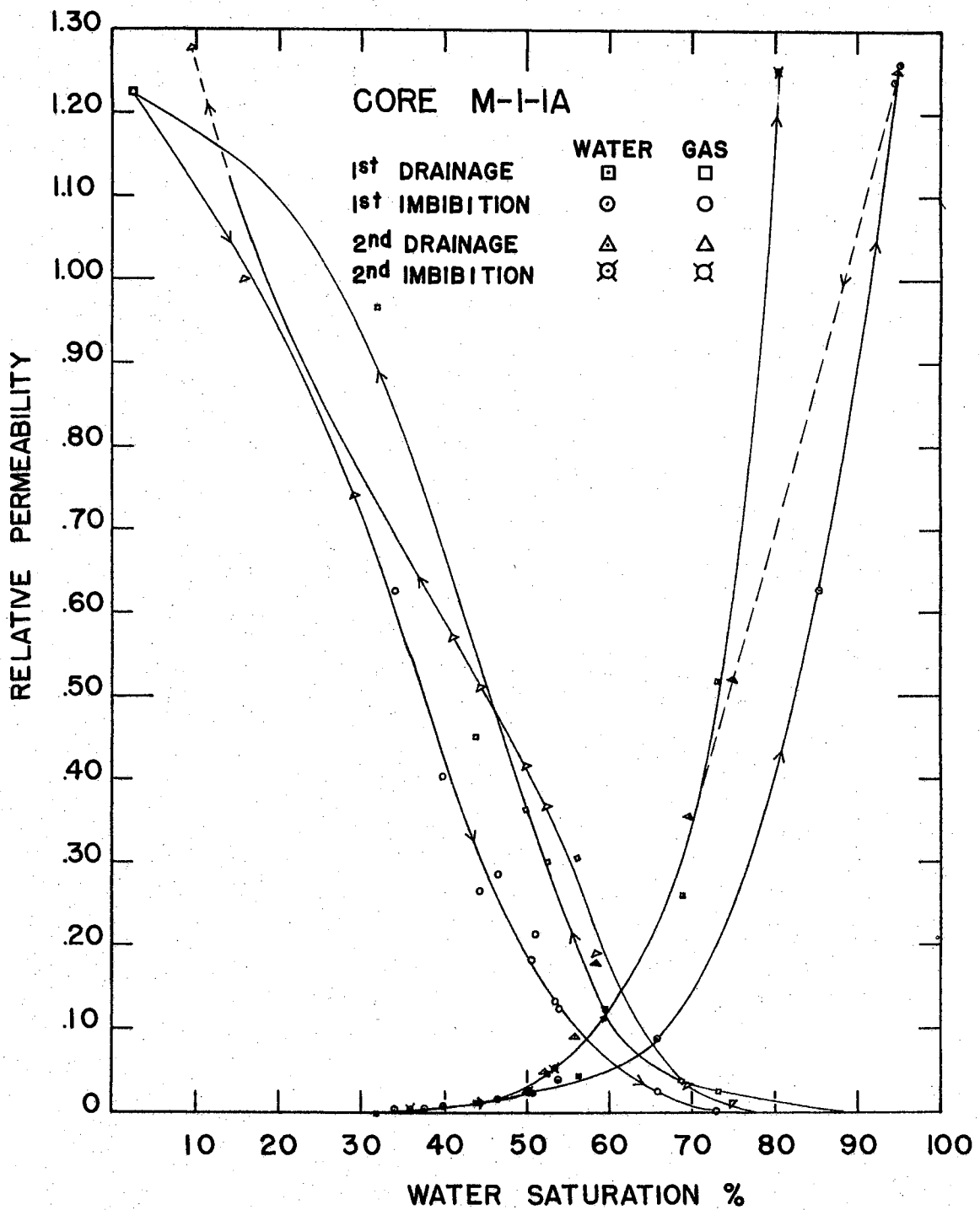


**FIG. 22 RELATIVE PERMEABILITY, CORE M-1-1A
(RUN 2)**

TABLE XIII

RELATIVE PERMEABILITY, CORE M-1-1A, RUN 1

Water Flow Rate, cc/sec	Gas Flow Rate, cc/sec	Flowing Temp., °F	Resistance at Temp., ohms	Pressure Drop, atm	Barom. Pressure, atm	Average Pressure, atm
0.03085	0.0468	82.5	18,000	0.0140	0.974	2.46
0.03085	0.0765	83.0	33,800	0.0826	0.974	2.86
0.03085	2.1900	83.0	34.0	0.0560	0.974	3.53
0.03085	14.9000	79.8	36,500	0.2415	0.974	4.56
0.03085	21.8000	77.5	38,500	0.3275	0.974	5.40
0.00271	66.6000	72.0	74,000	0.2180	0.974	6.32
0.00000	7.8300	77.0	122,000	0.0854	0.973	1.73
0.00271	7.3100	80.2	70,000	0.0602	0.973	4.91
0.00000	55.7000	81.5	88,000	0.1400	0.973	6.44
0.00271	0.0000	86.0	39,000	0.0280	0.973	----

Water Viscosity, cp	Gas Viscosity, cp	Relative Gas Perm.	Relative Water Perm.	R/R ₁₀₀	Water Saturation, %
0.829	0.01788	0.0114	0.88200	1.160	93.0
0.824	0.01789	0.2972	0.14900	2.190	68.0
0.824	0.01789	0.0960	0.22000	2.235	67.5
0.857	0.01783	0.1230	0.05570	2.280	67.0
0.885	0.01777	0.1027	0.04020	2.340	65.5
0.950	0.01764	0.2100	0.00568	4.200	49.0
-----	0.01776	0.4420	-----	-----	35.2
0.854	0.01783	0.2070	0.00300	4.380	46.0
0.840	0.01786	0.6160	-----	-----	30.8
0.797	-----	-----	0.03710	2.650	62.0

TABLE XIV
RELATIVE PERMEABILITY, CORE M-1-1A (RUN 2)

IDENTIFICATION	WATER FLOW RATE CC/SEC	GAS FLOW RATE CC/SEC	DIFF. PRESSURE ATM	MEAN PRESSURE ATM	RESISTANCE AT SAT. AND TEMP, KILOHOMS	TEMPERATURE F	CARD NO.
9060000004+	1344027850+		4359375049+	3129831151+	8150000051+	7150000052+	830000+
9060000008+	7789444449+	1917859650+	1181250050+	4622934251+	1260000052+	7450000052+	910000+
9060000014+	4115833349+	3206090050+	1321875050+	3839465551+	1510000052+	7000000052+	1030000+
9060000020+	2084305649+	1085693951+	1448437550+	4899793651+	2040000052+	6850000052+	1150000+
9060000025+	5194444448+	2150812051+	1054687550+	7350418651+	2750000052+	6680000052+	1250000+
9060000029+	5194444448+	2001810951+	1012500050+	6953059251+	2620000052+	6720000052+	1325000+
9060000038+	2596305648+	2126990751+	8859375049+	7671356151+	2910000052+	6650000052+	1510000+
9060000041+	9688611147+	2907093251+	9703125049+	9836274851+	3860000052+	6400000052+	1570000+
9060000052+		4398843251+	6890625049+	6383537351+	6200000052+	7000000052+	1790000+
9120000009+		1217078252+	1504687550+	4603142351+	2500000054+	6900000052+	1970000+
9130000014+	9663611147+	8698920651+	2095312550+	6247005751+	5950000052+	6702000052+	2310000+
9130000019+	2596305648+	7599440651+	2854687550+	6383787051+	4320000052+	6900000052+	2410000+
9130000022+	5194444448+	6388622551+	3417187550+	5423787051+	3290000052+	6850000052+	2470000+
9130000026+	9618888948+	5482079751+	3881250050+	4821177651+	2800000052+	6700000052+	2550000+
9130000030+	2084305649+	3800303151+	4640625050+	5089708951+	2500000052+	6750000052+	2630000+
9130000052+	1344027850+		9281250049+	5200521451+	8500000051+	6800000052+	3070000+
9130000057+	1344027850+		8718750049+	4341333951+	8000000051+	7150000052+	3170000+
9170000002+	1344027850+		4640625049+	2578150551+	7780000051+	7600000052+	3210000+
9170000007+	7789444449+	7131819049+	1195312550+	4393338051+	1220000052+	7400000052+	3330000+
9170000018+	4115833349+	2228023750+	9703125049+	3772744351+	1480000052+	7000000052+	3550000+
9170000023+	2084305649+	1222029251+	9843750049+	4876853751+	2090000052+	6950000052+	3650000+
9170000031+	9618888948+	1894072251+	9421875049+	5006494351+	2340000052+	6800000052+	3810000+
9170000035+	5194444448+	2255241251+	9281250049+	5466916251+	2620000052+	6750000052+	3890000+
9170000039+	2596305648+	2480217851+	9000000049+	6519509951+	2950000052+	6600000052+	3970000+
9170000049+	9663611147+	2521416351+	7453125049+	7925456451+	3720000052+	6550000052+	4170000+
9170000051+		2591255551+	6890625049+	7659143951+	4300000052+	6550000052+	4210000+
9170000065+		5861788051+	1195312550+	8804331451+	7150000052+	6800000052+	4490000+
9180000001+		1108530452+	1673437550+	5832109451+	1050000053+	6600000052+	4510000+
9180000003+		1134969252+	1335937550+	4530671951+	2080000053+	6650000052+	4550000+
9180000006+		1028328652+	5906250049+	1120606351+	2500000054+	6800000052+	4610000+
9190000016+	9663611147+	7308905351+	2053125050+	5061383351+	5300000052+	6200000052+	4990000+
9190000029+	5194444448+	5439417151+	3079687550+	4915086451+	3800000052+	6400000052+	5250000+
9190000035+	9618888948+	4235641651+	3515625050+	4732258351+	3000000052+	6350000052+	5370000+
9190000039+	2084305649+	3135790351+	3571875050+	4610320851+	2700000052+	6400000052+	5450000+
9190000057+	7789444449+		5484375049+	1955898951+	1200000052+	6600000052+	5810000+
9200000004+	1344027850+		7171875049+	2099770651+	9200000051+	6800000052+	5970000+

IDENTIFICATION	WATER VISCOSITY CP	GAS VISCOSITY CP	WATER RELATIVE PERMEABILITY	GAS RELATIVE PERMEABILITY	RESISTANCE RATIO	AREA CM	SATURATION PER CENT
9060000004+	9560126250+	1771191749+	2522090151+		1130539051+	506708665	94.0+
9060000008+	9192392650+	1780232549+	5187936350+	2474211549+	1821162551+	506708665	73.3+
9060000014+	9752969750+	1768120849+	2599497350+	3670983049+	2050675151+	506708665	69.5+
9060000020+	9952150050+	1765392049+	1225924350+	1132749550+	2711081951+	506708665	59.5+
9060000025+	1018590551+	1763544949+	429 375649+	3078578950+	3563945351+	506708665	56.3+
9060000029+	1013011651+	1764160549+	4488807349+	2985734950+	3415800151+	506708665	52.8+
9060000038+	1022807151+	1763103949+	2565851749+	3640512850+	3754365351+	506708665	50.0+
9060000041+	1059061551+	1758935949+	9052242648+	4511099850+	4792798351+	506708665	44.0+
9060000052+	9752969750+	1770664849+		9676121850+	6419990651+	506708665	32.0+
9120000009+	988503350+	1766358549+		1223027351+	3346655353+	506708665	2.5+
9130000014+	1015794951+	1762947849+	4010345348+	6265289050+	7734168851+	506708665	34.3+
			5				40.0+
9130000022+	9952150050+	1765916049+	1295007649+	2826139450+	4372284051+	506708665	46.5+
9130000026+	1015794951+	1761522049+	2154985849+	2129839650+	3639608851+	506708665	51.0+
9130000030+	1008859651+	1763054649+	3878830149+	1235926450+	3273902051+	506708665	54.0+
9130000052+	1002000051+	1764431149+	1242094451+		1121372051+	506708665	94.5+
9130000057+	9560126250+	1772403249+	1261545051+		1109731551+	506708665	95.0+
9170000002+	9017007650+	1781954649+	2235523851+		1147136451+	506708665	93.5+
9170000007+	9252081350+	1778744649+	5161186650+	9084845448+	1751513351+	506708665	75.0+
9170000018+	9752969750+	1768054049+	3141344250+	3475272249+	2009933251+	506708665	69.7+
9170000023+	9818645450+	1767897449+	1779661850+	1878274850+	2818077851+	506708665	58.9+
9170000031+	1002000051+	1764237149+	8756698649+	3035996450+	3087071251+	506708665	55.8+
9170000035+	1008859651+	1763431849+	4833352549+	3668008250+	3431049351+	506708665	52.0+
9170000039+	1029897351+	1760691649+	2543269249+	4153514250+	377335251+	506708665	50.5+
9170000049+	1037066651+	1760876749+	1151046349+	5099268350+	4727223551+	506708665	44.5+
9170000051+	1037066651+	1760560349+		5667449150+	5464267751+	506708665	41.2+
9170000065+	1002000051+	1768034949+		7422062150+	9432717651+	506708665	29.2+
9180000001+	1029897351+	1760004249+		9980146550+	1344482452+	506708665	16.0+
9180000003+	1022807151+	1759963249+		1279931251+	2683532652+	506708665	9.3+
9180000006+	1002000051+	1760351249+		2623641651+	3298153053+	506708665	2.5+
9190000029+	1059061551+	1754014749+	1529110049+	2651942150+	4718298951+	506708665	44.5+
9190000035+	1066559651+	1752569249+	2498000949+	1807494350+	3695871651+	506708665	50.5+
9190000039+	1059061551+	1753709949+	5290192149+	1317933950+	3352475551+	506708665	53.7+
9190000057+	1029897351+	1756128049+	1252155851+		1536551351+	506708665	80.3+
9200000004+	1002000051+	1761330449+	1607416251+		1213720351+	506708665	91.0+

was occurring. Equipment modification was made to insure that the injected gas in subsequent tests would be water saturated. This modification consisted of connecting into the gas inlet line a Lucite tube filled with the test liquid and glass beads.

The relative permeability test of Core M-2-1, as presented in Fig. 23 and Table XV, yielded results almost identical to those obtained for Core M-1-1A (Run 1). This identity might be expected since the cores were from the same well and were separated by only four feet. Nevertheless, it is significant in that this similarity occurred in cores having a water permeability ratio of 1.6. The trapped gas saturation of 35 per cent for Core M-2-1 compares with 38 per cent for Core M-1-1A and their residual water saturations under the imposed differential pressures were 30.8 and 30.7 per cent respectively. It is remarkable that the relative permeabilities, the trapped gas saturations, and the residual water saturation compared so closely even though the absolute permeabilities differed significantly.

The relative permeability characteristics, based on the Klinkenberg permeability, for Core N-3-1 are given in Fig. 24 and Table XVI. This core was the first one tested after the development of a pump transmission that would permit the imbibition curves to be obtained in detail. The effects of low pressure diffusion were also experienced for the first time in the testing of this core. This diffusion phenomenon appeared in the form of a break in the relative permeability curves when tests were temporarily stopped over night. An example of this is illustrated by the dashed portion of the second drainage gas permeability curve in Fig. 24. Although the reason for this behavior

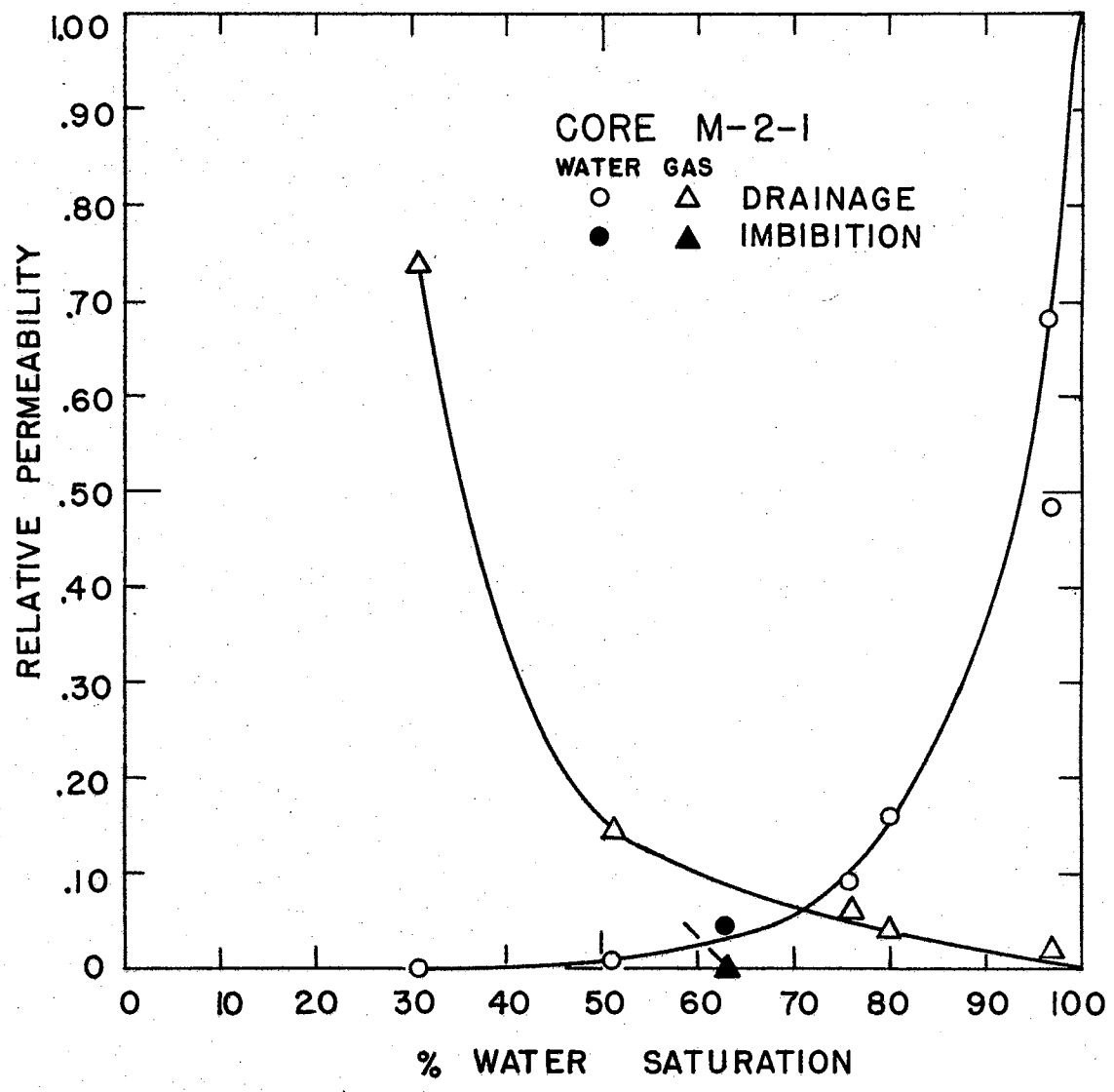


FIG. 23 RELATIVE PERMEABILITY, CORE M-2-1

TABLE XV

RELATIVE PERMEABILITY, CORE M-2-1

Water Flow Rate, cc/sec	Gas Flow Rate, cc/sec	Flowing Temp., °F	Resistance at Temp., ohms	Pressure Drop, atm	Barom. Pressure, atm	Average Pressure, atm
0.1875	1.65	87.0	24,500	0.3120	0.975	4.62
0.1875	1.20	87.0	24,500	0.2440	0.975	5.04
0.0308	1.72	86.8	36,300	0.1570	0.975	4.87
0.0308	4.85	87.0	40,000	0.2760	0.974	4.97
0.0027	11.95	88.5	75,500	0.2850	0.974	5.17
0.0000	16.70	86.0	117,000	0.0728	0.976	5.54
0.0027	0.00	88.0	58,000	0.0476	0.976	----

Water Viscosity, cp	Gas Viscosity, cp	Relative Gas Perm.	Relative Water Perm.	R/R ₁₀₀	Water Saturation, %
0.788	0.01810	0.0203	0.48100	1.065	97.0
0.788	0.01810	0.0172	0.61800	1.065	97.0
0.790	0.01809	0.0396	0.15700	1.575	80.0
0.788	0.01810	0.0648	0.08900	1.740	76.0
0.775	0.01813	0.1450	0.00748	3.340	51.0
0.797	9.01806	0.7400	-----	-----	30.7
0.779	0.01811	-----	0.04530	2.530	63.0

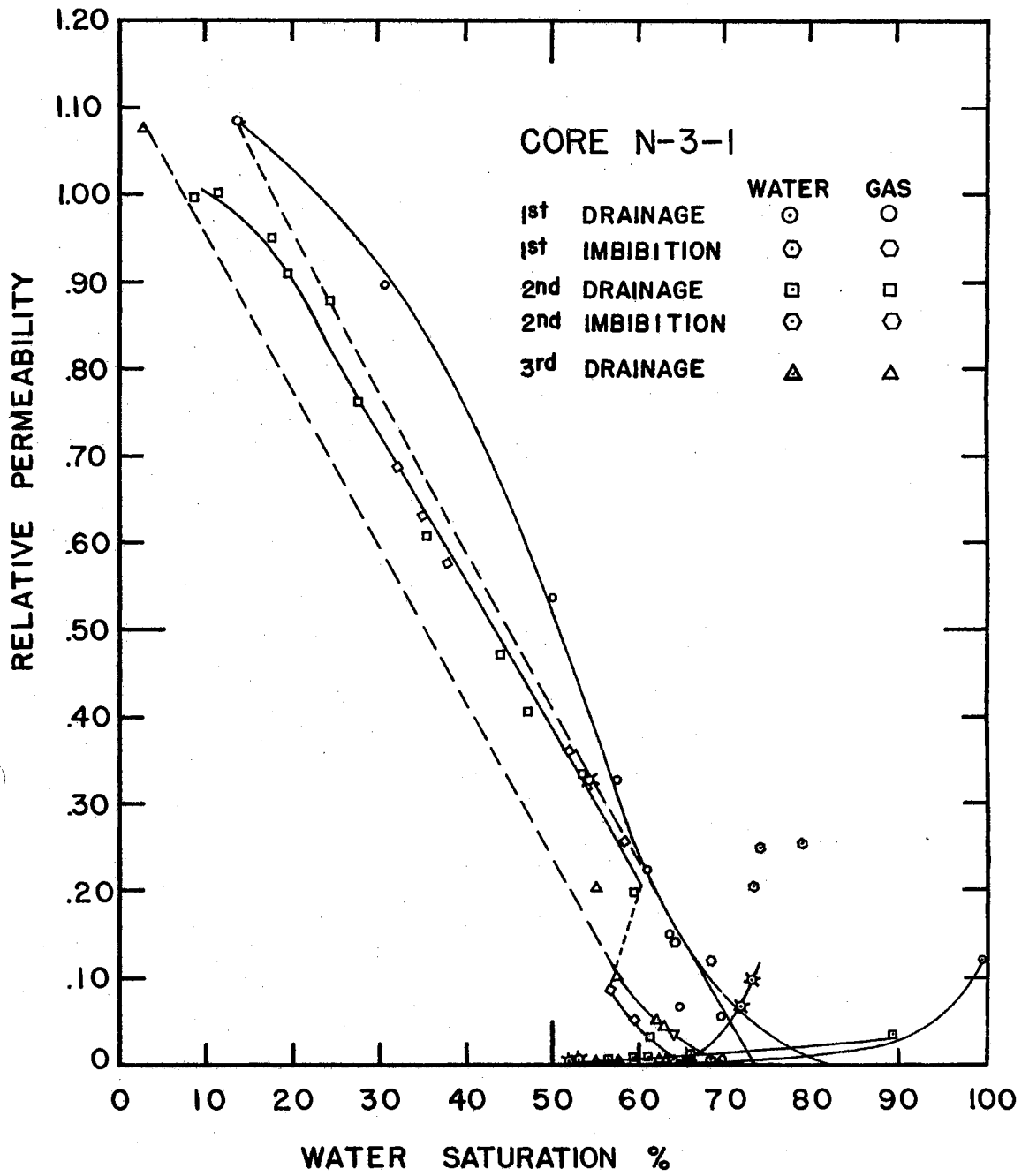


FIG. 24 RELATIVE PERMEABILITY, CORE N-3-1

TABLE XVI
RELATIVE PERMEABILITY, CORE N-3-I

IDENTIFICATION	WATER FLOW RATE CC/SEC	GAS FLOW RATE CC/SEC	DIFF. PRESSURE ATM	MEAN PRESSURE ATM	RESISTANCE AT SAT. AND TEMP., KILOHOMS	TEMPERATURE F	CARD NO.
3280000004+	2997222248+		2362500050+	1927025051+	1050000052+	8600000052+	270000+
3280000007+	1610555647+	1360870750+	5625000050+	6427950051+	4100000052+	8700000052+	330000+
3290000002+		6704163850+	9562500050+	6682988251+	5780000052+	8000000052+	390000+
3290000003+		1069183851+	1012500051+	7240113251+	6170000052+	8050000052+	410000+
3300000001+		3476822051+	2242000051+	7964873751+	7800000052+	7300000052+	450000+
3300000002+		6600262951+	2572400051+	7257223751+	1130000053+	6900000052+	470000+
3300000003+		1086360452+	2537000051+	8297523751+	3600000053+	7000000052+	490000+
3300000004+		1232177752+	2383600051+	8591123751+	2500000054+	7000000052+	510000+
3300000007+	1610555647+	9016955350+	1392400051+	5133123751+	3300000052+	7900000052+	570000+
3300000008+	3411111147+	8248624750+	1498600051+	5662323751+	3000000052+	7500000052+	590000+
4020000001+	6493055648+		3346875050+	6164817551+	2400000052+	7800000052+	610000+
4030000002+	6493055648+		2503125050+	4165330051+	1850000052+	8300000052+	650000+
4040000001+	2994444448+		1189440051+	4936526651+	1380000052+	8000000052+	10000+
4040000002+	1602777848+	3007464849+	1040760051+	4862186651+	3020000052+	8000000052+	30000+
4040000003+	6827777847+	1313110150+	9982800050+	4840946651+	3700000052+	8100000052+	50000+
4040000004+	3697222247+	2002120350+	8708400050+	4459851651+	3980000052+	8100000052+	70000+
4040000005+	1610555647+	3971618350+	9770400050+	4386001651+	4550000052+	8100000052+	90000+
4050000001+		1931068351+	2039040051+	6123289751+	4220000052+	7700000052+	110000+
4050000002+		2106179051+	1755840051+	5537364751+	4800000052+	7700000052+	130000+
4050000003+		4391800251+	2775360051+	6554924751+	5700000052+	7450000052+	150000+
4050000004+		4533719651+	2662080051+	6053959751+	6420000052+	7500000052+	170000+
4050000005+		4877202451+	2548800051+	5616469751+	7780000052+	7550000052+	190000+
4050000006+		5067045351+	2265600051+	5411394751+	1000000053+	7550000052+	210000+
4050000007+		5408975351+	1982400051+	5079369751+	1400000053+	7600000052+	230000+
4050000008+		5454593451+	1897440051+	5036889751+	1640000053+	7600000052+	250000+
4050000009+		5490882751+	1840800051+	5008569751+	1710000053+	7650000052+	270000+
4060000001+		8725523251+	2676240051+	7148599251+	2250000053+	7350000052+	290000+
4060000002+		9203311751+	2543136051+	6942402251+	3320000053+	7300000052+	310000+
4060000003+		9461642451+	2265600051+	6752854251+	4580000053+	7250000052+	330000+
4060000004+		1129515252+	2605440051+	7798729251+	6550000053+	7250000052+	350000+
4060000005+		1138496652+	2520480051+	7737206751+	7750000053+	7200000052+	370000+
4060000006+		1135693752+	2398704051+	7682666251+	1540000054+	7200000052+	390000+
4060000007+		1134427852+	2407200051+	7636134251+	2300000054+	7050000052+	410000+
4090000004+	1603166748+		1784160051+	7689085051+	1880000052+	8100000052+	530000+
4100000001+	2994444448+		4927500050+	2810813451+	1480000052+	7600000052+	550000+
4110000002+	1603055648+	3320643050+	2124000051+	5590284251+	4550000052+	7400000052+	610000+
4110000003+	6827777847+	3584231550+	1879740051+	5214254251+	4800000052+	7450000052+	630000+
4110000004+	3697222247+	3836088150+	1667340051+	4885891751+	5050000052+	7450000052+	650000+
4160000002+		1247697052+	2449680051+	8324651251+		7650000052+	830000+
4160000004+		7698057450+	1535625050+	7208330051+		8350000052+	870000+

IDENTIFICATION	WATER VISCOSITY CP	GAS VISCOSITY CP	WATER RELATIVE PERM EABILITY	GAS RELATIVE PERM EABILITY	RESISTANCE RATIO	AREA CM	SATURATION, PER CENT
3280000004+	7974488950+	1806271449+	1191961850+		1013695651+	506708665	100.0+
3280000007+	7881070250+	1813262249+	2658586348+	5168533649+	4004265851+	506708665	70.0+
3290000002+	8574864150+	1796076449+		1483577850+	5190839751+	506708665	63.5+
3290000003+	8522069150+	1797881849+		2236818950+	5575718451+	506708665	61.0+
3300000001+	9373351950+	1779804949+		3251858450+	6392007251+	506708665	57.5+
3300000002+	9885035350+	1769012649+		5347687350+	8752806451+	506708665	50.0+
3300000003+	9752969750+	1772578849+		8942755650+	2828917852+	506708665	30.5+
3300000004+	9752969750+	1772872449+		1079766351+	1964526353+	506708665	13.5+
3300000007+	8682057650+	1792022649+	1183168848+	1367262050+	2926582951+	506708665	64.3+
3300000008+	9133323150+	1782525749+	2449352648+	1155963150+	2525819551+	506708665	68.3+
4020000001+	8791438750+	1790551249+	2009472050+		2101481851+	506708665	73.2+
4030000002+	8265831650+	1801043649+	2526187050+		1723731551+	506708665	79.0+
4040000001+	8574864150+	1794329949+	2543392249+		1239335451+	506708665	89.5+
4040000002+	8574864150+	1794255649+	1555830749+	6108669648+	2712168851+	506708665	66.5+
4040000003+	8469799350+	1796732749+	6825154648+	2784483149+	3364391651+	506708665	61.3+
4040000004+	8469799350+	1796351749+	4236650848+	4865814449+	3618994251+	506708665	59.7+
4040000005+	8469799350+	1796277849+	1644935448+	8602823549+	4137292351+	506708665	56.6+
4050000001+	8903067850+	1788007449+		1995049150+	3647732451+	506708665	59.5+
4050000002+	8903067850+	1787421549+		2526095050+	4149079551+	506708665	56.5+
4050000003+	9192392650+	1782164549+		3322641150+	4767063351+	506708665	53.5+
4050000004+	9133323150+	1782917449+		3577479550+	5405253751+	506708665	52.0+
4050000005+	9074864350+	1783735549+		4021405250+	6593960551+	506708665	47.3+
4050000006+	9074864350+	1783530449+		4699638450+	8475527651+	506708665	44.0+
4050000007+	9017007650+	1784455845+		5736432650+	1194432052+	506708665	37.7+
4050000008+	9017007650+	1784413349+		6043689650+	1399191752+	506708665	35.5+
4050000009+	8959744850+	1785638049+		6275399250+	1468511552+	506708665	35.0+
4060000001+	9312398150+	1780243449+		6838457650+	1856477352+	506708665	31.8+
4060000002+	9373351950+	1778782449+		7584199350+	2720700552+	506708665	27.5+
4060000003+	9434951550+	1777333849+		8745097750+	3727548352+	506708665	24.3+
4060000004+	9434951550+	1778379649+		9083387650+	5330882452+	506708665	19.4+
4060000005+	9497206650+	1777060849+		9457212450+	6264032452+	506708665	17.5+
4060000006+	9497206650+	1777006349+		9912561350+	1244723853+	506708665	11.3+
4060000007+	9687998050+	1773179849+		9845319750+	1820273953+	506708665	8.6+
4090000004+	8469799350+	1799580949+	8966652948+		1709474651+	506708665	66.0+
4100000001+	9017007650+	1782187249+	6456013449+		1262685251+	506708665	71.8+
4100000002+	9017007650+	1782257449+	6283852949+		1262685251+	506708665	71.8+
4110000003+	9192392650+	1780823949+	3933892748+	4000659649+	4014369151+	506708665	63.0+
4110000004+	9192392650+	1780495549+	2401553848+	4826337149+	4223450851+	506708665	62.0+
4160000002+	8959744850+	1788954149+		1073522951+		506708665	2.8+
4160000004+	8216084050+	1805332949+		1066266251+		506708665	2.9+

of the relative permeability was unknown to the experimenters at the time, steps were taken to prevent its recurrence. The action taken was to test without interruption for any significant period of time except when the core was at residual water saturation or trapped gas saturation. It was later found that significant changes in permeability also occurred when testing was stopped at the trapped gas saturation. This change of permeability at the residual gas saturation occurred in the testing of Core AL-1-13 (Fig. 18).

Reference to Fig. 24 indicates that Core N-3-1, from the St. Peter formation, was highly reactive to water from this same formation. This reactivity is indicated by the water permeability of only 7 millidarcys as compared to a Klinkenberg permeability of 60 millidarcys. The trapped gas saturation for two different imbibition cycles was 27 and 30 per cent respectively. This volume of residual gas would amount to approximately one-third of the maximum gas saturation of 90 per cent as compared to the 50 per cent theoretical value.

CHAPTER VII

PREDICTED RESERVOIR PERFORMANCE

From an engineering point of view, the importance of theory and experimental work of the type presented bears a direct relationship to its utility in understanding and predicting the behavior of physical processes. In summarizing, therefore, it is desirable to demonstrate the utility of the work that has been presented.

The experimental relative permeabilities that have been presented may be combined with the theory given in Chapter III in order to predict reservoir behavior. The necessary calculations for this predicted behavior of a reservoir undergoing cyclic, two-phase flow are performed by using the computer programs described in Appendix B.

The experimental values of permeability must be curve-fitted, tabulated at intervals of one per cent gas saturation, and converted to values of gas fractional flow at each per cent of gas saturation. The fractional flow data is then similar to Fig. 2. The fractional flow values may then be used with the equations of Chapter III to calculate the saturation-radius characteristics, the saturation at the gas-water front, the produced volumes of water, and the producing water-gas ratio.

Example Problem

An example problem of injection, withdrawal, and re-injection into a radial single-well gas storage reservoir has been worked to illustrate

the method of analysis that has been presented. It is assumed that a fluid volume, equivalent to one-tenth of the maximum injected gas volume, is injected or withdrawn during each time increment.

The curve-fitted drainage curves and theoretical imbibition curve for Core N-3-1 are presented in Fig. 25. For this example, the critical gas saturation has been assumed to be 15 per cent ($S_{gc} = .15$), and the maximum gas saturation has been assumed to be 77 per cent ($S_{wr} = .23$). The corresponding drainage and imbibition gas fractional flow curves appear similar to Fig. 2. The saturation distribution for injection and withdrawal with hysteresis being neglected is similar to Fig. 1.

Reference to Fig. 26 for the non-hysteresis case shows the fraction of gas in place, $G/G_{i,max}$, the cumulative gas production, $G_p/G_{i,max}$ and cumulative water production, $W_p/G_{i,max}$. Of particular importance is the rapid decrease in gas production and rapid increase in water production after breakthrough. Even after the cumulative water production has reached 105 per cent of the initial gas injected, the gas recovered is only 44.5 per cent of the initial gas injected. The cumulative fraction of gas produced as a function of the fraction of water produced, Fig. 27, also illustrates the large water production required to recover a small volume of gas after breakthrough has occurred.

Figure 28 presents the injection-production performance for the case where the maximum theoretical hysteresis of the gas relative permeability characteristic is considered. The theory of Naar and Henderson⁽⁴²⁾ was used to obtain this imbibition gas permeability curve which is shown in Fig. 25.

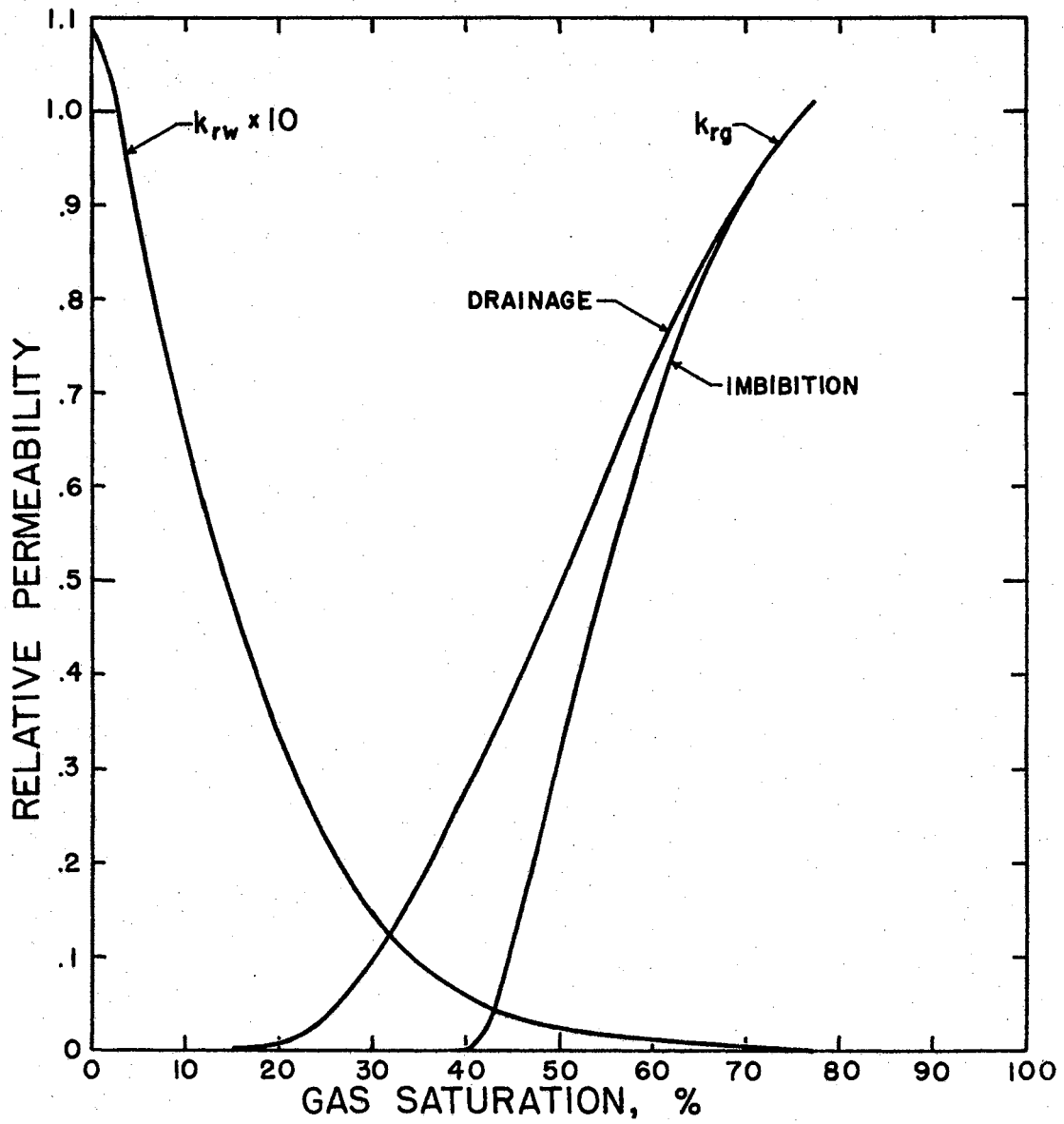


FIG. 25 RELATIVE PERMEABILITY, CORE N-3-1,
CURVE FITTED

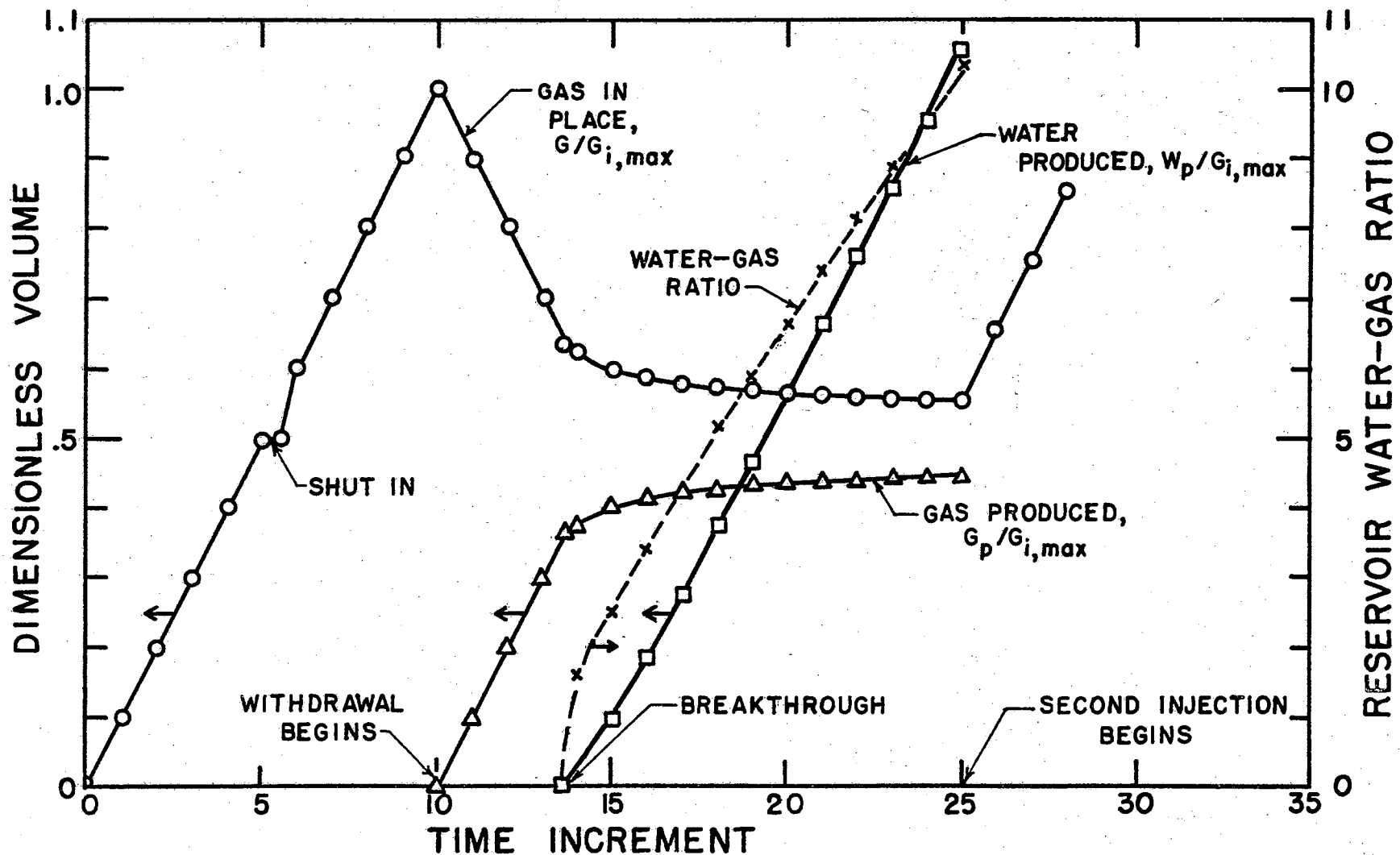


FIG. 26 INJECTION-PRODUCTION PERFORMANCE w/o HYSTERESIS

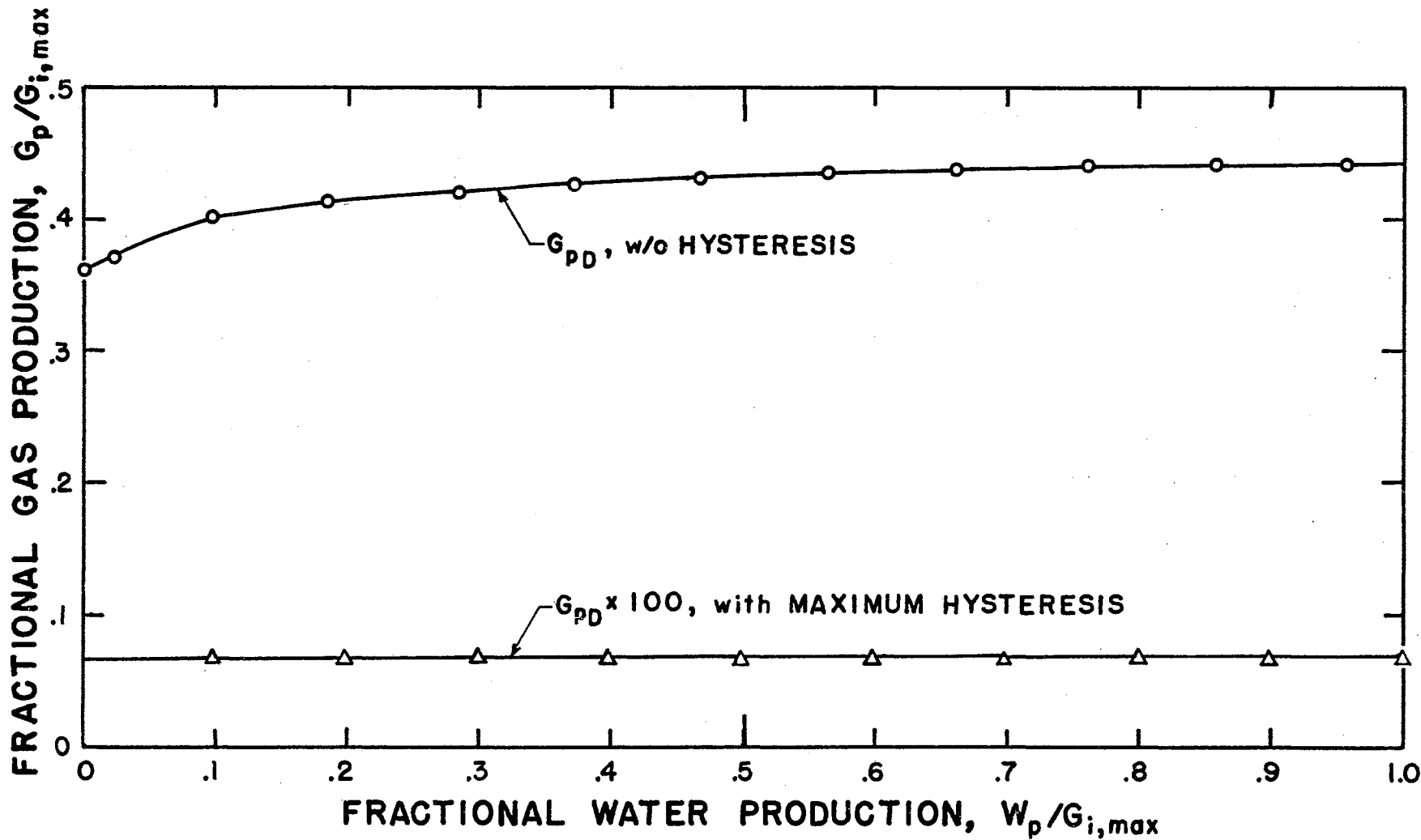


FIG. 27 GAS-WATER PRODUCTION

For the imbibition case breakthrough occurs almost immediately upon initiation of withdrawal and the gas recovery after water production of $1.05 G_{i, \max}$ is 0.0675 per cent of the initial volume of gas injected, $G_{i, \max}$. This volume of gas recovered is obviously an unrealistically low value.

It is worthwhile to consider the factors that affect the maximum recoverable gas volume. First, it is physically impossible to reduce the gas saturation below the critical gas saturation, S_{gc} , for the non-hysteresis case. In this example problem $S_{gc} = .15$ and the average saturation for injection was $\bar{S}_f = .23$. Therefore, a rough estimate of the fraction of residual gas is $G_{rd} = .15/.23 = 0.65$. Next, since there is a saturation distribution in the reservoir, the average gas saturation of the reservoir at breakthrough will be greater than S_{gc} . Yet, the saturation at breakthrough can not be greater than the saturation having the maximum fractional flow derivative, S_{md} , which for this example problem was $S_{md} = .20$. One can, therefore, estimate the loss of gas by having only the relative permeability characteristics and the fractional flow function.

Now consider the reason why the maximum hysteresis case resulted in essentially all of the gas being trapped. First, the maximum gas saturation is 77 per cent and the residual gas saturation, S_{gr} , must then be, by the Naar-Henderson imbibition theory, 38.5 per cent. This value of residual gas saturation means that the gas is immobile for any gas saturation equal to or less than 38.5 per cent. Because of the average saturation of 23 per cent and because of the nature of the fractional flow derivative for this core, which causes all saturations greater than 30 per cent to lie at dimensionless radii of less than

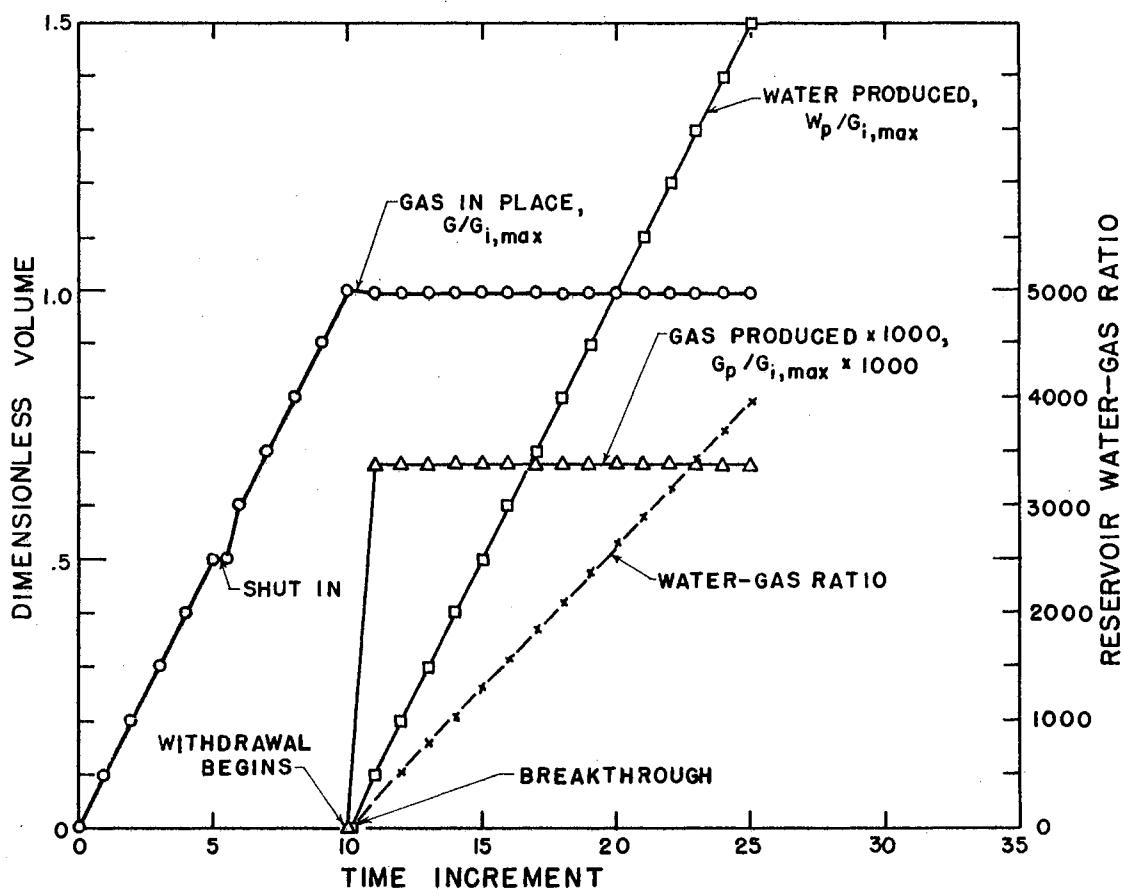


FIG. 28 INJECTION-PRODUCTION PERFORMANCE with HYSTERESIS

0.02, it can be stated that essentially all of the gas is immobile and very little, therefore, is produced.

It is possible to calculate theoretical imbibition curves originating from saturations other than the maximum gas saturation, but there is no theoretical or physical basis for doing this.

It is noted that much of the valuable information regarding the reservoir performance during cyclic operation is dependent on relative permeability values near to the critical gas saturation, S_{gc} , at which gas first starts to flow. It is unfortunate that the region near the critical gas saturation is the most difficult portion of the gas relative permeability curve to obtain accurately. Nevertheless, even with the present experimental techniques and equipment, the gas storage engineer has available to him, in the method that has been presented, a valuable tool to aid him in predicting the behavior of gas storage reservoirs.

CHAPTER VIII

SUMMARY AND CONCLUSIONS

The commercial utilization of virgin aquifers for natural gas storage is increasing steadily. A majority of these ventures have been undertaken at a high capital expenditure and with little original thought given to the actual mechanics of flow of the gas and water within the storage reservoir. Consequently, problems have developed concerning the pressure behavior of these reservoirs, the efficiency of displacement of water by gas and of gas by water, and the production of water during gas withdrawal. These problems facing the gas storage industry have presented the engineering profession with an enormous challenge. The writer of this dissertation has accepted this engineering challenge, and he has applied the two-phase-flow-in-porous-media concepts to the movement of gas and water within the storage region of gas storage aquifers.

In this dissertation, the writer has extended the two-phase flow theory in order to describe the cyclic, injection-withdrawal process to which gas storage reservoirs are subjected. Theoretical relationships for two-phase flow in a radial gas storage reservoir have been derived in detail from fundamental engineering concepts. The equations that have been developed were combined with experimental data to reveal important features of the gas storage process with regard to water pro-

duction and gas recovery. Computer programs are presented to facilitate the combining of theory and experimental data so that rapid, accurate comparisons of the effect of different operating conditions can be made.

An example gas storage problem for a hypothetical reservoir has been solved by using the theory, the experimental data and the computer programs that are presented in this dissertation. The behavior of this hypothetical reservoir shows that a significant volume of the injected gas cannot be recovered economically by present methods of production. The quantity of gas lost is in terms of the pore volume of the reservoir. Therefore, since gas density is pressure dependent, the application of gas production rates and methods that would reduce the gas zone pressure below the initial formation pressure, would reduce the mass of gas lost in the reservoir.

A significant improvement in the solution of the Two-Phase Gas Zone, Unsteady Aquifer Model ⁽⁶⁶⁾ for gas storage has been developed in this dissertation. The solution time for the model has been reduced by a factor of two. With this gas storage model the gas storage engineer can predict the well-bore pressures and gas zone radii that would be expected during the initial development of a gas storage field.

In the course of the work for this dissertation, experimental gas-water relative permeability tests were made on four natural sandstone cores and on two artificial cores. The result of the drainage and imbibition relative permeability tests showed that a significant volume of gas is physically trapped in a porous medium subjected to cyclic two-phase fluid flow. The volume of trapped gas amounted to 35 per cent of the pore volume in some cases.

Numerous experimental problems were encountered during experimental testing of the relative permeability of the cores. Among these problems were adequate mixing of the gas and water phases, determination of accurate water saturations, and establishment of a unique trapped gas saturation. Definite suggestions have been made in this dissertation for refining the test procedure to minimize these problems.

It is concluded that the mathematical methods and experimental information that have been presented in this study can serve as a valuable tool in giving the gas storage engineer greater insight into the operation and behavior of gas storage fields that have been developed, or are to be developed, in aquifers. Also, it is believed that this dissertation has made a significant contribution to the theory of two-phase flow in porous media.

CHAPTER IX

RECOMMENDATIONS FOR FUTURE STUDY

Many avenues are available for future study in the area of cyclic two-phase flow in porous media in both the experimental and the theoretical phases.

Two significant problems in the experimental phase are the obtaining of precise saturation measurements under flowing conditions and the uniform mixing of the gas and water phases at the core inlet. Automation of the experimental apparatus to the extent that the gas and water permeabilities could be directly recorded would provide for instantaneous recognition of many of the experimental difficulties that will occur. Such records would also permit a more detailed study of the drainage and imbibition relative permeability characteristics.

There is a need for experimental validation of the Naar-Henderson (42) imbibition theory and for the determination of imbibition gas permeability characteristics originating from initial gas saturations that are less than the maximum. That is, internal branches of the non-wetting phase imbibition relative permeability need to be determined to allow a more adequate theoretical description of the cyclic performance of a reservoir. There is also a need for checking for correlations between the trapped gas saturations and the pressure at which it is measured in order to determine the effects of low pressure gas

diffusion. Absolute permeability is a possible factor in a correlation of this type.

In the theoretical phase of describing the gas storage process, one could combine the Two-Phase Gas Zone, Unsteady Aquifer Model with the cyclic two-phase flow model to determine both the pressure and two-phase behavior of a reservoir undergoing cyclic operation. The accomplishment of such a combined model is dependent upon the availability of high speed computing facilities with adequate storage capacity (approximately 4000 words). It should also be of great interest to extend the present work to a multi-well system and to solve numerically the exact form of the differential equation for cyclic two-phase flow (Equation 18) in order that actual storage field conditions could be described more accurately. By including capillary and gravity effects and using a procedure similar to Sheffield and Brinkman⁽⁶¹⁾, one could possibly remove the necessity of having the many frontal equations needed to cover the different possible cases that arise.

The correlations between model performance and field performance might be improved by using the conical model of Welge, et al⁽⁶³⁾. Those persons desiring to develop a highly sophisticated mathematical model could solve the gas storage problems mentioned above and also include the effects of gas going into solution in the water and of the dry injected gas becoming water saturated as it travels through the porous medium.

The ultimate objective of these developments would be the adequate description of all phases of the behavior of a gas storage reservoir under any set of proposed operating conditions. The accomplishment of this objective would permit optimum development and operation of the reservoir.

BIBLIOGRAPHY

1. Baker, H. J. A Summary of Research of Two-Phase, Immiscible Fluid Flow in Porous Media, Master of Science Report, Oklahoma State University, Stillwater, Oklahoma (May, 1962).
2. Betz, H., P. B. Burcham, and G. M. Ewing. Differential Equations With Applications. Harper and Brothers, New York (1954).
3. Bizal, R. B. "Gas Storage Capacity Spurts," Oil and Gas Journal, (May 14, 1962), Vol. 60, No. 20, 125.
4. Buckley, S. E. and M. C. Leverett. "Mechanism of Fluid Displacement in Sands," Trans. AIME (1942) 146, 107.
5. Burdine, N. T. "Relative Permeability Calculations From Pore Size Distribution Data," Trans. AIME (1953) 198, 71.
6. Cardwell, W. T., Jr. "The Meaning of the Triple Value in Non-capillary Buckley-Leverett Theory," Trans. AIME (1959) 216, 271.
- ✓ 7. Collins, R. E. Flow of Fluids Through Porous Materials, Reinhold Publishing Corporation, New York, (1961).
8. Comer, A. G., E. G. Woods, E. W. Adams, and H. J. Baker. "Final Report on Gas Storage Project No. 2," Report to Northern Natural Gas Company (October 15, 1962).
- ✓ 9. Corey, A. T. "The Interrelation Between Gas and Oil Relative Permeabilities," Producers Monthly (1954) 19, No. 1, 38.
10. Coats, K. H., M. R. Tek, and D. L. Katz. "Method for Predicting the Behavior of Mutually Interfering Gas Storage Reservoirs," Trans. AIME (1959) 216, 247.
11. Coats, K. H., M. R. Tek, and D. L. Katz. "Unsteady State Liquid Flow Through Porous Media Having Elliptical Boundaries," Trans. AIME (1959), 216, 460.
12. Cornell, D. "Computer Application to a Gas-storage Aquifer," Oil and Gas Journal, (November 2, 1959), 57, No. 45, 72.

13. Cornell, D., E. G. Woods, H. J. Baker, and A. G. Comer. "Fluid Mechanics of Gas Storage Aquifers -- Final Report," Northern Natural Gas Company, Gas Storage Project No. 1, Oklahoma State University (September 1960).
14. Dietz, D. N. "A Theoretical Approach to the Problem of Encroaching and Bypassing Edgewater," Koninkl, Ned, Akad Wetenschap., Proc. (1953) B256, 83.
15. Douglas, J., Jr., P. M. Blair, and R. J. Wagner. "Calculation of Linear Waterflood Behavior Including the Effects of Capillary Pressure," Trans. AIME (1958) 213, 96.
- ✓ 16. Downie, J. and F. E. Crane. "Effect of Viscosity on Relative Permeability," SPE Journal (June, 1961) 1, No. 2, 59.
17. Erickson, A. R. and R. F. Svoboda. "Geological Report Redfield Gas Storage Field Northern Natural Gas Co.," Presented at Chicago before A.A.P.G. (April 23, 1956).
- ✓ 18. Fatt, I. and H. Dykstra. "Relative Permeability Studies," Trans. AIME (1951) 192, 249.
19. Fayers, F. L. and J. W. Sheldon. "The Effect of Capillary Pressure and Gravity on Two-Phase Fluid Flow in a Porous Medium," Trans. AIME (1959) 216, 147.
- ✓ 20. Frick, T. C., ed. Petroleum Production Handbook: Vol. II, Reservoir Engineering, McGraw-Hill Book Company, Inc., New York (1962).
21. Gardner, G. H. F., J. Downie, and M. R. J. Wyllie. "Problems in the Recovery of Gas from Aquifers Used for Gas Storage," Journal of the Institute of Petroleum (Jan. 1962), 48, No. 457, 1.
22. Gardner, G. H. F., J. H. Messner and W. Woodside. "Effective Porosity and Gas Relative Permeability on the Liquid Imbibition Cycle," Theory of Flow in Porous Media Conference Proceedings, University of Oklahoma, Norman, Oklahoma, (C. G. Dodd, ed), (1959).
23. Geffen, T. M., W. W. Owens, D. R. Parrish, and R. A. Morse. "Experimental Investigation of Factors Affecting Relative Permeability Measurements," Trans. AIME (1951) 192, 99.
24. Geffen, T. M., D. R. Parrish, G. W. Haynes, and R. A. Morse. "Efficiency of Gas Displacement from Porous Media by Liquid Flooding," Trans. AIME (1952) 195, 29.
- ✓ 25. Hawthorne, R. G. "Two-Phase Flow in Two-Dimensional Systems -- Effects of Rate, Viscosity and Density on Fluid Displacement in Porous Media," Trans. AIME (1960) 219, 81.

26. Hovanessian, S. A. and F. J. Fayers. "Linear Water Flood With Gravity and Capillary Effects," SPE Journal (March, 1961) 1, No. 1, 32.
27. Johnston, E. F., D. P. Bossler, and V. O. Naumann. "Calculation of Relative Permeability From Displacement Experiments," Trans. AIME (1959) 216, 370.
28. Katz, D. L. et al. Handbook of Natural Gas Engineering, McGraw-Hill, New York (1959), 413.
29. Katz, D. L., M. R. Tek, and S. C. Jones. "A Generalized Model For Predicting the Performance of Gas Reservoirs Subject to Water Drive," SPE Paper 428, 37th Annual Fall Meeting of SPE of AIME, Los Angeles, (October 7-10, 1962).
30. Katz, D. L., M. R. Tek, and K. H. Coats. "Effect of Unsteady-State Aquifer Motion on the Size of an Adjacent Gas Storage Reservoir," Trans. AIME (1959) 216, 18.
31. Kruger, W. D., The Effect of Saturation History on the Residual Gas Content of Cores after Water Flooding. M. S. Thesis. Texas A&M (August, 1954).
32. Kyte, J. R. and L. A. Rapoport. "Linear Waterflood Behavior and End Effects in Water-wet Porous Media," Trans. AIME (1958) 213, 423.
33. Kyte, J. R., V. O. Naumann, and C. C. Mattax. "Effect of Reservoir Environment on Water-Oil Displacements," Journal of Petroleum Technology (June, 1961) 13, No. 6, 579.
34. Lee, E. H. and F. J. Fayers. "The Use of the Method of Characteristics in Determining Boundary Conditions for Problems in Reservoir Analysis," Trans. AIME (1959) 216, 284.
35. Leverett, M. D. "Capillary Behavior in Porous Solids," Trans. AIME (1941) 142, 152.
36. Levine, J. S. "Displacement Experiments in a Consolidated Porous Media," Trans. AIME (1954) 201, 57.
37. Martinson, E. V. "Review of Aquifer Gas Storage Projects," Presented at Transmission Conference, American Gas Assoc., Denver, Colorado, (May 25, 27, 1961).
38. Masse, L. "On the Displacement of Immiscible Fluids," Theory of Fluid Flow in Porous Media Conference Proceedings, University of Oklahoma, Norman, Oklahoma (C. G. Dodd, ed.), (1959) 131.
39. McEwen, C. R. "A Numerical Solution of the Linear Displacement Equation With Capillary Pressure," Trans. AIME (1959) 216, 412.

40. Morse, R. A., P. L. Terwilliger, and S. T. Yuster. "Relative Permeability Measurements on Small Core Samples," Oil and Gas Journal (August 23, 1947) 109.
41. Muskat, M. The Flow of Homogeneous Fluids Through Porous Media, McGraw-Hill Book Company, Inc., New York (1937).
42. Naar, J. and J. H. Henderson. "An Imbibition Model -- Its Application to Flow Behavior and the Prediction of Oil Recovery," SPE Journal (June, 1961) 1, No. 2, 61.
43. Naar, J., R. J. Wygal and J. H. Henderson. "Imbibition Relative Permeability in Unconsolidated Porous Media," SPE Journal (March, 1962), 2, No. 1, 13.
- ✓✓ 44. Odeh, A. S. "Effect of Viscosity Ratio on Relative Permeability," Trans. AIME (1959) 216, 346.
45. Osoba, J. S., J. G. Richardson, J. K. Kerver, J. A. Hafford, and P. M. Blair. "Laboratory Measurements of Relative Permeability," Trans. AIME (1951) 192, 47.
46. Owens, W. W., D. R. Parrish, and W. E. Lamoreaux. "An Evaluation of a Gas Drive Method for Determining Relative Permeability Relationships," Trans. AIME (1956) 207, 275.
47. Patnode, H. W. and M. R. J. Wyllie. "The Presence of Conductive Solids in Reservoir Rocks as a Factor in Electric Log Interpretation," Trans. AIME (1950) 189, 47.
48. Pirson, S. J. Oil Reservoir Engineering, McGraw-Hill Book Company, Inc., New York (1958).
49. Rapoport, L. A. and W. J. Leas. "Relative Permeability to Liquid in Liquid-Gas Systems," Trans. AIME (1951) 192, 83.
50. Rapoport, L. A. and W. J. Leas. "Properties of Linear Waterfloods," Trans. AIME (1953) 198, 139.
51. Ribe, K. H. "Production Behavior of a Water-Blocked Oil Well," Trans. AIME (1960) 219, 1.
52. Richardson, J. G., J. K. Kerver, J. A. Hafford, and J. S. Osoba. "Laboratory Determination of Relative Permeability," Trans. AIME (1952) 195, 187.
53. Richardson, J. G. and F. M. Perkins, Jr. "A Laboratory Investigation of the Effect of Rate on Recovery of Oil by Water Flooding," Trans. AIME (1957) 210, 114.
54. Rose, W. "Theoretical Generalizations Leading to the Evaluation of Relative Permeability," Trans. AIME (1949) 186, 111.

55. Root, P. J. and J. C. Calhoun, Jr. "Displacement of Gas by Water from Unconsolidated Sands," Producers Monthly (August 1954) 18, No. 10, 18.
56. Rzepczynski, W. M., D. L. Katz, M. R. Tek, and K. H. Coats. "How the Mount Simon Gas-Storage Project was Developed," Oil and Gas Journal (1961) 59, no. 25, 86.
57. Salvadori, M. G. and M. L. Baron. Numerical Methods in Engineering. Prentice-Hall, Inc. Englewood Cliffs, N.J. (1952).
58. Sandberg, C. R. and L. S. Gournay. "The Effect of Fluid-Flow Rate and Viscosity on Laboratory Determinations of Oil-Water Relative Permeabilities," Trans. AIME (1958) 213, 36.
59. Scheidegger, A. E. The Physics of Flow Through Porous Media. The Macmillan Company, New York (1960).
60. Sheldon, J. W., B. Zondek, and W. T. Cardwell. "One Dimensional, Incompressible, Non-capillary, Two-phase Fluid Flow in a Porous Medium," Trans. AIME (1959) 216, 290.
61. Sheffield, M. and F. H. Brinkman. "Improvement of Reservoir Studies Through Use of Two-Dimensional Mathematical Analysis," SPE Paper 416, 37th Annual Fall Meeting of SPE of AIME, Los Angeles (October 7-10, 1962).
62. Snedecor, G. W. and W. G. Cochran. Statistical Methods Applied to Experiments in Agriculture and Biology. Iowa State College Press, Ames (1956) 122.
63. Welge, H. J. "A Simplified Method for Computing Oil Recovery by Gas or Water Drive," Trans. AIME (1952) 195, 91.
64. Wegle, H. J., E. F. Johnson, A. L. Hicks, and F. H. Brinkman. "An Analysis for Predicting the Performance of Cone-Shaped Reservoirs Receiving Gas or Water Injection," Jour. Pet. Tech. (August, 1962) XIV, No. 8, 894.
65. West, W. J., W. W. Garvin, and J. W. Sheldon. "Solution of the Equations of Unsteady State Two-Phase Flow in Oil Reservoirs," Trans. AIME (1954) 201, 217.
66. Woods, E. G. and A. G. Comer. "Saturation Distribution and Injection Pressure for a Radial Gas Storage Reservoir," Jour. Pet. Tech. (Dec. 1962) XIV, No. 12, 1389.
67. Wyllie, M. R. J. and M. B. Spangler. "Application of Electrical Resistivity Measurements to the Problem of Fluid Flow in Porous Media," Bulletin of American Association of Petroleum Geologists (February, 1952) 36, No. 2, 359.

68. Van Everdingen, A. F., and W. Hurst, "The Application of the Laplace Transformation to Flow Problems in Reservoirs," Trans., AIME (1949) 186, 305.
69. Yoo, H. D., D. L. Katz, and M. R. Tek. "Study of Gas Reservoirs Subject to Water Drive on Electronic Differential Analyzer," Trans. AIME (1961) 222, II-287.

APPENDIX A

DERIVATION OF EQUATIONS

Material Balance

Equation (1) may be derived in the following manner (7). Let $\bar{\rho}\bar{u}$ be the mass flux across the surface of a unit volume and let the mass concentration within the volume be $\phi\rho S$. Then for material balance the integral of the mass flux over surface of the volume plus the time rate of change of the integral of the mass concentration over the volume must be zero as is stated in Equation (A-1).

$$\iint_A \bar{\rho}\bar{u} \cdot d\bar{A} + \frac{d}{dt} \iiint_V \phi\rho S dV = 0 \quad (\text{A-1})$$

The surface integral may be transformed to a volume integral by the divergence theorem, and by noting that the limits of the volume integral are not functions of time, one may differentiate under the integral sign. The result is Equation (A-2).

$$\iiint_V (\nabla \cdot \bar{\rho}\bar{u} + \phi \frac{\partial(\rho S)}{\partial t}) dV = 0 \quad (\text{A-2})$$

Since Equation (A-2) must hold for any arbitrary volume, the integrand must be zero. Therefore the continuity equation for two-phase is obtained.

$$\nabla \cdot (\bar{\rho}\bar{u}_i) + \phi \frac{\partial(\rho S)}{\partial t} = 0, \quad i = g, w \quad (\text{A-3})$$

For incompressible flow for which ρ is constant, Equation (A-3) takes the form of Equation (5).

$$\nabla \cdot \bar{u}_i + \phi \frac{\partial S_i}{\partial t} = 0 \quad (5)$$

Fractional Flow

The fractional flow function may be derived in terms of the relative permeability characteristics by using Darcy's equation

$$\bar{u}_i = -\frac{k k_{ri}}{\mu_i} \nabla (p_i + \rho_i g z) \quad (A-4)$$

for each phase and by use of the capillary pressure relationship

$$P_c = p_g - p_w \quad (A-5)$$

These equations are combined to eliminate the pressure term in the following manner. Let the fractional flow be defined as

$$f_i = \frac{\bar{u}_i \cdot \bar{u}_t}{|\bar{u}_t|^2} \quad (A-6a)$$

and

$$f_j = 1 - f_i \quad (A-6b)$$

Then Equation (A-4) for the water phase may be rearranged as

$$\nabla p_w = -\frac{\bar{u}_w \mu_w}{k k_{rw}} - \bar{j} \rho_w g \quad (A-7)$$

where \bar{j} is a positive upward unit vector. Upon substituting Equations (A-5) and A-7) into Equation(A-4) the following result is obtained.

$$\bar{u}_g = -\frac{k k_{rg}}{\mu_g} \left(-\frac{\bar{u}_w \mu_w}{k k_{rw}} + \nabla P_c + \Delta \rho g \right) \quad (A-8)$$

where

$$\Delta \rho = \rho_g - \rho_w \quad (A-9)$$

By then substituting Equation (A-6) for each fluid into Equation(A-8), Equation (A-10) is obtained,

$$f_g = \left[1 - \frac{k_{rw} \bar{u}_t}{|u_t|} \cdot (\nabla P_c + \bar{j} \Delta \rho g) \right] \div \left[1 + \frac{k_{rw} \mu_g}{k_{rg} \mu_w} \right] \quad (A-10)$$

Upon neglecting capillary and gravity effects as justified previously this equation becomes Equation (7)

$$f_i = 1 \div \left(1 + \frac{k_{rj} \mu_i}{k_{ri} \mu_j} \right), \quad i = g, w; \quad j = w, g. \quad (7)$$

Two-Phase Flow

The two-phase flow equation can be obtained by combining Equations (5) and (A-11) to obtain Equation (A-12).

$$\bar{u}_g = \frac{f \bar{q}_t}{A} = \frac{f \bar{q}_t}{2\pi hr} \quad (A-11)$$

$$\nabla \cdot \bar{q}_t f_g + \phi \frac{\partial S}{\partial t} = 0 \quad (A-12)$$

The two-phase flow equation as given by Equation (A-12) is independent of geometry. By recalling the general form of $\nabla \cdot \bar{B}$ where

$$\nabla \cdot \bar{B} = \frac{1}{h_1 h_2 h_3} \left[\frac{\partial (h_2 h_3 B_1)}{\partial X_1} + \frac{\partial (h_3 h_1 B_2)}{\partial X_2} + \frac{\partial (h_1 h_2 B_3)}{\partial X_3} \right]. \quad (A-13)$$

Equation (A-12) may be adapted to a particular geometry by knowing the scale factors, h_i . For a radial system $h_1 = 1$, $h_2 = r$, $h_3 = 1$. If we choose a radial system where \bar{q}_t is independent of angular position, θ , and height, z , then Equation (A-12) becomes Equation (A-14).

$$\frac{q_t}{2\pi h \phi r} \frac{\partial f_g}{\partial r} + \frac{\partial S}{\partial t} = 0 \quad (\text{A-14})$$

On neglecting capillary and gravity effects and considering flow that is non-cyclic or without permeability hysteresis, f_g becomes a function of saturation, S , only. Then Equation (A-14) takes the form of Equation (9).

$$\frac{q_t}{2\pi h \phi r} \frac{df}{dS} \frac{\partial S}{\partial r} + \frac{\partial S}{\partial t} = 0 \quad (9)$$

This equation yields to solution by the method of characteristics. If Equation (9) is compared with the total derivative of saturation as given by Equation (A-15),

$$dS = \frac{\partial S}{\partial r} dr + \frac{\partial S}{\partial t} dt \quad (\text{A-15})$$

it is seen that

$$\frac{dS}{dt} = 0 \quad (\text{A-16})$$

and

$$\frac{dr}{dt} = \frac{q_t}{2\pi h \phi r} \frac{df}{dS} \quad (\text{A-17})$$

These ordinary differential equations, Equation (A-16) and (A-17), then have the solutions

$$S = \text{constant} \quad (10)$$

along surfaces of constant radius and

$$r_{k,m} = \left[\frac{\Delta Q}{\pi h \phi} \frac{df_k}{dS} + r_{k,m-1}^2 \right]^{1/2} \quad (11)$$

where "k" designates a particular saturation and

$$\Delta Q = \int_{t_{m-1}}^{t_m} q_t dt \quad (\text{A-18})$$

is the total volume of fluid (gas) injected or fluid (gas or gas and water) withdrawn during the "m"th time interval. Consider the volume injected to be algebraically positive and volume withdrawn to be negative.

Two-Phase Flow With Hysteresis

For radial two-phase flow with relative permeability hysteresis one may begin with Equation (A-14) since no assumptions were made concerning the fractional flow function, f_g , up to this point. If capillary and gravity effects are again neglected in Equation (A-10), it reduces to Equation (7) which indicates that f_g is a function of the relative permeability ratio. In the cyclic flow case with hysteresis, relative permeability becomes a function not only of saturation, but also of direction of approach and the initial saturation at a point when the flow direction was reversed; that is $f = f(S, S_{gi})$ and by chain rule differentiation

$$\frac{\partial f}{\partial r} = \frac{\partial f}{\partial S} \frac{\partial S}{\partial r} + \frac{\partial f}{\partial S_{gi}} \frac{\partial S_{gi}}{\partial r} \quad (\text{A-19})$$

with S_{gi} indicating the initial saturation at r . However, application of Equation (11) indicates that the initial saturation distribution at the end of the initial injection period is some function of radius; that is, $S_{gi} = g(r)$. Now Equation (A-19) becomes Equation (A-20)

$$\frac{\partial f}{\partial r} = \frac{\partial f}{\partial S} \frac{\partial S}{\partial r} + \frac{\partial f}{\partial S_{gi}} \frac{\partial g}{\partial r} \quad (\text{A-20})$$

and Equation (A-14) becomes

$$\frac{q_t}{2\pi h\phi r} \left(\frac{\partial f}{\partial S} \frac{\partial S}{\partial r} + \frac{\partial f}{\partial S_{gi}} \frac{\partial g}{\partial r} \right) + \frac{\partial S}{\partial t} = 0. \quad (18)$$

Frontal Development, First Injection

The saturation at the gas-water front during injection is readily determined by a material balance procedure. Consider the volume of gas injected in relation to the saturation distribution in the reservoir as given by Equation (A-21).

$$G_i = \pi h\phi \int_0^1 (r_k^2 - r_w^2) dS \quad (A-21)$$

The radius terms may be eliminated from the equation by making use of Equation (11). The radii of $S \leq S_f$ will be given by

$$r_k^2 - r_w^2 = \frac{G_i}{\pi h\phi} f'_f, \quad \dots \quad S \leq S_f \quad (A-22)$$

with f'_f being a constant. The radii of $S \geq S_f$ is given by

$$r_k^2 - r_w^2 = \frac{G_i f'_k}{\pi h\phi}, \quad S \geq S_f. \quad (A-23)$$

Substitution of these equations into Equation (A-21) then yields

$$G_i = G_i f'_f \int_0^{S_f} dS + G_i \int_{S_f}^1 f'_k dS \quad (A-24a)$$

$$= G_i (f'_f S_f + 1 - f'_f) \quad (A-24b)$$

since

$$\int_{S_f}^1 \left(\frac{df_k}{dS} \right) dS = \int_{S_f}^1 df = 1 - f'_f. \quad (A-25)$$

On solving Equation (A-24b) for f'_f , one obtains Equation (A-26) which is equivalent to Equation (12).

$$f'_f = \frac{f_f}{S_f} \quad (A-26)$$

The saturation at the front can now be determined by simply drawing a line from the origin that is tangent to the fractional flow curve as shown in Fig. 2.

One numerical method of finding the combination that satisfies Equation (12) is to consider the function (f/S) which is the slope of a line from the origin to a point on the fractional flow curve. The maxima and minima may be investigated by setting the first derivative of function equation to zero.

$$\frac{d(f/S)}{dS} = \frac{Sf' - f}{S^2} = 0 \quad (\text{A-27a})$$

or

$$f' = \frac{f}{S} \cdot \quad (\text{A-27b})$$

Equation (A-27b) is identical to Equation (12) and reference to Fig. 2 shows that f/S is a maximum when Equation (A-27b) is satisfied. Therefore, f'_f , f_f and S_f can be determined by finding the maximum value of f/S .

Frontal Development, Withdrawal

The material balance equations for determination of the saturations at the front during withdrawal will be derived for the hysteresis case. Equation (21) for the hysteresis case then readily reduces to Equation (14) for the non-hysteresis case.

Consider the saturation distribution for withdrawal given in Fig. 1 for the non-hysteresis and hysteresis ($S_{gr} < S_f$) withdrawal cases respectively along with the general material balance given by Equation (A-28).

$$Q_p = \pi h \phi \int_0^1 (r_{j2}^2 - r_{j1}^2) ds \quad (\text{A-28})$$

The subscript 'j' designates the gas saturation and '1' and '2' designate values calculated from the drainage and imbibition fractional flow curves respectively. The saturation range is covered by the following three equations of radius.

$$r_{j2}^2 - r_{j1}^2 = \frac{Q_p f'_{j2}}{\pi h \phi}, \dots, 0 \leq j \leq S_{**} < S_f, \dots, S_* \leq j \leq 1 \quad (\text{A-29})$$

$$\begin{aligned} r_{*2}^2 - r_{f1}^2 &= (r_{*1}^2 - r_w^2) - (r_{f1}^2 - r_w^2) + (r_{*2}^2 - r_{*1}^2) \\ &= \frac{G_i (f'_{*1} - f_{f1})}{\pi h \phi} + \frac{Q_p f'_{*2}}{\pi h \phi}, \dots, S_{**} \leq j \leq S_f \end{aligned} \quad (\text{A-30})$$

$$\begin{aligned} r_{*2}^2 - r_{j1}^2 &= (r_{*1}^2 - r_w^2) - (r_{j1}^2 - r_w^2) + (r_{*2}^2 - r_{*1}^2) \\ &= \left[G_i (f'_{*1} - f'_{j1}) + Q_p f'_{*2} \right] / \pi h \phi, \dots, S_f \leq j \leq S_* \end{aligned} \quad (\text{A-31})$$

Now upon remembering that f'_{*2} , f'_{*1} and f_{f1} are constants, Equation (A-28) may be broken into four parts covering the entire saturation range and may then be integrated as was Equation (A-24a). Algebraic rearrangement of the integrated form of Equation (A-28) then yields the equation of the front for the condition that the trapped gas saturation, S_{gr} , is less than S_f . This frontal condition is determined by

$$\begin{aligned} f_{*2} &= \frac{1}{(S_* - S_{**})} \left\{ f_{*2} - f_{**2} + \frac{G_i}{Q_p} \left[f_{*1} - f'_f S_{**} - f'_{*1} (S_* - S_{**}) \right] \right\}, \\ S_{gr} &< S_f. \end{aligned} \quad (\text{21})$$

If all subscripts '2' are replaced by '1', this equation reduces to Equation (14) for the non-hysteresis case.

$$f'_* = \frac{1}{(S_* - S_{**})} \frac{G_i}{(1 + \frac{G_i}{Q_p})} \left\{ f_* - f_{**} + \frac{G_i}{Q_p} [f_* - f'_f S_{**}] \right\} \quad (14)$$

Now consider the saturation distribution depicted by Fig. 3 for the withdrawal case having hysteresis and $S_{gr} > S_f$. The same general material balance equation, Equation (A-28), holds for this case. Equation (A-29) holds for the same saturation ranges; but without the restriction of $S_{**} < S_f$, and Equation (A-31) is now valid for $S_{**} \leq j \leq S_*$. On substituting these two equations into Equation (A-28) the integral is broken into three parts, covering the saturation range. Integration of the resulting equation and rearrangement yields Equation (22).

$$f'_{*2} = \frac{1}{(S_* - S_{**})} \left\{ f_{*2} - f_{**2} + \frac{G_i}{Q_p} [f_{*1} - f_{**1} - f'_{*1} (S_* - S_{**})] \right\},$$

$$S_{gr} > S_f \quad (22)$$

Frontal Development, Injection after Withdrawal

Consider the saturation distribution in Fig. 1 for the second injection phase. The material balance for the injected gas volume is given by Equation (A-32),

$$G_{i2} = \pi h \phi \int_0^1 (r_{j2i}^2 - r_{j1w}^2) ds \quad (A-32)$$

where the subscripts 'i' and 'w' refer to the second injection and withdrawal respectively. The four saturation-radius equations covering the saturation interval are as follows:

$$r_{j2i}^2 - r_{j2w}^2 = \frac{G_{i2}}{\pi h \phi} f'_{j2}, \quad \dots \quad 0 \leq j \leq S_-, \quad S_+ \leq j \leq 1 \quad (A-33)$$

$$r_+^2 - r_{j2w}^2 = (r_{*1}^2 - r_w^2) - (r_{f1}^2 - r_w^2) + (r_{*2}^2 - r_{*1}^2) - (r_{j2w}^2 - r_{f1}^2) + (r_+^2 - r_{*2}^2) \quad (A-34a)$$

$$= \left[G_{i1} (f'_{*1} - f'_{f1}) + Q_p (f'_{*2} - f'_{j2w}) + G_{i2} f'_{+2} \right] / \pi h \phi, \dots$$

$$S_- \leq j \leq S_{**} \quad (A-34b)$$

$$r_+^2 - r_*^2 = \frac{G_{i2}}{\pi h \phi} f'_{+2}, \dots \dots S_{**} \leq j \leq S_+ \quad (A-35)$$

$$r_j^2 - r_{*2} = \frac{G_{i2}}{\pi h \phi} f'_{j2}, \dots \dots S_+ \leq j \leq S_* \quad (A-36)$$

These equations may now be substituted into Equation (A-32), thereby breaking it into the sum of five integrals covering the saturation range. Since f'_{*1} , f'_{*2} , f'_{-2} and f'_{f1} are constants, the integrated equation may be arranged as Equation (22).

$$f_{+2} = \frac{1}{(S_+ - S_-)} \left\{ f_{+2} - f_{-2} + \frac{Q_p}{G_{i2}} (f_{**2} - f_{-2}) + (S_{**} - S_-) \right. \\ \left. \left[\frac{G_{i1}}{G_{i2}} (f'_{f1} - f'_{*1}) - \frac{Q_p}{G_{i2}} f'_{*2} \right] \right\}, \dots \dots S_{gr} < S_f \quad (22)$$

G_{i1} and G_{i2} are the volumes of gas injected during the first and second injections respectively and Q_p is the algebraically negative total volume of fluid produced. Change of the subscript '2' to '1' in Equation (22) yields Equation (16) for the non-hysteresis case.

For the second injection case where $S_{gr} > S_f$ Equations (A-33), (A-35) and (A-36) hold for the same saturation ranges, and since the range from S_- to S_{**} is no longer influenced by $S < S_f$, the constant f'_f in Equation (34b) is in effect, replaced by the variable f'_j which results in Equation (A-37).

$$r_+^2 - r_{j2w} = \left[G_{i2} (f'_{*1} - f'_{j1}) + Q_p (f'_{*2} - f'_{j2w}) + G_{i2} f'_{+2} \right] /$$

$$\pi h \phi, \dots \dots S_- \leq j \leq S_{**} \quad (A-37)$$

By following the procedure of integration that was used for Equation (A-24a), Equation (23) is obtained.

$$f'_{+2} = \frac{1}{(S_+ - S_-)} \left\{ f_{+2} - f_{-2} + \frac{G_{i1}}{G_{i2}} [f_{**1} - f_{-1} - f'_{*1} (S_{**} - S_-)] \right. \\ \left. + \frac{Q_p}{G_{i2}} [f_{**2} - f_{-2} - f'_{*2} (S_{**} - S_-)] \right\}, \dots S_{gr} > S_f \quad (23)$$

If breakthrough occurred during the withdrawal process for the condition of non-hysteresis or $S_{gr} < S_f$ then the equations defining the saturation-radius relationship become as follows:

$$r_{j2i}^2 - r_{j2w}^2 = \frac{G_{i2} f'_{j2}}{\pi h \phi}, \dots 0 \leq j \leq S_-, \dots S_+ \leq j \leq 1 \quad (A-38)$$

$$r_{+2}^2 - r_w^2 = \frac{G_{i2} f'_{+2}}{\pi h \phi}, \dots S_{wb} \leq j \leq S_+ \quad (A-39)$$

$$r_+^2 - r_{j2w}^2 = (r_+^2 - r_w^2) - [(r_f^2 - r_w^2) + (r_{j2w}^2 - r_f^2)] \quad (A-40a)$$

$$= [G_{i2} f'_{+2} - F_{i2} f'_{f1} - Q_p f'_{j2w}] / \pi h \phi, \dots \\ S_- \leq j \leq S_{wb}. \quad (A-40b)$$

Substituting these equations into Equation (A-32) and integrating as before yields Equation (17) for the non-hysteresis and hysteresis ($S_{gr} < S_f$) cases.

$$f'_+ = \frac{1}{(S_+ - S_-)} \left\{ f_{+2} - f_{-2} + \frac{G_{i1}}{G_{i2}} f'_{f1} (S_{wb} - S_-) + \frac{Q_p}{G_{i2}} \right. \\ \left. (f_{wb} - f_{-2}) \right\}, \dots S_{gr} < S_f \quad (17)$$

The subscript 'wb' again designates 'at the well bore' at the end of the withdrawal phase.

The handling of the $S_{gr} > S_f$ case is the same with the constant f'_f again, in effect, being replaced by the variable f'_{ji} . The equation of the front then becomes Equation (24b) after Equation (A-32) is integrated.

$$f'_{+2} = \frac{1}{(S_+ - S_-)} \left\{ f_{+2} - f_{-2} + \frac{G_{i1}}{G_{i2}} (f_{wb1} - f_{-1}) + \frac{Q_p}{G_{i2}} (f_{wb2} - f_{-2}) \right\}, \dots S_{gr} > S_f \quad (24b)$$

Water Production

The cumulative volume of water produced, W_p , at any time after breakthrough is also derived readily from material balance. First, consider the gas remaining in the reservoir as depicted by the saturation distribution in Fig. 4.

$$G_r = \pi h \phi \int_{r_0}^{S_{wb}} (r_{j2}^2 - r_w^2) dS \quad (A-41)$$

where

$$r_{j2}^2 - r_w^2 = (r_f^2 - r_w^2) + (r_{j2}^2 - r_f^2) \quad (A-42a)$$

$$= \frac{G_i}{\pi h \phi} f'_f + Q_p f_{wb2} \quad (A-42b)$$

Upon substitution of Equation (A-42) in Equation (A-41), dividing by G_i and integrating, the equation for the fraction of the initial injected gas still remaining in the reservoir becomes Equation (25a).

$$G_{rD} = \frac{G_r}{G_i} = f'_{f1} S_{wb} + \frac{Q_p}{G_i} f_{wb2} \quad (25a)$$

The total gas produced, G_p , must necessarily be given by

$$G_p = - (G_i - G_r) \quad (A-43)$$

with the produced volumes being considered negative. Then the water produced must be the total fluid produced less the total gas produced.

$$W_p = Q_p + G_i - G_r \quad (25b)$$

This equation holds for the non-hysteresis case. It also holds for hysteresis with $S_{gr} < S_f$ if there has not been water production before breakthrough.

For the hysteresis case considered it is possible for water production to occur before breakthrough since for the fractional flow of water the physical condition holds that $f_w > 0$ for $S_g < S_{gmax}$. This water production is then found by integrating over the volume bounded by the well bore and the hypothetical saturation distribution, as given by Equation (11), lying to the left of the well bore as shown in Fig. 3.

$$W_p = \int_{S_{wb}}^1 (r_{j2}^2 - r_w^2) dS \quad (A-44)$$

where

$$r_{j2}^2 - r_w^2 = (r_{j1}^2 - r_w^2) + (r_{j2}^2 - r_{j1}^2) \quad (A-45a)$$

$$= (G_i f'_{j1} + Q_p f'_{j2}) / \pi h \phi \quad (A-45b)$$

The combination and integration of these equations give the volume of water produced.

$$W_p = G_i (1 - f_{wb,1}) + Q_p (1 - f_{wb,2}) \quad (26)$$

This equation evaluated at breakthrough gives the volume to be added to Equation (25b) if there was water production before breakthrough for the $S_{gr} < S_f$ hysteresis case.

The water production when $S_{gr} > S_f$ may be found by the same

methods. Combining Equations (12), (A-22) and (46b) with Equation (A-41)

$$r_{j2}^2 - r_w^2 = (r_{j1}^2 - r_w^2) + (r_{j2}^2 - r_{j1}^2) \quad (\text{A-46a})$$

$$= (G_i f'_{j1} + Q_p f'_{j2}) / \pi h \phi \quad (\text{A-46b})$$

results in the fraction of gas remaining in the reservoir.

$$G_{rD} = \frac{G_r}{G_i} = f_{wb1} + \frac{Q_p}{G_i} f_{wb2} \quad (27)$$

Using Equation (27) and the total water produced before breakthrough as given by Equation (26) yields the cumulative water production for the case where $S_{gr} > S_f$.

$$W_{p,t} = Q_p + G_i - G_r + W_{p,bt} \dots S_{gr} > S_f \quad (28)$$

The produced gas-water ratio follows from the definition of fractional flow from Equation (A-6).

$$f_g = \frac{q_g}{q_t}, \quad f_w = \frac{q_w}{q_t} = 1 - f_g \quad (\text{A-47})$$

The equation for the producing ratio at surface conditions is then given by Equation (29) (7,48).

$$R_{wg} = \frac{q_w}{q_g} = \left(\frac{1}{f_g} - 1 \right) \frac{B_g}{B_w} \quad (29)$$

Average Saturation

The average saturation behind any saturation, i , is given by

$$\bar{S} = \frac{\int_0^{V_k} S dV}{\int_0^{V_k} dV} \quad (\text{A-48})$$

where $dV = 2\pi h \phi r dr = \pi h \phi dr^2$. Now on setting up the integral for separation into parts, Equation (A-48) becomes

$$\bar{S} = \frac{1}{r_k^2 - r_w^2} \int_{r_w}^{r_k} S (dr^2) \quad (\text{A-49})$$

or by using Equation (11)

$$\bar{S} = \frac{1}{r_k^2 - r_w^2} \left[(S_k r_k^2 - 1.0 r_w^2) - \int_1^{S_k} \left(\frac{G_i}{\pi h \phi} f'_k + r_w^2 \right) dS \right], \quad (\text{A-50})$$

On completing the integration and again applying Equation (11) this becomes

$$\bar{S} = S_k + \frac{1 - f_k}{f'_k}. \quad (\text{A-51})$$

If S_k is allowed to become S_f , the saturation at the front, and it is remembered from Equation (12) that $f_f = f'_f S_f$, then the average saturation behind the front becomes

$$\bar{S}_f = \frac{1}{f'_f}$$

with it being noted that \bar{S}_f may be found by extending the tangent used to determine S_f , (Fig. 2), to $f = 1$.

Two-Phase Gas Zone-Unsteady Aquifer Model

To obtain the pressure equation for this model, Equation (36), it is necessary to algebraically combine the equations giving the pressure increments in the three zones (semi-compressible gas, incompressible water, and compressible water) of the model. In the following derivation primed, ($'$), values of rates and volume indicate "at standard conditions."

Equation (A-52) gives the pressure increment in the two-phase gas zone in terms of the injection rate, i'_g and is equivalent to Equation (31).

$$\Delta p_{1,n} = \frac{i'_g}{0.07952\pi hk} \frac{Z_n T_{sc} p_{sc}}{Z_{sc} T_{sc} \bar{p}_{g,n}} \int_{r_w}^{r_f} \frac{dr/r}{\frac{k_{rg}(r)}{\mu_g} + \frac{k_{rw}(r)}{\mu_w}} \quad (\text{A-52a})$$

$$= \alpha_2 \gamma_1 \frac{Z_n}{\bar{p}_{g,n}} \quad (\text{A-52b})$$

$$\alpha_2 = \frac{p_{sc} T_{sc} \mu_w}{Z_{sc} T_{sc} hk \Delta t_n} \quad (40)$$

$$\gamma_1 = \frac{i'_g}{0.07952\pi \mu_w} \int_{r_w}^{r_f} \frac{dr/r}{\frac{k_{rg}}{\mu_g} + \frac{k_{rw}}{\mu_w}} \quad (42)$$

$$\Delta t_n = t_j - t_{j-1} \quad (43)$$

The equation for the pressure increment in the incompressible water zone is given by Equation (A-53) which is equivalent to Equation (32).

$$\Delta p_{2,n} = \frac{\mu_w}{0.07952\pi hk \Delta t_n} \cdot \frac{p_{sc} T_{sc}}{Z_{sc} T_{sc}} \ln \frac{r_c}{r_{f,n}} \left[\frac{Z_n}{\bar{p}_{g,n}} G'_{i,n} - G_{i,n-1} \right] \quad (\text{A-53a})$$

$$= \alpha_2 \beta_3 \left[\frac{Z_n}{\bar{p}_{g,n}} G'_{i,n} - G_{i,n-1} \right] \quad (\text{A-53b})$$

$$\beta_3 = \frac{1}{0.07952\pi} \ln \frac{r_c}{r_{f,n}} \quad (\text{A-54})$$

The pressure at the inner boundary of the compressible aquifer is now given by Equation (A-55) which is equivalent to Equation (33).

$$p_{c,n} = p_i + \frac{25.1\mu_w}{hk_w} \left\{ \sum_{j=1}^{n-1} \left[\left(\frac{\Delta G_i}{\Delta t} \right)_j - \left(\frac{\Delta G_i}{\Delta t} \right)_{j-1} \right] p_{t,j} \right. \\ \left. + \left[\frac{p_{sc} T_{sc}}{Z_{sc} T_{sc} \Delta t_n} \left(\frac{Z_n}{\bar{p}_{g,n}} G'_{i,n} - G_{i,n-1} \right) - \left(\frac{\Delta G_i}{\Delta t} \right)_{n-1} \right] p_{t,n} \right\} \quad (\text{A-55a})$$

$$= \alpha_3 + 25.1\alpha_2 \left(\frac{Z_n}{\bar{p}_{g,n}} G_{i,n} - G_{i,n-1} \right) P_{t,n} \quad (\text{A-55b})$$

$$\alpha_3 = p_i + \frac{25.1\mu_w}{hk_w} \left\{ \sum_{j=1}^{n-1} \left[\left(\frac{\Delta G_i}{\Delta t} \right)_j - \left(\frac{\Delta G_i}{\Delta t} \right)_{j-1} \right] P_{t,j} \right. \\ \left. - \left(\frac{\Delta G_i}{\Delta t} \right)_{n-1} P_{t,n} \right\} \quad (\text{A-56})$$

Now if the assumptions are made that

$$Z_n = a \bar{p}_{g,n} + b \quad (\text{A-57a})$$

or

$$\frac{Z_n}{\bar{p}_{g,n}} = a + \frac{b}{\bar{p}_{g,n}} \quad (\text{A-57b})$$

and on the basis of the volumetric average pressure for single-phase, radial flow that

$$\frac{\bar{\Delta p}_1}{\Delta p_1} = \frac{\bar{p}_g - p_f}{p_w - p_f} \approx 0.1 \quad (\text{A-58})$$

then Equations (A-52b), A-53b), A-55b) and A-57b) may be substituted in Equation (A-58) to obtain an expression for the average pressure, $\bar{p}_{g,n}$, in the gas zone at the end of the 'n'th time step.

$$\bar{p}_{g,n} = \frac{\bar{\Delta p}_1}{\Delta p_1} \Delta p_{1,n} + \Delta p_{2,n} + p_{c,n} + p_{sc} \quad (\text{A-59a})$$

$$= 0.1 \alpha_2 \gamma_1 \left(a + \frac{b}{\bar{p}_{g,n}} \right) + \alpha_2 \beta_3 \left[\left(a \frac{b}{\bar{p}_{g,n}} \right) G'_{i,n} - G_{i,n-1} \right] \\ + \alpha_3 + 25.1\alpha_2 \left[\left(a + \frac{b}{\bar{p}_{g,n}} \right) G'_{i,n} - G_{i,n-1} \right] + p_{sc} \quad (\text{A-59b})$$

$$\begin{aligned} \bar{p}_{g,n} &= 0.1 \alpha_2 \gamma_1^a + \alpha_2 (\beta_3 + 25.0) (aG'_{i,n} - G_{i,n-1}) \\ &+ \alpha_3 + p_{sc} + \left[0.1 \alpha_2 \gamma_1 + \alpha_2 (\beta_3 + 25.1) G'_{i,n} \right] \frac{b}{\bar{p}_{g,n}} \end{aligned} \quad (\text{A-59c})$$

$$= \alpha_1 + \frac{\beta_1}{\bar{p}_{g,n}} \quad (\text{A-59d})$$

or

$$\bar{p}_{g,n}^{-2} - \alpha_1 \bar{p}_{g,n} - \beta_1 = 0 \quad (\text{A-60})$$

and by the quadratic formula

$$\bar{p}_{g,n} = \left[\alpha_1 + (\alpha_1^2 + 4\beta_1)^{\frac{1}{2}} \right] / 2 \quad (37)$$

The other possible root is an extraneous root which was introduced by multiplying Equation (A-59b) by \bar{p}_g to obtain Equation (A-60).

APPENDIX B

COMPUTER PROGRAMS

As this investigation progressed, several computer programs were written to facilitate the data processing. These programs permit the calculation of Klinkenberg permeability, relative permeability, and saturation-resistance data from the observed experimental data; tabulation of relative permeability; calculation of fractional flow characteristics; and the prediction of reservoir performance for a radial gas storage reservoir. All of these programs were written in IBM 650 FORTRAN computer language, and they were all compiled with optional print and/or punch output. The input and output variables are in fixed point or in floating point form as identified by the first letter of the mnemonic name of each variable according to the rules of FORTRAN. The symbol lists for these programs are included in Appendix C.

Relative Permeability

The computer processing of experimental relative permeability data increases the practicality of calculating a larger number of data points and, thereby allows an observation of the trends taking place during the experimental testing. A flow chart of the program is given in Fig. 29 and a program listing in Table XVII.

The program is based on Darcy's equation for each phase in

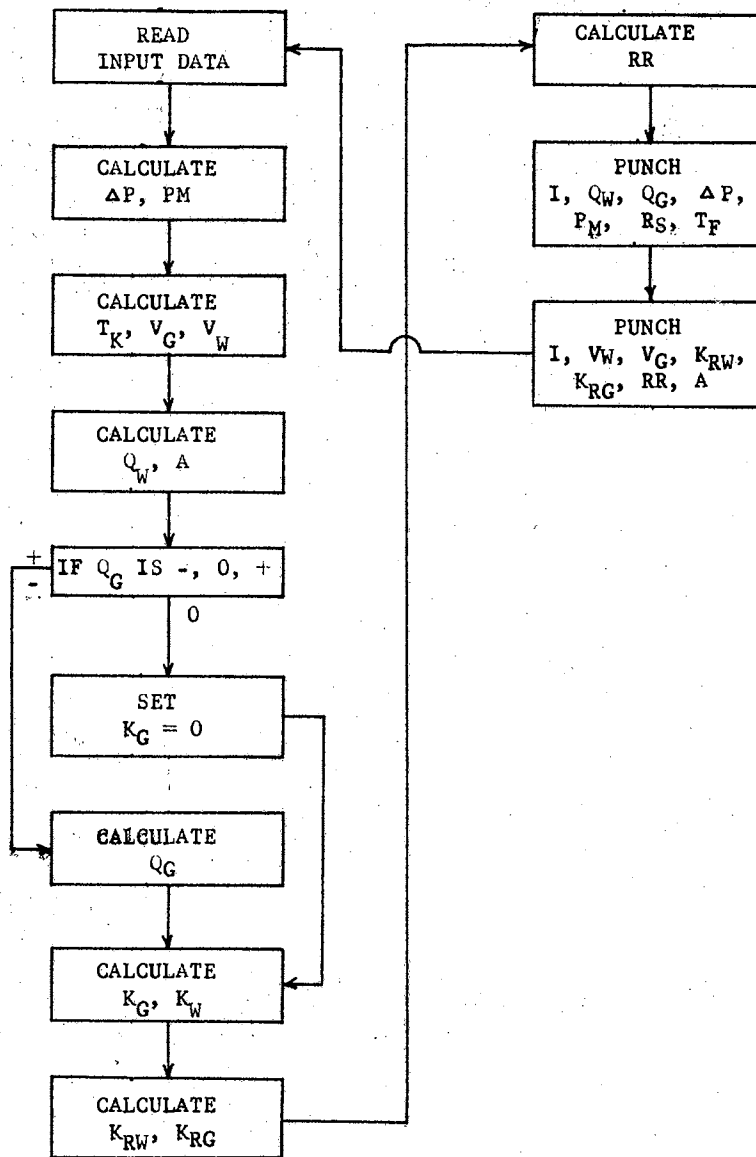


FIG. 29 FLOW CHART, RELATIVE PERMEABILITY

TABLE XVII

RELATIVE PERMEABILITY COMPUTER PROGRAM

```

C 0000 0 RELATIVE PERMEABILITY
      1 0 READ1,X,D,RS1,BK
      2 0 READ2,I,QW,QG,T,DP,P2,RS,TR,
      2 1 PB,DMV,GMV
      3 0 IF(DMV-10.0) 4,4,6
      4 0 DP=DP*DMV*1.35E-3
      5 0 GO TO 10
      6 0 IF(DMV-20.0) 7,7,9
      7 0 DP=DP*DMV*1.416E-3
      8 0 GO TO 10
      9 0 DP=DP*DMV*1.468E-3
     10 0 PM=(6.324E-3)*P2*GMV+(PB/760.0
     10 1 )+0.5*DP
    1010 0 TK=0.55555555*(TR-32.0)+273.15
     11 0 VG=((13.85E-4)*TK**1.5)/(TK
     11 1 +102.0)+(1.0E-5)*PM
     12 0 VW=1.002*EXP((0.686*(68.0-TR
     12 1 )-(4.53E-4)*(TR-68.0)**2)/(78.
     12 2 22222+0.55555555*TR))
     13 0 QW=QW/3600.0
     17 0 A=(D**2)*0.7854
     14 0 IF(QG) 16,15,16
     15 0 GK=0.0
    1015 0 GO TO 19
     16 0 QG=(QG*PB/(PM*T*760.0))-QW
     18 0 GK=VG*QG*X*1000./(A*DP)
     19 0 WK=VW*QW*X*1000./(A*DP)
     20 0 RWK=WK/BK
     21 0 RGK=GK/BK
     22 0 RR=RS*TR/(68.0*RS1)
     23 0 PUNCH1,I,QW,QG,DP,PM,RS,TR
     24 0 PUNCH2,I,VW,VG,RWK,RGK,RR,A
     25 0 GO TO 2
     26 0 END

```

the following form

$$k_i = - \frac{\mu_i q_i L}{A \Delta p}, \dots i = g, w \quad (\text{B-1})$$

and on equations for the fluid viscosities from API Recommended Practices No. 27.

$$\mu_{N_2} = \frac{13.85(10^{-4})(T)^{1.5}}{T + 102} \quad (\text{B-2})$$

$$\mu_w = 1.002 \exp_{10} \left(\frac{0.686(68-T) - 4.53(10^{-4})(T-68)^2}{96 + 5/9(T-32)} \right) \quad (\text{B-3})$$

The gas rate, q_g in Equation (B-1) is the measured rate corrected to the mean core pressure; the nitrogen viscosity is based on temperature °K and pressure in atmospheres with a pressure correction term of $[10^{-5} \bar{p}(\text{atm})]$ being added. The water viscosity was based on temperature in °F.

The resistance calculations are in the form of a ratio corrected to a temperature of 68°F as given by Equation (B-4).

$$R_R = \frac{R_i \times T}{R_{100,68} \times 68} \quad (\text{B-4})$$

where R_i is the measured resistance, T is the temperature in °F, and $R_{100,68}$ is the resistance at 100 per cent water saturation as corrected to 68°F.

The input data for each core is 1) length, 2) diameter, 3) resistance at $S_w = 100$, and 4) the base permeability. The input data for each experimental data point consists of 1) an identification number, 2) water rate, 3) gas volume, 4) time, 5) differential pressure, 6) downstream pressure, 7) electrical resistance, 8) flowing temperature, 9) barometric pressure, 10) differential pressure recorder scale range,

and 11) gauge pressure scale range. The output data then consists of 1) the identification number, 2) water rate, 3) gas rate, 4) differential pressure, 5) mean pressure, 6) electrical resistance, 7) temperature, 8) water viscosity, 9) gas viscosity, 10) water relative permeability, 11) gas relative permeability, 12) electrical resistance ratio, and 13) flow area.

Saturation-Resistance

A computer program was written to process the core weight and electrical resistance data in order that a saturation-resistance correlation might be obtained. A flow chart is given in Fig. 30 and a program listed in Table XVIII.

The basic equations are as follows:

$$S_{w,i} = \frac{w_i - w_0}{w_{100} - w_0} \quad (\text{B-5})$$

$$\phi = \frac{w_{100} - w_0}{\pi/4 d^2 L \rho} \quad (\text{B-6})$$

where w_i is the weight of the core at a saturation of 'i'. The temperature corrected resistance ratio was obtained from Equation (B-4).

The input data for each core consisted of 1) an identification number, 2) core length, 3) core diameter, and 4) resistance at 100 per cent saturation. For each data point the input information was 1) an identification number, 2) core weight at a saturation to be calculated, 3) dry weight of core, 4) electrical resistance, 5) fluid temperature, and 6) a drainage or imbibition cyclic identification index to identify the conditions under which the data was obtained, i.e. $K = 1$ for first drainage; $K = 2$ for first imbibition, etc.

TABLE XVIII

SATURATION-RESISTANCE
COMPUTER PROGRAM

```

C 0000 0 SATURATION-RESISTANCE
    1 0 DIMENSION ID(60),RS(60),TR(60)
    1 1 ,RSC(60),WW(60),WS(60),WD(60)
    3 0 WMAX=0.0
    6 0 READ1,ID(1),XL,DIA,RMIN
106 0 DO 315 J=1,60
    7 0 READ2,ID(J),WS(J),WD(J),RS(J),
    7 1 TR(J),K
    8 0 IF(ID(J)) 9,16,9
    9 0 ID(J)=ID(J)+1000*K
C 0000 0 WEIGHT OF WATER
    10 0 WW(J)=WS(J)-WD(J)
C 0000 0 TEMPERATURE CORRECTED
C 0000 1 RESISTANCE
    13 0 RSC(J)=RS(J)*TR(J)/68.0
    14 0 IF(RSC(J)) 15,15,11
    15 0 PUNCH,ID(J),J,RSC(J),RMIN,WW(J)
    15 1 ),WMAX
    115 0 GO TO 7
    11 0 IF(WMAX-WW(J)) 12,315,315
    12 0 WMAX=WW(J)
    112 0 RMIN=RSC(J)
    315 0 CONTINUE
    16 0 JE=J-1
C 0000 0 POROSITY
    51 0 POR=WMAX / (XL*0.7854*DIA**2)
    52 0 PUNCH1,ID(1),RMIN,WMAX,POR
    53 0 DO159 J=1,JE
C 0000 0 SATURATION
    153 0 SW=WW(J)/WMAX
C 0000 0 RESISTANCE RATIO
    54 0 RR=RSC(J)/RMIN
    55 0 PUNCH2,ID(J),WS(J),WD(J),RS(J)
    55 1 ,TR(J),RR,SW
    159 0 CONTINUE
    60 0 GO TO 3
      END

```

The output information for each core was 1) the identification number, 2) minimum resistance at 100 per cent water saturation, 3) maximum weight of water in the core, and 4) porosity. Then for each data point the following information was punched: 1) identification and cycle index, 2) weight of water in the core, 3) weight of the core at the calculated saturation, 4) dry weight, 5) electrical resistance, 6) fluid temperature, 7) temperature corrected resistance ratio, and 8) water saturation.

Each set of input data, not to exceed 60 data points must be followed by a card with zeros in its first word (card columns 1-10). If it is desired, continuous processing of several sets of data may be accomplished by stacking the sets, each with its "trigger card," one behind another.

Klinkenberg Permeability, Model II, Bivariate

This computer program permits determination of the Klinkenberg permeability, k_k , which is defined as the gas permeability at infinite mean pressure ($1/\bar{p} = 0$); it is sometimes referred to as the equivalent liquid permeability. The purpose of the program is to apply linear regression to the gas permeability data as a linear function of reciprocal mean pressure. That is, a statistical model of the form

$$k_{gi} = \alpha + \beta [1/\bar{p}_i - \overline{(1/\bar{p})}] \quad (\text{B-7})$$

is used where k_{gi} is the gas permeability at a mean pressure of p_i . The Klinkenberg permeability is then given by

$$k_k = \alpha - \beta \overline{(1/\bar{p})}. \quad (\text{B-8})$$

A statistical estimate of Equation (48), as given by Snedecor (62), is

$$\hat{k}_{gi} = \bar{k} + b[1/\bar{p}_i - \overline{(1/p)}] \quad (\text{B-9})$$

in which \hat{k}_{gi} is the estimated value of gas permeability at $1/\bar{p}_i$, \bar{k} is the arithmetic average permeability (an estimator of α), and b is an estimator of the population regression coefficient β .

The following six statistical quantities are required to evaluate b , k_k , and their confidence intervals (62):

- 1) the number of data points, n ,
- 2) the average permeability, $\bar{k} = \frac{\sum k}{n}$
- 3) the average reciprocal mean pressure, $\overline{(1/p)} = \frac{\sum(1/\bar{p})}{n}$
- 4) $\sum X^2 = \sum_1^n (1/\bar{p})^2 - (\sum_1^n 1/\bar{p})^2/n$
- 5) $\sum Y^2 = \sum_1^n k_i^2 - (\sum_1^n k)^2/n$
- 6) $\sum XY = \sum_1^n (k_i/\bar{p}_i) - (\sum_1^n k_i \sum_1^n 1/\bar{p}_i)/n$

The equation giving the sample regression coefficient "b" is Equation (B-10).

$$b = \frac{\sum XY}{\sum X^2} \quad (\text{B-10})$$

The Klinkenberg permeability is then estimated by

$$\hat{k}_k = \bar{k} - b \overline{(1/p)}. \quad (\text{B-11})$$

The equation giving the least squares estimates of each experimental point is Equation (B-12) which may be written as

$$\hat{k}_i = \hat{k}_k + b/\bar{p}_i \quad (\text{B-12})$$

and the deviation from regression at each point is then

$$d_i = k_i - \hat{k}_i. \quad (\text{B-13})$$

The calculation of the different standard deviations allows the placing of interval estimates on the values of the regression coefficient, β , and the Klinkenberg permeability, k_k . The standard deviation from regression is given by

$$s_{y \cdot x} = \left\{ \left[\Sigma y^2 - (\Sigma xy)^2 / \Sigma x^2 \right] / (n-2) \right\}^{\frac{1}{2}} \quad (\text{B-14})$$

the sample standard deviation of the regression coefficient by

$$s_b = s_{y \cdot x} / (\Sigma x^2)^{\frac{1}{2}} \quad (\text{B-15})$$

and the sample standard deviation of \hat{k} by

$$s_{\hat{k}, i} = s_{y \cdot x} \left\{ 1/n + \left[1/\bar{p}_i - \overline{(1/\bar{p})} \right]^2 / \Sigma x^2 \right\}^{\frac{1}{2}}. \quad (\text{B-16})$$

These statistical parameters may now be used along with Student's "t" distribution to set a 95 per cent confidence interval on β and k_k as indicated by Equations (B-17) and B-18).

$$b - s_b t_{.05, n-2} \leq \beta \leq b + s_b t_{.05, n-2} \quad (\text{B-17})$$

$$\hat{k}_k - s_{\hat{k}, 0} t_{.05, n-2} \leq k_k \leq \hat{k}_k + s_{\hat{k}, 0} t_{.05, n-2} \quad (\text{B-18})$$

with $s_{\hat{k}, 0}$ being the sample standard deviation of \hat{k} evaluated at $1/\bar{p} = 0$ and $t_{.05, n-2}$ being Student's "t" at the 5 per cent level for n-2 degrees of freedom⁽⁶²⁾.

The input data for this program consists of a table of Student's "t" values for 1 to 49 degrees of freedom and of the output from the relative permeability program when it has processed gas permeability data with a base permeability of 1 md. This use of a base permeability of 1 md. provides effective permeability data for this program instead of relative permeability data.

The output data for each set of input data consists of three types of cards. The first card contains 1) an identification number; 2) the estimated Klinkenberg permeability, \hat{k}_k ; 3) the lower limit of its confidence interval; 4) its upper limit; 5) the per cent deviation for the half interval, $s_{k,0} t_{.05, n-2}$; 6) the standard deviation from regression, $s_{y.x}$; and 7) the degrees of freedom. The second card is comprised of 1) an identification; 2) the estimate of the regression coefficient; 3) the lower limit of its confidence interval; 4) its upper limit; 5) the per cent deviation for the half interval, $s_b t_{.05}$; 6) the sample standard deviation of the regression coefficient, s_b ; and 7) Student's "t". Following these two cards are 'n' cards with 1) an identification number; 2) an experimental value of gas permeability; 3) its estimate by regression; 4) the reciprocal mean pressure; 5) the mean pressure; 6) the deviation between the permeability and its estimate.

Each set of data must be followed by a card with a non-zero number in word two (columns 11-20) since the program determines 'n' by a card count. The value of 'n' may not exceed 50.

A number of sets of data may be placed in the read hopper at one time for continuous processing. Each set must be separated by a card of the above type.

The program flow chart is shown in Fig. 31 and the program listing in Table XIX.

Relative Permeability Tabulation

The purpose of this program is to tabulate relative permeability curves at saturation intervals of one per cent to be used in a program

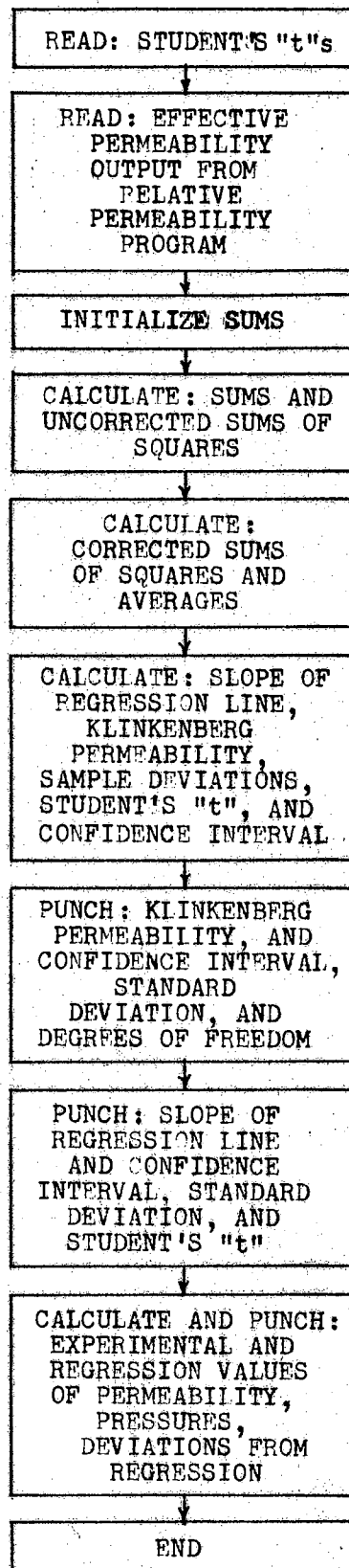


FIG. 31 FLOW CHART, KLINKENBERG PERMEABILITY

TABLE XIX
KLINKENBERG PERMEABILITY COMPUTER PROGRAM

```

C 0000 0 KLINKENBERG PERMEABILITY,
C 0000 1 MODEL 2, BIVARIATE
  1 0 DIMENSION ID(50),PM(50),GK(50)
  1 1 ,RPM(50),TS(50)
101 0 READ3,(TS(I),I=1,49)
  2 0 J=1
  3 0 READ1, ID(J),QW,QG,DR,
  3 1 PM(J),RS,TR
  4 0 IF(QW) 8,5,8
  5 0 READ2, ID(J),VW,VG,WK,GK(J),RR,
  5 1 A
  6 0 J=J+1
  7 0 GO TO 3
  8 0 SUMP=0.0
  9 0 SUMK=0.0
10 0 SUMP=0.0
11 0 SKS=0.0
12 0 SPS=0.0
13 0 JM=J-1
14 0 DO 20 J=1,JM
15 0 RPM(J)=1.0/PM(J)
C 0000 0 SUMS AND SUMS OF SQUARES
16 0 SUMK=SUMK+GK(J)
17 0 SUMP=SUMP+RPM(J)
18 0 SUMPK=SUMPK+GK(J)*RPM(J)
19 0 SKS=SKS+GK(J)**2
20 0 SPS=SPS+RPM(J)**2
21 0 FN=JM
22 0 C=SUMK*SUMP/FN
23 0 SXY=SUMPK-C
24 0 SYS=SKS-((SUMK)**2)/FN
25 0 SXS=SPS-((SUMP)**2)/FN
26 0 AK=SUMK/FN
27 0 ARPM=SUMP/FN
28 0 B=SXY/SXS
C 0000 0 KLINKENBERG PERMEABILITY
29 0 GKK=AK-B*ARPM
129 0 IDF=JM-2
30 0 DF=IDF
31 0 IF(DF) 32,32,36
32 0 SD=99999999.
33 0 SB=99999999.
34 0 T=99999999.
35 0 GO TO 39
36 0 SD=(( SYS-(SXY)**2 /SXS)/DF)**
36 1 0.5
37 0 SB=SD/(SXS)**0.5
38 0 T=B/SB
138 0 SYH=SD*(1./FN+ARPM**2/SXS)**.5
238 0 TS1=TS(IDF)
C 0000 0 CONFIDENCE INTERVAL
338 0 GKHI=SYH*TS1
438 0 GKKL=GKK-GKHI
538 0 GKKU=GKK+GKHI
638 0 PERGK=GKHI*100./GKK
738 0 BHI=SB*TS1
838 0 BL=B-BHI
938 0 BU=B+BHI
1038 0 PERB=BHI*100./B
  39 0 PUNCH1, ID(1),GKK,GKKL,GKKU,PER
  39 1 GK,SD,IDF
139 0 PUNCH3, ID(1),B,BL,BU,PERB,SB,T
  40 0 DO 44 J=1,JM
  41 0 ESK=GKK+B*RPM(J)
  42 0 D=GK(J)-ESK
  43 0 PUNCH2, ID(J),GK(J),ESK,RPM(J),
  43 1 PM(J),D
  44 0 CONTINUE
  45 0 GO TO 2
  46 0 END

```

for calculation of the fractional flow characteristics and two-phase frontal displacement. If the sign of the computer console is set to minus instead of plus, the program also tabulates the theoretical non-wetting phase (gas) imbibition relative permeability curve corresponding to an experimental drainage relative permeability curve. This imbibition curve is based on the theory of Naar and Henderson ⁽⁴²⁾. The program flow chart is shown in Fig. 32 and the program itself in Table XX.

The input source is the coefficients of a least-squares polynomial fit of experimental relative permeability data. This curve fitting is done by a program named LS-3, IBM Program Library No. 6.0.024, which was written by Mr. Gene Pulley of the Oklahoma State University Computing Center. It fits first, second, third, and fourth degree polynomials through the input data, calculates the standard deviation, and also, calculates the least squares estimate and deviation at each point.

The basic equations for the relative permeability tabulator program are the fourth degree polynomial

$$k_{ri} = a_0 + a_1 S_g + a_2 S_g^2 + a_3 S_g^3 + a_4 S_g^4 \quad (\text{B-19})$$

for the drainage relative permeability curve and

$$S_{g,imb} = [S_{g,max} (2S_{g,dr} - S_{g,max})]^{\frac{1}{2}} \quad (\text{B-20})$$

In Equation (B-20) $S_{g,imb}$ is a gas saturation on the imbibition curve, originating from $S_{g,max}$, which has the same relative permeability as the gas saturation $S_{g,dr}$ on the drainage relative permeability curve. The imbibition curve is represented pictorially by Fig. 25. The imbibition relative permeabilities are then tabulated by picking the proper value from the table of drainage relative permeabilities.

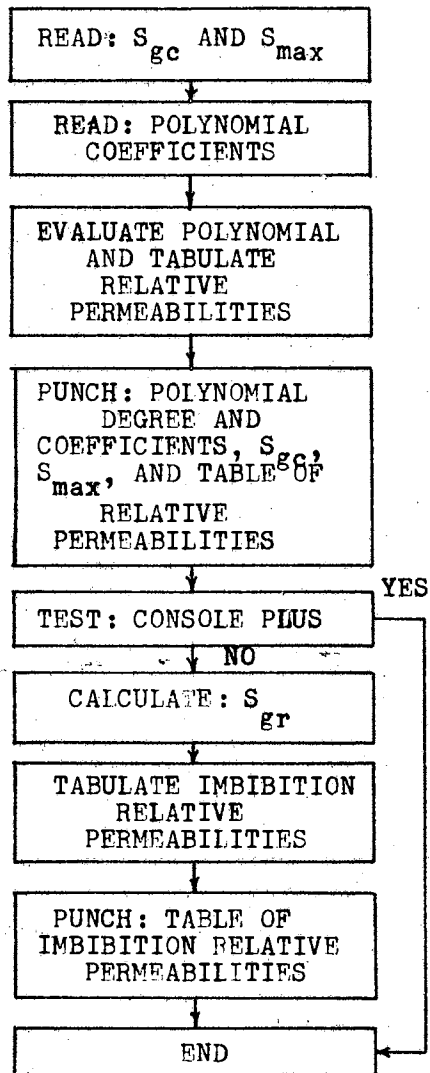


FIG. 32 FLOW CHART, RELATIVE PERMEABILITY TABULATION

TABLE XX

**RELATIVE PERMEABILITY
TABULATION COMPUTER
PROGRAM**

```

C 0000 0 RELATIVE PERMEABILITY
C 0000 1 TABULATION
      DIMENSION RK(100),RKI(100)
      1 0 READ1, ID, IL, IU
      2 0 READ2, N1, A0, A1, A2, A3, A4
      3 0 SG=(FLOTF(IL))/100.
      4 0 DO 5 I=1, IL
      5 0 RK(I)=0.
105 0 IL1=IL+1
      6 0 DO 8 I=IL1, IU
      7 0 SG=SG+.01
      8 0 RK(I)=A0+A1*SG+(A2*SG**2)+(A3*
      8 1 SG**3)+A4*SG**4
      9 0 N=N1/10-1
     10 0 PUNCH1, ID, IL, IU, N, A0, A1, A2, A3,
     10 1 A4
     11 0 PUNCH2, (RK(I), I=1, IU)
C 0000 0 CALCULATED IMBIBITION
C 0000 1 PERMEABILITY
     12 0 IF(XCONF(1)) 13, 23, 23
     13 0 ILW=(IU+1)/2
     14 0 SG=(FLOTF(ILW))/100.
     15 0 SGU=(FLOTF(IU))/100.
     16 0 DO 17 K=1, ILW
     17 0 RKI(K)=0.
117 0 ILW1=ILW+1
     18 0 DO 21 K=ILW1, IU
     19 0 SG=SG+.01
     20 0 I=.5+(SGU*(2.*SG-SGU))**.5
     21 0 RKI(K)=RK(I)
     22 0 PUNCH3, (RKI(K), K=1, IU)
     23 0 END

```

The input data for each core are 1) an identification number, 2) lower limit of gas saturation, S_{gc} , 3) maximum gas saturation (one minus residual water saturation). The input data for each curve to be tabulated is then the coefficient cards from the LS-3 program with the following data: 1) degree of polynomial plus one, 2) a_0 , 3) a_1 , 4) a_2 , 5) a_3 , 6) a_4 . The output data is 1) the identification, 2) lower limit of gas saturation, 3) maximum gas saturation, 4) degree of polynomial, 5) a_0 , 6) a_1 , 7) a_2 , 8) a_3 , 9) a_4 . Following this are the tabulated values of permeability punched seven values per card. The imbibition curve, if it is desired, is also punched as seven values per card.

Fractional Flow-Saturation Distribution

This program converts the output from the relative permeability tabulator program into fractional flow data and calculates the saturation distribution for the injection case. The flow chart is shown in Fig. 33, and the program is listed in Table XI.

The equations used by this program are the fractional flow equation

$$f_g = \frac{1}{1 + \frac{k_{rw} \mu_g}{k_{rg} \mu_w}} \quad (7)$$

and the equation for the saturation of the front

$$f'_f = f_f / S_f \quad (12)$$

where the proper value of saturation is found by finding the maximum value of f/S as suggested in Appendix A. The average saturation for injection is calculated from Equation (30).

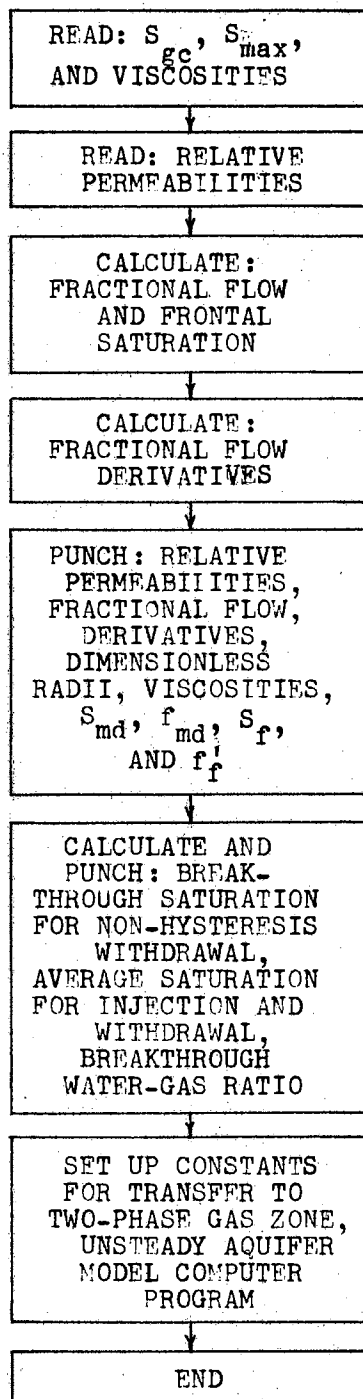


FIG. 33 FLOW CHART, FRACTIONAL FLOW — SATURATION DISTRIBUTION

TABLE XXI
FRACTIONAL FLOW—SATURATION DISTRIBUTION
COMPUTER PROGRAM

```

C 0000 0 FRACTIONAL FLOW-SATURATION
C 0000 1 DISTRIBUTION
  1 0 DIMENSION FD(100),DFD(100),RK(
  1 1 100,2),RSD2(100)
  2 0 READ1,ID,IL,IU,V1,V2
  3 0 READ2,(RK(I,1),I=1,IU)
  4 0 READ3,(RK(I,2),I=1,IU)
  5 0 DO 6 I=IU,100
1005 0 DFD(I)=0.
  6 0 FD(I)=1.0
  7 0 DO 8 I=1,IL
1007 0 DFD(I)=0.
  8 0 FD(I)=0.0
1008 0 DFDB=0.
2008 0 DFDM=0.
C 0000 0 FRACTIONAL FLOW
  9 0 DO 18 I=IL,IU
 10 0 FD(I)=RK(I,1)/(RK(I,1)+RK(I,2)
 10 1 *V1/V2)
C 0000 0 FRONTAL SATURATION
 14 0 SI=(FLOTF(I))/100.
 15 0 FS=FD(I)/SI
 16 0 IF(DFDB-FS) 17,18,18
 17 0 DFDB=FS
1017 0 ISB=I
 18 0 CONTINUE
C 0000 0 DERIVATIVE OF FRACTIONAL FLOW
 21 0 DO 28 I=1,IU
1021 0 IF(I-IL) 2013,2013,11
 11 0 IF(IL+2-I) 12,1011,1011
1011 0 DFD(I)=(-3.*FD(I)+4.*FD(I+1)-
1011 1 FD(I+2))/0.02
2011 0 GO TO 1013
 12 0 IF(98-I) 1012,13,13
1012 0 DFD(I)=(FD(I-2)-4.*FD(I-1)+3.
1012 1 *FD(I))/0.02
2012 0 GO TO 1013
 13 0 DFD(I)=(FD(I-2)-FD(I+2)+8.*
 13 1 (FD(I+1)-FD(I-1)))/0.12
1013 0 IF(DFD(I)) 2013,3013,3013
2013 0 DFD(I)=0.
3013 0 IF(DFDM-DFD(I)) 4013,4013,22
4013 0 DFDM=DFD(I)
5013 0 IMD=I
 22 0 RSD2(I)=DFD(I)/DFDB
 23 0 IF(I-ISB) 24,24,26
 24 0 RSD=1.
 25 0 GO TO 1026
 26 0 RSD=(RSD2(I))**.5
1026 0 IDS=ID+I
 20 0 DFD(IU)=0.0
1020 0 DFD(IL)=0.
 27 0 PUNCH2,IDS,RK(I,1),RK(I,2),
 27 1 FD(I),DFD(I),RSD,RSD2(I)
 28 0 CONTINUE
 19 0 PUNCH1,IDS,IL,IU,IMD,DFDM,ISB,
 19 1 DFDB,V1,V2
C 0000 0 BREAKTHROUGH SATURATION
1019 0 FMIN=99.0E19
2019 0 IB=IL+1
 29 0 DO 35 I=IB,IMD
 30 0 SI=(FLOTF(I))/100.
1030 0 IF(DFD(I)) 42,42,31
 31 0 F1=ABSF(1.-FD(I)+(FD(I)-DFDB*
 31 1 SI)/(1.-DFDB/DFD(I)))
 32 0 IF(FMIN-F1) 35,33,33
 33 0 ISBT=I
 34 0 FMIN=F1
 35 0 CONTINUE
C 0000 0 AVERAGE SATURATION, INJECTION
 36 0 ISAI=100./DFDB
C 0000 0 AVERAGE SATURATION, WITHDRAWAL
1036 0 IF(ISBT) 43,43,37
 37 0 SBT=(FLOTF(ISBT))/100.
 38 0 ISAW=(SBT-FD(ISBT)/DFD(ISBT))
 38 1 *100.
C 0000 0 BREAKTHROUGH WGR
 39 0 WGRBH=1./FD(ISBT)-1.
C 0000 0 FRACTION OF GAS IN RESERVOIR
 40 0 GDBT=1.-DFDB/DFD(ISBT)
 41 0 PUNCH,ID,ISAI,ISBT,ISAW,WGRBH,
 41 1 GDBT
C 0000 0 STOP 1111, DFD=0,1030
 42 0 STOP 1111
C 0000 0 STOP 1222, ISBT=0, 1036
 43 0 STOP 1222
      IUX=IU
      ISBX=ISB
      DFDBX=DFDB
      IMDX=IMD
      DFDMX=DFDM
      ILX=IL
      END

```

$$\bar{S}_g = 1/f'_f \quad (30)$$

A dimensionless radius squared for each saturation as a fraction of the radius to the front is given by

$$r_{iD}^2 = \frac{r_i^2 - r_w^2}{r_f^2 - r_w^2} = \frac{f'_i}{f'_f} \cdot \quad (B-21)$$

This squared dimensionless radius given by Equation (B-21) is also equivalent to the dimensionless distance in a linear system; that is,

$$X_{iD} = X_i/L = r_{iD}^2 \cdot \quad (B-22)$$

Also, the well bore saturation, the average saturation, the producing water-gas ratio, and the fraction of injected gas in place are calculated at breakthrough for the withdrawal without hysteresis case. The well-bore saturation at breakthrough is found by minimizing ϵ in Equation (B-23)

$$1 - f'_i + \frac{f'_i - f'_f S_i}{1 - f'_f/f'_i} = \epsilon \cdot \quad (B-23)$$

The average gas saturation at breakthrough is found from

$$\bar{S} = S_{wb} - f_{wb}/f'_{wb} \quad (B-24)$$

and the fraction of the injected gas remaining in the reservoir at this time by Equation (67).

$$G_{rD} = 1 - f'_f/f'_{wb} \quad (B-25)$$

The bottom-hole, water-gas ratio is then determined by Equation (29)

which with the formation volume factors of unity becomes Equation (B-26)

$$R_{wg} = \frac{1}{f_{wb}} - 1 \cdot \quad (B-26)$$

The input data is comprised of 1) an identification number, 2) gas saturation at zero gas permeability, 3) gas saturation at the

maximum gas permeability (residual water saturation), 4) gas viscosity, 5) water viscosity, 6) the tabulated values of gas relative permeability, and 7) the tabulated values of water relative permeability.

The output data consists of the following values at each per cent of gas saturation: 1) identification and saturation, 2) gas relative permeability, 3) water relative permeability, 4) gas fractional flow, 5) derivative of the fractional flow, 6) the approximate dimensionless radius, and 7) the dimensionless radius squared. Also punched out are 1) the identification, 2) the minimum saturation, 3) the maximum saturation, 4) the saturation at which f' is a maximum, 5) the maximum f' , 6) the saturation at the injection front, 7) f_f^0 at the front, 8) gas viscosity, and 9) water viscosity.

The last six statements of the program permit the machine program deck to be modified readily to continue automatically into the program for the Two-Phase Gas Zone, Unsteady Aquifer Model while retaining the necessary fractional flow data in the computer memory.

Two-Phase Gas Zone-Unsteady Aquifer Model

This computer program solves the equations describing the radius of the gas zone and the well-bore pressure of the mathematical model discussed under the above title in Chapter III. The program is described by the flow chart in Fig. 34 and the listing in Table XXII.

The basic equations are for the well bore pressure,

$$p_{w,n} = \bar{p}_{g,n} + 0.9 \Delta p_{l,n} - p_{sc} \quad (36)$$

and for the radius of the gas zone obtained by modifying Equation (11) to the form of Equation (B-27)

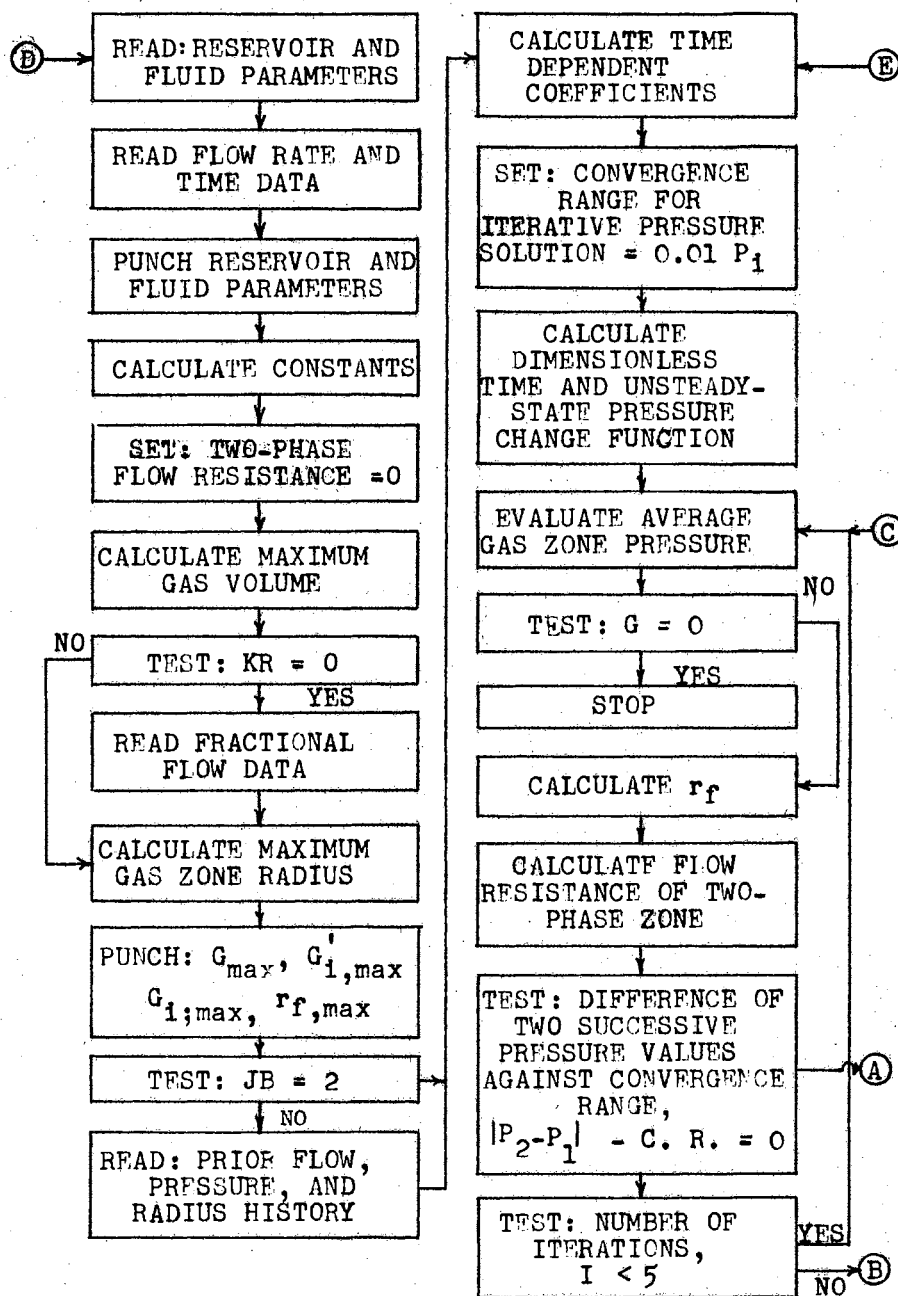


FIG. 34 FLOW CHART, TWO-PHASE GAS ZONE, UNSTEADY AQUIFER MODEL

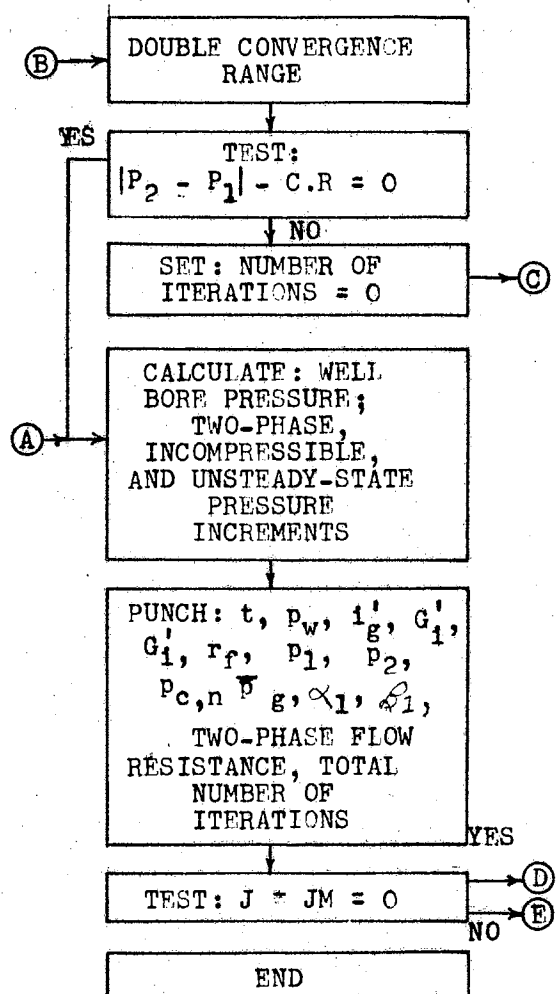


FIG. 34 (CONTINUED)

TABLE XXII

TWO-PHASE GAS ZONE, UNSTEADY AQUIFER MODEL COMPUTER PROGRAM

```

C 0000 0 TWO-PHASE GAS ZONE, UNSTEADY
C 0000 1 AQUIFER MODEL
  100 0 DIMENSION QD(200),RK(100,2),
  100 1 RSD(100),T(200)
  101 0 READ4,JM,JB,PG,BK,P,H,RW,C,ZM,
  101 1 ZC,V1,V2,PB,PO,TB,TR,KR
  102 0 READ5,(QD(J),J=1,JM)
  103 0 READ6,(T(J),J=1,JM)
  104 0 PUNCH3,BK,P,H,V1,TR,PO,PG
  105 0 RB=RW
  106 0 GC=PB*TR/TB
  107 0 PIHP=3.1415927*H*P
  108 0 HBKG=GC/(0.2498194*H*BK)
  109 0 CU=25.1*V2/(H*BK)
  110 0 TPR=0.0
  112 0 SUMQS=QD(1)*T(1)
  113 0 QMAX=0.0
  114 0 DO 119 J=2,JM
  115 0 SUMQS=SUMQS+QD(J)*(T(J)-T(J-1))
  115 1 )
  117 0 IF(QMAX-SUMQS) 118,119,119
  118 0 QMAX=SUMQS
  119 0 CONTINUE
  1119 0 IF(KR) 120,2119,120
  2119 0 READ10,X,X,IU,ISB,DFDB,X,X
  3119 0 DO 5119 I=1,IU
  4119 0 READ9,X,RK(I,1),RK(I,2),X,X,RS
  4119 1 D(I),X
  5119 0 CONTINUE
  120 0 SUMQ=QMAX*GC*(ZM+ZC/PG)
C 0000 0 MAXIMUM GAS ZONE RADIUS
  121 0 RA=(RW**2+(SUMQ*DFDB/PIHP))**
  121 1 0.5
  123 0 CTD=(6.3216E-3)*BK/(V2*P*C*
  123 1 RA**2)
  124 0 PUNCH4,JM,RA,QMAX,SUMQS,SUMQ
  1124 0 SUMQS=QD(1)*T(1)
  125 0 IF(JB-2) 192,128,126
  126 0 JC=JB-1
  127 0 DO 3127 J=2,JC
  1127 0 READ7,X,X,X,X,SUMQS,RB,X
  2127 0 READ8,X,X,X,X,PG,QD(J),TPR
  3127 0 CONTINUE
C 0000 0 PRESSURE CALCULATION
  128 0 ZPG=ZM+ZC/PG
  129 0 DO 190 J=JB,JM
  1129 0 DT=T(J)-T(J-1)
  2129 0 SQS1=SUMQS*ZPG
  130 0 SUMQS=SUMQS+QD(J)*DT
  131 0 AIC=V2*HBKG/DT
  132 0 ATP=0.9*QD(J)*HBKG
  1132 0 AGS=ZM*SUMQS-SQS1
  2132 0 BQS=ZC*SUMQS
  3132 0 DPO=0.01*PO
  160 0 DPU1=0.0
  161 0 DO 177 K=2,J
  162 0 TD=CTD*(T(J)-T(K-1))
  163 0 IF(TD-2.0) 165,174,164
  164 0 IF(TD-100.0) 174,176,176
  165 0 IF(TD-0.09) 166,172,172
  166 0 IF(TD-0.01) 167,167,169
  167 0 PT=2.0*(TD/3.1415927)**0.5
  168 0 GO TO 1176
  169 0 PT=0.1745831*LOGEF((TD+0.03)/
  169 1 0.021536)
  171 0 GO TO 1176
  172 0 PT=0.3551249*LOGEF((TD+0.2)/
  172 1 0.10225)
  173 0 GO TO 1176
  174 0 PT=0.4845196*LOGEF((TD+1.0)/
  174 1 0.36588)
  175 0 GO TO 1176
  176 0 PT=0.5*LOGEF(2.2458*TD)
  1176 0 IF(K-J) 177,1177,192
  177 0 DPU1=DPU1+(QD(K)-QD(K-1))*PT
  1177 0 DPU2=(DPU1-QD(K-1)*PT)*CU
  2177 0 AU=CU*GC*PT/DT
  3177 0 LM=0
  178 0 DO2157 L=1,5
  179 0 PG2=PG
  1179 0 RLN=LOGEF(RA/RB)
  180 0 AIU=AU+AIC*RLN
  181 0 ATPR=ATP*TPR
  182 0 AA=AIU*AQS+DPU2+ATPR*ZM+PO+PB
  183 0 BB=BQS*AIU+ATPR*ZC
C 0000 0 AVERAGE GAS ZONE PRESSURE
  184 0 PG=((AA**2+4.*BB)**.5)+AA)/2.
  1184 0 ZPG=ZM+ZC/PG
  134 0 SUMQ=SUMQS*GC*ZPG
  1134 0 IF(SUMQ) 192,135,135
C 0000 0 GAS ZONE RADIUS
  135 0 RB=(RW**2+(SUMQ*DFDB/PIHP))**
  135 1 0.5
  142 0 RWD=RW/RB
  143 0 IF(L-2) 1057,144,1057
  144 0 TPR=0.0
  149 0 B=(RSD(ISB)**2+RWD**2)**0.5
  150 0 IM=IU-1
  151 0 DO 157 I=ISB,IM
  152 0 A=B
  153 0 IF(RSD(I+1)/RWD-7.0) 154,156,
  153 1 156
  154 0 B=(RSD(I+1)**2+RWD**2)**0.5
  155 0 GO TO 157
  156 0 B=RSD(I+1)
  157 0 TPR=TPR+2.0*(A-B)/(B*(RK(I+1,1)
  157 1 )/V1+RK(I+1,2)/V2)+A*(RK(I,1)/
  157 2 V1+RK(I,2)/V2))
  1057 0 ADP=ABSF(PG-PG2)
  2057 0 LM=LM+1
  1157 0 IF(ADP-DPO) 158,158,2157
  2157 0 CONTINUE
  2257 0 IF(PG-PB) 2357,3157,3157
  2357 0 PG=PB
  2457 0 ZPG=ZM+ZC/PG
  2557 0 GO TO 158
  3157 0 DPO=2.0*DPO
  4157 0 IF(ADP-DPO) 158,158,178
C 0000 0 TWO-PHASE-ZONE PRESSURE
C 0000 1 INCREMENT
  158 0 DPTP=QD(J)*TPR*HBKG*ZPG
  1158 0 QUS=(SUMQ-SQS1*GC)/DT
C 0000 0 INCOMPRESSIBLE-ZONE PRESSURE
C 0000 1 INCREMENT
  159 0 DPIC=V2*HBKG*QUS*RLN/GC
  1159 0 DPU=DPU2+QUS*CU*PT
C 0000 0 WELL BORE PRESSURE
  2159 0 PW=PG+0.1*DPTP-PB
  185 0 JP=J+10000
  186 0 PUNCH5,JP,T(J),PW,QD(J),SUMQS,
  186 1 RB,SUMQ
  1186 0 QD(J)=QUS
  187 0 JP=J+20000
  188 0 PUNCH6,JP,DPTP,DPIC,DPU,PG,
  188 1 QD(J),TPR
  1188 0 JP=J+30000
  189 0 PUNCH7,JP,LM,ADP,DPO,AA,BB,
  189 1 DPU2
  190 0 CONTINUE
  191 0 GO TO 101
  192 0 END

```

$$r_{f,n} = \left[\frac{G_i f'_f}{\pi h \phi} + r_w^2 \right]^{\frac{1}{2}} \quad (\text{B-27})$$

The basic data input for this program is comprised of three different sets of data: reservoir parameters, flow rates, and times at which these flow rates ended. One or two additional sets of data are required if the following conditions exist: 1) this program is being used independently of the fractional flow computer program; that is, the fractional data is not already in the computer memory in which case it may be read in by setting equal to zero an index (KR) in the basic data set, 2) a problem has been partially processed and it is desired to pick up the calculation where it left off.

The reservoir parameters consist of 1) the number of constant-flow rate time steps to be considered ($JM \leq 200$); 2) the time step with which calculations are to begin ($JB \geq 2$); 3) the average gas zone pressure at time step $JB-1$; 4) base permeability; 5) porosity; 6) formation thickness; 7) well-bore radius; 8) the combined compressibility of the formation and its in situ fluid; 9) the slope of linearized gas compressibility factor equation; 10) the intercept of this equation; 11) gas viscosity; 12) water viscosity; 13) initial reservoir pressure; 14) base temperature for gas volume measurement; 15) reservoir temperature; 16) an index (KR), defining whether or not the fractional flow data is in the computer memory. The flow rate (the initial rate must be zero). The time data indicates at what time after injection began that each flow rate ended (the initial time must be zero).

The fractional flow data, if it is to be read into the computer, must be headed by the card giving the minimum, maximum and frontal

values of saturation and the fractional flow derivative at the front (which is the next to the last card of the output deck of the fractional flow program; the last card should be discarded), and the index KR must be set to zero. In the case where calculation is to be resumed at an intermediate time step, the necessary quantities from the previously calculated answers can be read into the computer by setting the index JB in the basic data set equal to the number of the time step at which the calculations are to be resumed.

The output data at each time step consists of three cards. On the first card is 1) the number of the time step; 2) total time elapsed from beginning of injection; 3) well bore pressure at the end of the time step; 4) gas injection rate at standard conditions; 5) cumulative volume of gas injected at standard conditions; 6) the radius of the gas zone; and 7) the cumulative volume of gas at reservoir conditions. On the second card is 1) the number of the time step; 2) the pressure increment in the two-phase zone; 3) the pressure increment in the incompressible water zone; 4) the unsteady-state pressure increment; 5) the average gas zone pressure; 6) the gas injection rate corrected to reservoir conditions; and 7) the two-phase flow resistance represented by the integral in Equation (42). The third card then contains several of the partial products making up Equation (36).

Cyclic Two-Phase Flow

A computer program was developed to study the theoretical aspects, as developed in Chapter III, of cyclic two-phase flow in a reservoir.

The major objectives were to determine saturation distributions, water production, producing water-gas ratios, and the fraction of gas recovered at breakthrough. The program flow chart is shown in Fig. 35 and the program listing in Table XXIII.

The basic equations, in addition to those computations necessary to separate and define the various cases, were the equations for the square of the dimensionless radius of the saturation as developed from Equation (11) and as given by Equation (B-28).

$$r_{iD}^2 = \frac{r_i^2 - r_w^2}{r_f^2 - r_w^2} \quad (\text{B-28})$$

and, also, the various equations for the saturation at the front for the various cases. These equations are represented by Equations (12), (14), (16), (17), (21), (22), (23), and (24a,b).

The input data may be divided into reservoir parameters, two sets of fractional flow data, and fluid volume data. The reservoir parameters are 1) reservoir identification; 2) formation thickness; and 3) wellbore radius. The fractional flow data consists of two complete sets of output data from the fractional flow program each headed by the card containing saturation limits and saturation and fractional flow derivative at the front (the last card, containing the computed average saturations, is discarded from these decks). If hysteresis is not to be considered, both of these sets should be fractional flow data from the drainage relative permeability curves. If hysteresis is being considered, the first set should be for drainage conditions and the second set for imbibition conditions. The fluid volume data includes 1) an identification number, and 2) the volume of gas, at reservoir

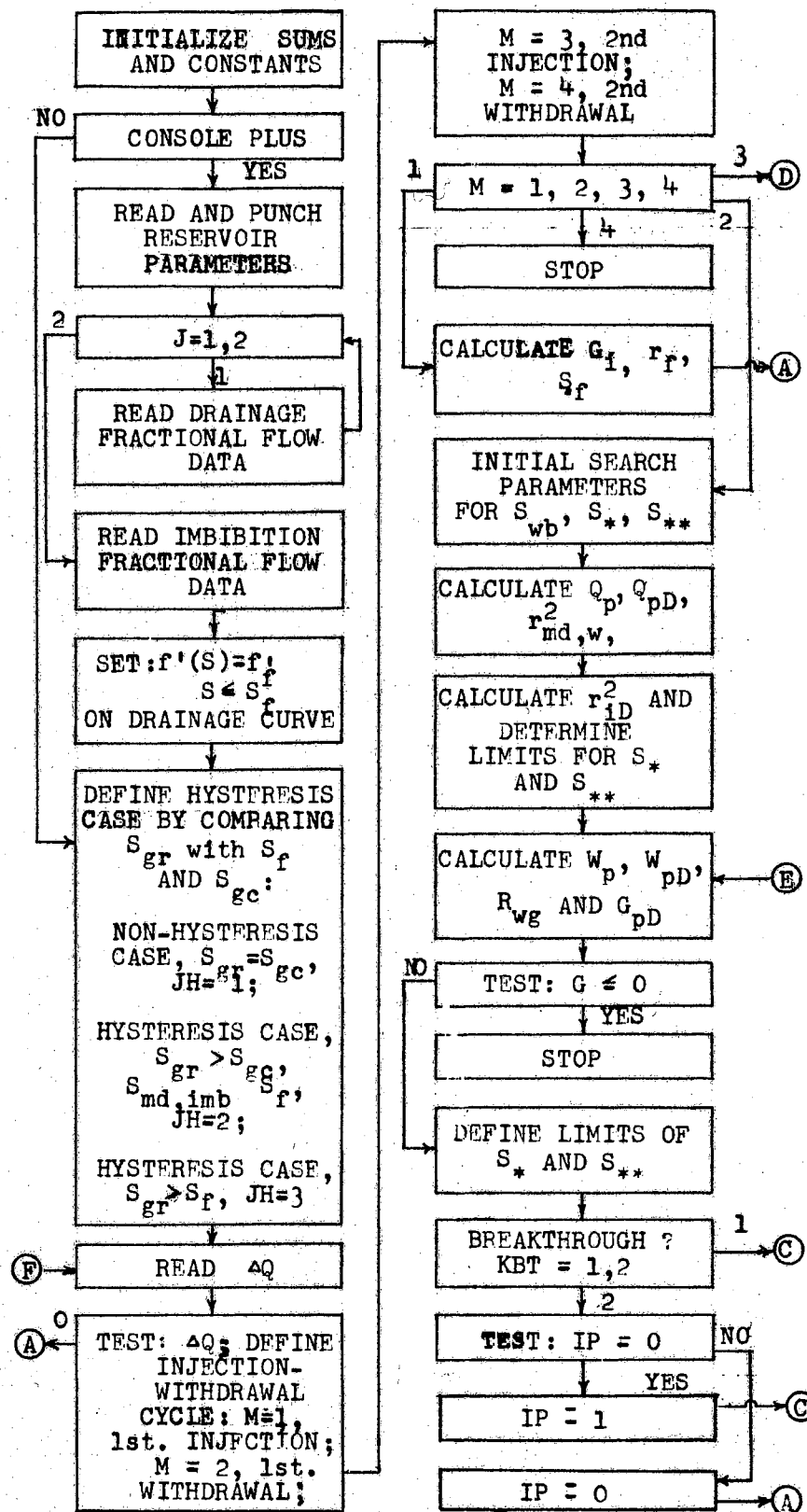


FIG. 35 FLOW CHART, CYCLIC TWO-PHASE FLOW

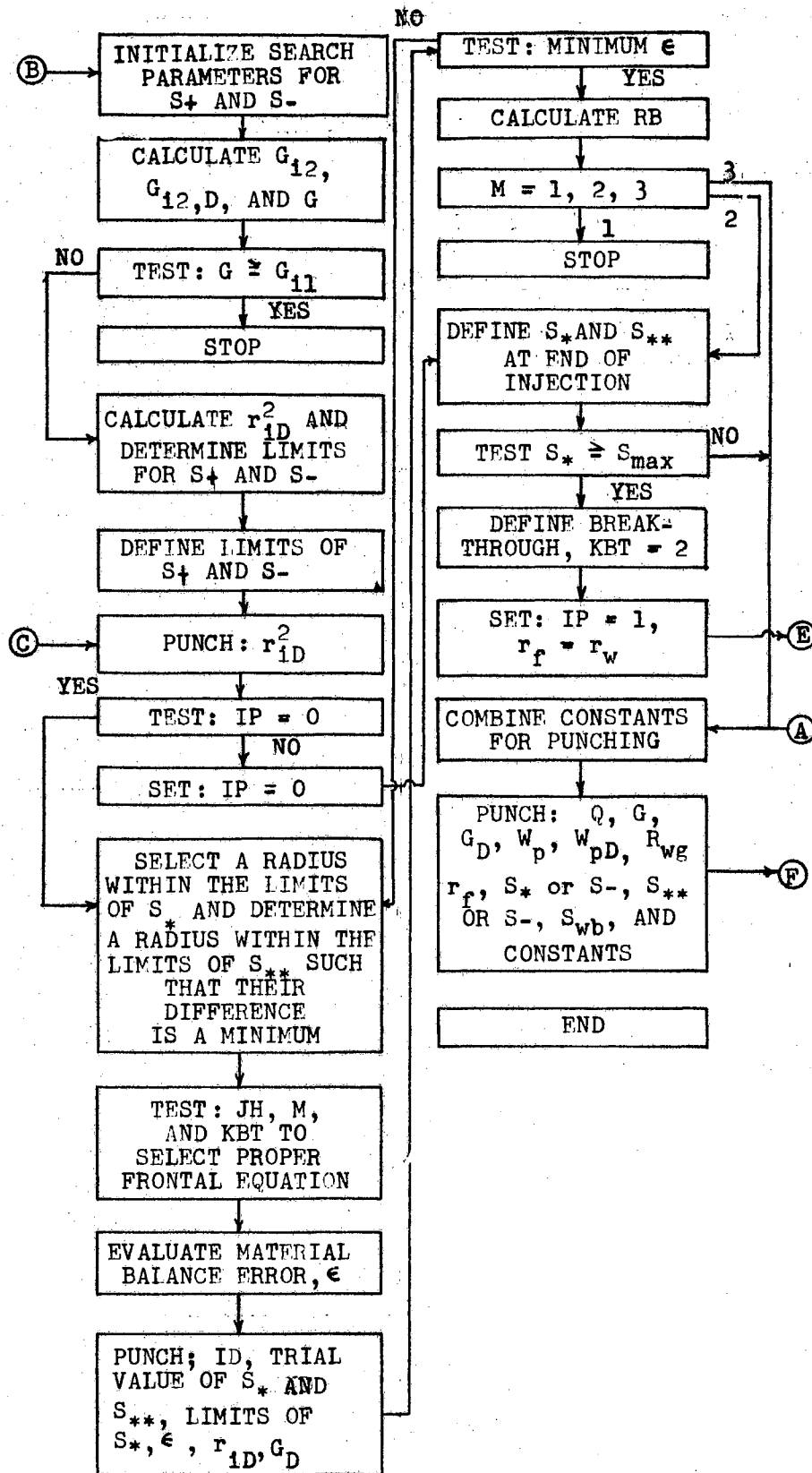


FIG. 35 (CONTINUED)

TABLE XXIII
CYCLIC, TWO-PHASE FLOW COMPUTER PROGRAM

```

C 0000 0 CYCLIC, TWO-PHASE FLOW
C 0000 1 RADIAL CASE
      1 0 DIMENSION D(100,2),DFD(100,2)
      1 1 ,RSDW2(100)
      30 0 GI=0.
      31 0 GI2=0.
    1031 0 FP=0.
    2031 0 GP=0.
    3031 0 WP=0.
    4031 0 GD=0.
    5031 0 WPD=0.
    6031 0 KBT=1
    7031 0 WGR=0.
    8031 0 JWB=0
    9031 0 KIW=1
    9131 0 IP=0
    9231 0 WPB=0.
    9331 0 KWB=0.
    9431 0 JB=0
      32 0 M=1
    1032 0 N=0
C 0000 0 READ FRACTIONAL FLOW DATA
    1132 0 IF(XCONF(1)) 35,2032,2032
    2032 0 READ5,ID,H,P,RW
    3032 0 PUNCH5,ID,H,P,RW
    4032 0 DO 8132 J=1,2
    4132 0 GO TO (5032,5232),J
    5032 0 READ6,X,IL,IU,IMD,DFDM,ISB,
    5032 1 DFDB
    5132 0 GO TO 6032
    5232 0 READ,X,ILW,X,IMDW,DFDMW,X,X
    6032 0 DO 8032 I=1,IU
    7032 0 READ7,X,X,X,FD(I,J),DFD(I,J),
    7032 1 X,X
    8032 0 CONTINUE
    8132 0 CONTINUE
    9032 0 DO 9132 I=1,ISB
    9132 0 DFD(I,1)=DFDB
      33 0 RW2=RW**2
      34 0 PIHP=3.1415927*H*P
    1034 0 DO 2034 I=IU,100
    2034 0 RSDW2(I)=0.
      35 0 ISWBU=IU
      36 0 ISWBL=0
    1036 0 ISB2=ILW
      37 0 IF(ILW=IL) 108,1037,3037
    1037 0 JH=1
    2037 0 GO TO 38
    3037 0 IF(IMDW=ISB) 4037,4037,6037
    4037 0 JH=2
    5037 0 GO TO 38
    6037 0 IF(ILW=ISB) 108,7037,7037
    7037 0 JH=3
C 0000 0 READ FLOW RATE
      38 0 READ4,JP,DELV
      39 0 IF(DELV) 41,102,40
      40 0 IF(KIW) 43,105,44
      41 0 M=2+N
    1041 0 KIW=-1
      42 0 GO TO 45
      43 0 N=N+2
      44 0 M=1+N
    1044 0 KIW=1
      45 0 GO TO(46,52,66,104),M
C 0000 0 INJECTION
      46 0 GI=GI+DELV
    1046 0 RB2=RW2+GI*DFDB/PIHP
      47 0 RB=(RB2)**.5
      48 0 G=GI
      49 0 ISBU=ISB
      50 0 ISBL=0
      51 0 GO TO 102
C 0000 0 INJECTION=WITHDRAWAL
      52 0 JWB=1
      53 0 IB=ISB
    1053 0 JB=1
    2053 0 KWB=1
      54 0 FP=FP+DELV
      55 0 FPD=FP/GI
      56 0 RM2=(DFD(IMDW,1)+DFDMW*FPD)/
      56 1 DFDB
      57 0 DO 62 I=1,IU
      58 0 RSDW2(I)=(DFD(I,1)+FPD*DFD(I,2
      58 1 ))/DFDB
    1058 0 GO TO (1061,2058,2058),JH
    2058 0 GO TO (1061,3058,1061),JB
    3058 0 IF(RSDW2(I)-RSDW2(I-1))4058,
    3058 1 1061,1061
    4058 0 IB=I-1
    5058 0 JB=3
    6058 0 KWB=2
    1061 0 IF(RSDW2(I)) 7061,2061,2061
    2061 0 GO TO (3061,5061,62),JWB
    3061 0 ISWBL=I
    4061 0 GO TO 59
    5061 0 ISWBU=I
    6061 0 GO TO 59
    7061 0 GO TO (7161,7361),KWB
    7161 0 JWB=2
    7261 0 GO TO 8061
    7361 0 JWB=3
    8061 0 GO TO (59,3062),KBT
      59 0 IF(RM2-RSDW2(I)) 61,1060,60
      60 0 GO TO (160,62,62),JH
    160 0 ISWBU=IU
    260 0 GO TO 5062
    1060 0 JB=2
    2060 0 GO TO (3060,61),JWB
    3060 0 JWB=2
    4060 0 ISWBL=0
      61 0 ISM=I
      62 0 CONTINUE
    1062 0 IF(RSDW2(ISWBU+1)+RSDW2(ISWBU)
    1062 1 )3062,3062,2062
    2062 0 ISWBU=ISWBU+1
    3062 0 IF(ISWBL) 4162,4162,3162
    3162 0 RATIO=RSDW2(ISWBL)/(RSDW2(ISWB
    3162 1 L)+ABSF(RSDW2(ISWBL+1)))
    3262 0 SWBL=(RATIO+FLOTF(ISWBL))/100
    3262 1 .
    3362 0 FDWBL=FD(ISWBL,2)+RATIO*(FD(
    3362 1 ISWBL+1,2)-FD(ISWBL,2))
    3462 0 FDWBL=FD(ISWB,1)+RATIO*(FD(ISW
    3462 1 BL+1,1)-FD(ISWBL,1))
    3562 0 IF(RSDW2(ISWBL+1)+RSDW2(ISWBL)
    3562 1 ) 4162,4162,4062
    4062 0 ISWBL=ISWBL+1
    4162 0 GO TO (5062,4262),KBT
    4262 0 ISWBU=ISWBL
    4362 0 ISBU=ISWBL
    4462 0 ISBL=ISWBL
    4562 0 GO TO (4662,4862,4862),JH
    4662 0 WP=GI*(1.-DFDB*SWBL-FPD*FDWBL)
    4662 1 +FP
    4762 0 GO TO 4962
    4862 0 WP=GI*(1.-FDWBL-FPD*FDWBL)+FP
    4862 1 +WPB
    4962 0 WGR=1./FDWBL-1.
      GO TO 6062
    5062 0 WP=(1.-FD(ISWBU,1)+FPD*(1.-
    5062 1 FD(ISWBU,2)))*GI
    5162 0 WPB=WP
    5262 0 WGR=1./FD(ISWBU,2)-1.
    6062 0 GD=(FP-WP)/GI
    7062 0 WPD=WP/GI
    8062 0 G=GI*(1.+GD)

```

TABLE XXIII (CONTINUED)

```

63 0 IF(G) 106,64,64
64 0 IE=ISM
1064 0 I1U=IMDW
2064 0 I1L=ILW
65 0 GO TO(80,1065),KBT
1065 0 IF(IP) 2065,2065,4065
2065 0 IP=1
3065 0 GO TO 1080
4065 0 IP=0
5065 0 GO TO 102
C 0000 0 INJECTION-WITHDRAWAL-INJECTION
66 0 ISWBU=0
67 0 ISWBL=0
1067 0 WGR=0.
68 0 GI2=GI2+DELV
69 0 GID=GI2/GI
1069 0 GD=GID
2069 0 GFD=GI2/FP
3069 0 G=GI+GI2+FP-WP
4069 0 IF(GI-G) 107,70,70
70 0 DO 75 I=1,IU
71 0 IF(I-ISB2) 72,1073,1073
72 0 RSDW2(I)=(DFD(I,1)+(FPD+GID)*
72 1 DFD(I,2))/DFDB
73 0 GO TO 75
1073 0 GO TO (74,2074),KBT
74 0 RSDW2(I)=(DFD(ISB1,1)+FPD*DFD(
74 1 ISB1,2)+GID*DFD(I,2))/DFDB
1074 0 GO TO 75
2074 0 RSDW2(I)=DFD(I,2)*GID/DFDB
75 0 CONTINUE
77 0 IB=IMD
78 0 IE=IU
79 0 I1U=ISB2
1079 0 I1L=ILW
C 0000 0 MATERIAL BALANCE
80 0 FDEL=99.0E19
1080 0 PUNCH,RSDW2
2080 0 IF(IP) 81,81,3080
3080 0 IP=0
4080 0 GO TO 2100
81 0 DO 100 I=IB,IE
1081 0 DR1=99.0E19
82 0 DO 93 IBL=I1L,I1U
94 0 DR=ABSF(RSDW2(I)-RSDW2(IBL))
95 0 IF(DR-DR1) 96,96,83
96 0 DR1=DR
98 0 L=IBL
93 0 CONTINUE
83 0 DS=(FLOTF(I-L))/100.
84 0 SI=(FLOTF(L))/100.
85 0 F1=DFD(I,2)*DS-DFD(I,2)+FD(L,2)
1085 0 GO TO (105,86,88,104),M
86 0 GO TO (1086,1086,3086),JH
1086 0 FUN=F1-(FD(I,1)-DFDB*SI-
1086 1 DFD(I,1)*DS)/FPD
2086 0 GO TO 90
3086 0 FUN=F1-(FD(I,1)-FD(L,1)-DFD(I,
3086 1 1)*DS)/FPD
87 0 GO TO 90
88 0 DS1=(FLOTF(ISB2-L))/100.
89 0 GO TO (2089,1089),KBT
1089 0 GO TO (2089,2089,8089),JH
2089 0 FUN=F1-(FD(ISB2,2)-FD(L,2))/GF
2089 1 D-DS1*DFDB/GID
3089 0 GO TO (4089,90),KBT
4089 0 FUN=FUN+DS1*(DFD(ISB1,1)/GID+D
4089 1 FD(ISB1,2)*GFD)
5089 0 GO TO (90,90,6089),JH
6089 0 FUN=FUN+(DFDB*DS1-DFD(ISB2,1)+
6089 1 FD(L,1))/GID
7089 0 GO TO 90
8089 0 FUN=F1-(FD(ISB2,1)-FD(L,1))/GI
8089 1 D-(FD(ISB2,2)-FD(L,2))*GFD
90 0 FUN=ABSF(FUN)
1090 0 IF(FDEL-FUN) 1097,91,91
91 0 ISBL=L
92 0 FDEL=FUN
97 0 ISBU=I
1097 0 I1LU=I1L*10000+I1U
2097 0 IBIE=IB*10000+IE
3097 0 IDJP=ID+JP
99 0 PUNCH,IDJP,I,L,I1LU,IBIE,FUN,
99 1 DR1,GD
100 0 CONTINUE
3101 0 RB=(RSDW2(ISBU)*(RB2-RW2)+RW2)
3101 1 **.5
1100 0 GO TO (105,2100,102),M
2100 0 ISB1=ISBU
3100 0 ISB2=ISBL
101 0 IF(ISBU-ISWBU) 102,1101,1101
1101 0 KBT=2
RB=RW
IP=1
GO TO 4262
102 0 KP=JP+M*1000000+10000
1102 0 PUNCH4,KP,DELV,G,WP,GD,WPD,
1102 1 WGR,RB
2102 0 KP=KP+10000
3102 0 KWB=KWB*10000+JWB*100+JB
4102 0 PUNCH5,KP,ISBU,ISBL,ISWBU,
4102 1 ISWBL,JH,KBT,KJWB
103 0 GO TO 38
C 0000 0 STOP 1444, M=4, 45,85
104 0 STOP 1444
C 0000 0 STOP 1111, M=1, 40,85,1100
105 0 STOP 1111
C 0000 0 STOP 1999, G=0., 4064
106 0 STOP 1999
C 0000 0 STOP 1333, G=GI, M=3, 4069
107 0 STOP 1333
C 0000 0 STOP 1888, ILW, 37,6037
108 0 STOP 1888
END

```

conditions, injected or volume of fluid (gas or gas and water) withdrawn during a time period. The injected volumes are considered positive, and the produced volumes are considered negative.

Since the calculations are based upon volumes instead of rates, no real values of time are required; only the cumulative volumes of flow within time periods. Therefore, the number of time periods is unlimited except that calculation stops at the beginning of the second withdrawal.

The data output contains two cards for each fluid volume input. The first card has the following values: 1) volume identification; 2) fluid volume; 3) volume of gas in place; 4) cumulative volume of water produced; 5) fraction of initial gas volume that has been produced or re-injected; 6) water production as a fraction of initial injected gas volume; 7) producing water gas ratio at the end of the time period; and 8) the radius of the gas-water front. The second card has 1) the volume identification; 2) the upper saturation at the front; 3) the lower saturation at the front; 4) the upper saturation at the well-bore; 5) the hypothetical lower saturation at the well-bore; 6) an index identifying the hysteresis case (JH=1 for non-hysteresis and for $S_{gr} \leq S_f$; JH = 3 for $S_{gr} \geq S_f$); 7) an index identifying breakthrough (KBT = 1, before breakthrough; KBT = 2 after breakthrough); and 8) a combination of several indices used in the calculation.

APPENDIX C

SYMBOLS

TABLE XXIV

SYMBOL LIST FOR THE TEXT

A	Area, ft^2 .
a	Coefficient of linear term in linear equation for gas compressibility factor, Z.
a	Statistical estimate of ordinal intercept, α , of least squares regression line for Klinkenberg permeability.
a_0	Constant term of fourth degree polynomial for least squares fit of relative permeability function.
a_1	Coefficient of linear term of fourth degree polynomial.
a_2	Coefficient of quadratic term of fourth degree polynomial.
a_3	Coefficient of cubic term of fourth degree polynomial.
a_4	Coefficient of quartic term of fourth degree polynomial.
B	Fluid formation volume factor, vol./vol.
b	Constant term in linear equation for gas compressibility factor, Z.
b	Statistical estimate of regression coefficient, β , in least squares regression line for Klinkenberg permeability.
c	Combined compressibility of formation and water, psi^{-1} .
f_f, f_{fl}	Drainage fractional flow at gas-water front during injection.
f'_f, f'_{fl}	Derivative of f_f with respect to saturation.
f_i	Fractional flow of fluid "i".
f'_i	Derivative of f_i with respect to saturation.
f_{wb}, f_{wbl}	Drainage fractional flow at the well-bore saturation.

TABLE XXIV (CONTINUED)

f_{*}, f_{*1}	Drainage fractional flow at upper saturation of the front during withdrawal.
f_{*}, f'_{*1}	Derivative of f_{*}, f_{*1} with respect to saturation.
f_{*2}	Imbibition fractional flow at the upper saturation of the front during withdrawal.
f'_{*2}	Derivative of f_{*2} with respect to saturation.
f_{**}, f_{**1}	Drainage fractional flow at the lower saturation of the front during withdrawal.
f'_{**1}	Derivative of f_{**1} with respect to saturation.
f_{**2}	Imbibition fractional flow at the lower saturation of the front during withdrawal.
f_{+}, f_{+1}	Drainage fractional flow at the upper saturation of the front during re-injection.
f'_{+}, f_{+1}	Derivative of f_{+}, f_{+1} with respect to saturation.
f_{+2}	Imbibition fractional flow at the upper saturation of the front during re-injection.
f'_{+2}	Derivative of f_{+2} with respect to saturation.
f_{-}, f_{-1}	Drainage fractional flow at the lower saturation of the front during re-injection.
f'_{-}, f'_{-1}	Derivative of f_{-}, f_{-1} with respect to saturation.
f_{-2}	Imbibition fractional flow at the lower saturation of the front during re-injection.
f'_{-2}	Derivative of f_{-2} with respect to saturation.
G_i	Cumulative volume of injected gas at reservoir conditions, ft^3 .
ΔG_i	Change of injected gas volume at reservoir conditions during time interval Δt , ft^3 .
$\Delta G'_i$	Change of injected gas volume at standard conditions during time interval Δt , ft^3 .
$G_{i,1}$	Volume of gas injected during first injection, ft^3 .

TABLE XXIV (CONTINUED)

$G_{i,2}$	Volume of gas injected during second injection, ft ³ .
G_p	Cumulative volume of gas produced at reservoir conditions, ft ³ .
G_r	Volume of residual gas in reservoir at end of withdrawal.
G_{rD}	Ratio of residual gas volume to initial injected gas volume.
g	Undetermined mathematical function.
h	Formation thickness, ft.
i_g	Gas injection rate at reservoir conditions, ft ³ /da.
i'_g	Gas injection rate at standard conditions, ft ³ /da.
\bar{j}	Upward directed unit normal vector.
k	Absolute permeability, millidarcys, darcys.
k_g	Single-phase gas permeability.
k_k	Klinkenberg permeability.
k_{ri}	Relative permeability to fluid "i".
k_w	Single phase water permeability
\bar{k}	Average permeability
\hat{k}	Statistical estimate of permeability
L	Reservoir length, ft.
P_c	Capillary pressure.
$P_{c,n}$	Pressure at outer radius of incompressible core (inner radius of aquifer) at time "n", psi.
$\bar{P}_{g,n}$	Average pressure in the gas zone at time "n", psia.
P_i	Pressure in fluid "i", atm.
P_{sc}	Pressure at standard conditions, psia.
$P_{w,n}$	Well-bore pressure at time "n", psi.

TABLE XXIV (CONTINUED)

$\Delta p_{1,n}$	Pressure increment in the two-phase gas zone at time "n", psi.
$\Delta p_{2,n}$	Pressure increment in the incompressible water zone at time "n", psi.
q_i	Flow rate of fluid "i",
Q_p	Cumulative volume of fluid produced, ft ³ .
q_t	Total flow rate.
r_f	Radius of the gas-water front during injection, ft.
R_i	Electrical resistance at saturation "i", ohms.
r_i	Radius of saturation "i", ft.
r_{iD}	Dimensionless radius of saturation "i".
$r_{k,m}$	Radius of saturation "k" at time "m", ft.
r_{md}	Radius of the saturation having the maximum derivative of fractional flow, ft.
R_R	Electrical resistance ratio.
r_w	Well-bore radius, ft.
$R_{100,68}$	Electrical resistance at $S_w = 100\%$ and 68°F., ohms.
r_*	Radius of the upper saturations of the front during withdrawal, ft.
r_{**}	Radius of the lower saturation of the front during withdrawal, ft.
r_+	Radius of the upper saturation of the front during re-injection.
r_-	Radius of the lower saturation of the front during re-injection, ft.
s_b	Sample standard deviation of the regression coefficient.
S_f	Saturation of the front during injection, fraction.
\bar{S}_f	Average saturation behind the front during injection.
S_g	Gas saturation, fraction.

TABLE XXIV (CONTINUED)

\bar{S}_g	Average gas saturation, fraction.
$S_{g,dr}$	Gas saturation on the drainage relative permeability curve, fraction.
S_{gi}	Initial gas saturation, fraction.
$S_{g,imb}$	Gas saturation on the imbibition relative permeability curve, fraction.
S_{gr}	Residual gas saturation, fraction.
S_i	Saturation of fluid "i", fraction.
$s_{\hat{k},i}$	Sample standard deviation of \hat{k} at the value "i" of the independent variable.
S_{max}	Maximum gas saturation, fraction.
S_{md}	Saturation with the maximum derivative of fractional flow, fraction.
S_{wb}	Well-bore saturation, fraction.
$s_{y \cdot x}$	Standard deviation from regression.
S_*	Upper saturation of the front during withdrawal, fraction.
S_{**}	Lower saturation of the front during withdrawal, fraction.
S_+	Upper saturation of the front during re-injection.
S_-	Lower saturation of the front during re-injection.
T	Temperature, °K, °R or °F.
t	Time, seconds or days.
$t_{i,n}$	Student's "t" at confidence level "i" for "n" degrees of freedom.
T_r	Reservoir temperature, °R.
T_{sc}	Temperatures at standard conditions, °R.
\bar{u}_i	Velocity vector for fluid "i".
V	Volume, ft ³ .

TABLE XXIV (CONTINUED)

V_k	Volume enclosed by saturation "k", ft ³ .
w_i	Core weight at saturation "i", gm.
W_p	Volume of water production, ft ³ .
w_0	Dry weight of core, gm.
X	Statistical deviation of independent variable from its mean.
x_i	Linear distance to saturation "i", ft.
x_{iD}	Dimensionless Linear distance to saturation "i", ft.
y	Statistical deviation of dependent variable from its mean.
z	Coordinate axis in the direction of \bar{j} .
Z	Gas compressibility factor.
Z_{sc}	Gas compressibility factor at standard conditions
α	Constant term of the regression line,
α_1	Term defined by Equation (38).
α_2	Term defined by Equation (40).
α_3	Term defined by Equation (A-56).
β	Slope of the regression line.
β_1	Term defined by Equation (39).
β_2	Term defined by Equation (41).
β_3	Term defined by Equation (A-54).
γ_1	Term defined by Equation (42).
∇	Differential vector operator.
π	Constant, 3.1415927.
μ_i	Viscosity of fluid "i", cp.
ρ_i	Density of fluid "i".
\emptyset	Porosity, fraction.

TABLE XXV

SYMBOLS FOR THE RELATIVE PERMEABILITY COMPUTER PROGRAM

A	area of core
BK	base permeability, md
D	diameter of core, cm
DMV	differential pressure recorder range, mv.
DP	differential pressure, chart divisions
GK	gas effective permeability, md
GMV	downstream pressure recorder range, mv.
I	identification number
PB	barometric pressure, mm Hg
PM	mean core pressure, atm
P2	downstream pressure, chart divisions
QG	gas flow rate, cc/sec
QW	water flow rate, cc/sec
RGK	gas relative permeability
RWK	water relative permeability
RR	resistance ratio
RS	A-C resistance of core at $S_w = S$
RS1	A-C resistance of core at $S_w = 100\%$
T	time, sec
TK	temperature, °K

TABLE XXV (CONTINUED)

TR	flowing temperature, °F
VG	gas viscosity, c;
VW	water viscosity, cp
WK	water effective permeability, md.
X	length of core, cm

TABLE XXVI

SYMBOL LIST FOR SATURATION-RESISTANCE COMPUTER PROGRAM

DIA	Core diameter, in.
ID	Identification number.
J	Subscript.
JE	Maximum value of J.
K	A number identifying whether saturation was obtained under drainage or imbibition conditions.
POR	Porosity, ϕ , fraction.
RMIN	Electrical saturation at $S_w = 100\%$ and 68°F , $R_{100,68}$, ohms or kilohms.
RR	Electrical resistance ratio of RSC to RMIN, R_R , fraction.
RS	Electrical resistance at a saturation to be calculated and at a measured temperature, R_i , ohms or kilohms.
RSC	Electrical resistance RS corrected to 68°F , ohms or kilohms.
TR	Fluid temperature at core outlet, T, $^\circ\text{F}$.
WD	Dry weight of core, gm.
WMAX	Weight of core at $S_w = 100\%$, fraction.
WS	Weight of core at a resistance RS, gm.
WW	Weight of water in core at a resistance RS, gm.
XL	Core Length, cm.

TABLE XXVII

SYMBOL LIST FOR RELATIVE PERMEABILITY TABULATOR COMPUTER PROGRAM

A0	Constant term of fourth degree least squares polynomial, a_0 .
A1	Linear term of fourth degree polynomial a_1 .
A2	Quadratic term of fourth degree polynomial, a_2 .
A3	Cubic term of fourth degree polynomial, a_3 .
A4	Quartic term of fourth degree polynomial, a_4 .
I	Subscript.
ID	Identification number.
IL	Critical gas saturation, S_{gc} , per cent.
IL1	IL-1.
ILW	Residual gas saturation, S_{gr} , per cent.
ILW1	ILW-1.
IU	Maximum gas saturation, S_{max} , per cent.
K	Subscript.
N	Degree of least squares polynomial.
N1	N+1.
RK	Relative permeability, k_{ri} , md.
RKI	Imbibition relative permeability.
SG	Gas saturation, S_g , per cent.
SGU	Maximum gas saturation, S_{max} , per cent.

TABLE XXVIII

SYMBOL LIST FOR KLINKENBERG PERMEABILITY COMPUTER PROGRAM

A	Flow area of core, cm^2 .
AK	Average permeability, \bar{k} , md.
ARPM	Average reciprocal mean pressure, $\overline{(1/p)}$, atm^{-1} .
B	Sample regression coefficient, b .
BHI	One-half of confidence interval for the regression coefficient.
BL	Lower limit of confidence interval on the population regression coefficient β .
BU	Upper limit of confidence interval on the population regression coefficient β .
C	Sum of squares correction for the mean.
DF	Degrees of freedom.
DP	Differential pressure, atm.
ESK	Least squares estimate of permeability, \hat{k} , md.
FN	Number of data points.
GK	Gas permeability, k_g , md.
GKHI	One-half of confidence interval on Klinkenberg permeability, md.
GKK	Klinkenberg permeability, k_k , md.
GKKL	Lower limit of confidence interval on Klinkenberg permeability, md.
GKKU	Upper limit of confidence interval on Klinkenberg permeability, md.

TABLE XXVIII (CONTINUED)

ID	Identification number.
IDF	Degrees of freedom.
J	Subscript.
JM	Maximum value of J.
PERB	Ratio of half confidence interval of the regression coefficient to its estimate, per cent.
PERGK	Ratio of half confidence interval of Klinkenberg permeability to its estimate, per cent.
PM	Mean core pressure, \bar{p} , atm.
QG	Gas flow rate, q_g , cc/sec.
QW	Water flow rate, q_w , cc/sec.
RPM	Reciprocal mean pressure, $1/\bar{p}$, atm ⁻¹ .
RR	Electrical resistance ratio, R_R .
RS	Measured electrical core resistance, R_i , ohms or kilohms.
SB	Sample standard deviation of the regression coefficient, s_b .
SD	Sample standard deviation, S_d .
SKS	Sum of squares of sample permeabilities.
SPS	Sum of squares of sample reciprocal mean pressures.
SUMK	Sum of sample permeabilities.
SUMP	Sum of reciprocal mean pressures.
SUMPK	Sum of permeability -- reciprocal mean pressure products.
SXS	Corrected sum of squares for reciprocal mean pressure, x^2 .
SXY	Corrected sum of squares for permeability -- reciprocal mean pressure products.
SYH	Sample standard deviation of \hat{k} .
SYS	Corrected sum of squares for permeability, y^2 .

TABLE XXVIII (CONTINUED)

T	Calculated Student's "t" for the sample.
TR	Fluid temperature.
TS	Student's "t" (62).
TS1	Significant Student's "t" at the 5% level for IDF degrees of freedom.
VG	Gas viscosity, μ_g , cp.
VW	Water viscosity, μ_w , cp.
WK	Water permeability, k_w , md.

TABLE XXIX

SYMBOL LIST FOR FRACTIONAL FLOW COMPUTER PROGRAM

DFD	Derivative of fractional flow, f' .
DFDB	Derivative of fraction flow at the front, f'_f .
DFDM	Maximum derivative of fractional flow f'_{md} .
FD	Fractional flow, f .
FMIN	Minimum value of f/S .
FS	Ratio of fractional flow to its saturation, f/S .
F1	Material balance function at breakthrough, Equation (B-23).
GDBT	Fraction of injected gas remaining in the reservoir at breakthrough, G_r .
IB	$IL + 1$.
ID	Identification number.
IDS	Combined identification and saturation.
IL	Critical gas saturation, S_{gc} .
IMD	Saturation for DFDM.
ISAI	Average saturation behind the front for injection, \bar{S}_f , per cent.
ISAW	Average saturation behind the front at breakthrough (non-hysteresis), per cent.
ISB	Saturation at the front, S_f , per cent.
ISBT	Saturation at the front at breakthrough (non-hysteresis), S_{**} , per cent.

TABLE XXIX (CONTINUED)

IU	Maximum gas saturation, S_{\max} , per cent.
RK(I,1)	Injected phase relative permeability, k_{rg} , fraction.
RK(I,2)	Displaced phase relative permeability, k_{rw} , fraction.
RSD	Dimensionless radius of a saturation, fraction.
RSD2	Square of dimension radius of a saturation, fraction.
SBT	Frontal saturation at breakthrough (non-hysteresis), S_{**} , per cent.
SI	Gas saturation, S_g , fraction.
V1	Injected phase viscosity, μ_g , cp.
V2	Displaced phase viscosity, μ_w , cp.
WGRBH	Well bore water-gas ratio, R_{wg} , vol./vol.

TABLE XXX

SYMBOL LIST FOR TWO-PHASE GAS ZONE-UNSTEADY AQUIFER COMPUTER PROGRAM

A	Defined by Statement 152.
AA	Defined by Statement 182, α_1 , psia.
ADP	Pressure convergence difference, psia.
AIC	Defined by Statement 131.
AIU	Defined by Statement 180.
AQS	Defined by Statement 1132.
ATP	Defined by Statement 132.
ATPR	Defined by Statement 181.
AU	Defined by Statement 2177.
B	Defined by Statements 149, 154, or 156.
BB	Defined by Statement 183, β_1 , psi ² .
BK	Base (single-phase) permeability for relative permeability functions, md.
C	Combined compressibility of formation water and rock, psi ⁻¹ .
CTD	Dimensionless time constant.
CU	Unsteady flow constant.
DFDB	Derivative of fractional flow at the front, f'_f , fraction.
DPIC	Pressure increment due to liquid flow in the incompressible zone between RB and RA, psi.
DPO	Allowable pressure convergence difference, psia.
DPTP	Pressure increment due to unsteady compressible liquid flow beyond RA, psi.

TABLE XXX (CONTINUED)

DPU	Unsteady-state pressure increment for compressible liquid flow in the aquifer, psi.
DPU1	Defined by Statement 177
DPU2	Defined by Statement 1177.
DT	Time increment, days.
FD	Gas fractional flow, f_g , fraction.
GC	Gas volume constant, psi.
H	Formation thickness, h, ft.
HBKG	Incompressible flow constant.
I	Gas saturation, S_g , per cent.
IL	Critical gas saturation, S_{gc} , per cent.
IU	Maximum gas saturation, S_{max} , per cent.
J	Subscript.
JB	Number of the gas injection period at which calculation are to begin.
JC	JB-1.
JM	Maximum number of constant gas injection rates included in the problem.
JP	Sorting number based on Statements 185, 187, and 189.
K	Subscript.
KR	Index: 0-read in fractional flow values; 1 - values already on drum.
L	Subscript.
LM	Number of iterations for pressure convergence.
P	Porosity, ϕ , fraction.
PB	Pressure at standard conditions, p_{sc} , psia.
PG	Average gas zone pressure, \bar{p}_g , psia.

TABLE XXX (CONTINUED)

PG2	Previous value of average gas zone pressure, psia.
PIHP	Constant defined by Statement 107.
PO	Initial reservoir pressure, p_i , psi.
PT	Dimensionless unsteady-state pressure change function (28, 68).
PW	Well-bore pressure, p_w , psi.
QD	Gas injection rate, i_g , scf/day.
QMAX	Maximum volume of injected gas, $G_{i,max}$, scf.
RA	Maximum radius of gas zone (radius of assumed incompressible zone), r_c , ft.
RK(I,1)	Injected phase relative permeability, k_{rg} , md.
RK(I,2)	Displaced phase relative permeability, k_{rw} , md.
RLN	Logarithm of radius ratio.
RSD	Dimensionless radius of saturation, r_{iD} , fraction.
RW	Well bore radius, r_w , ft.
RWD	Dimensionless well bore radius, r_w/r_b , fraction.
SQS1	Defined by Statement 2129.
SUMQ	Cumulative volume of gas in place at reservoir conditions, G , ft^3 .
SUMQS	Cumulative volume of gas in place at standard conditions, G_{sc} , scf.
T(J)	Time elapsed from beginning of injection to end of Jth flow rate, t , days.
TB	Gas temperature at standard conditions, T_{sc} , °R.
ID	Dimensionless time, t_d (28, 68).
TPR	Flow resistance integral for two-phase zone.
TR	Reservoir temperature, T_r , °R.

TABLE XXX (CONTINUED)

V1	Injected phase viscosity, μ_g , cp.
V2	Displaced phase viscosity, μ_w , cp.
ZC	Constant for linear gas compressibility equation, b.
ZM	Slope of linear gas compressibility equation, a.
ZPG	Ratio of gas compressibility to average gas zone pressure, psi^{-1} .

TABLE XXXI

SYMBOL LIST FOR CYCLIC TWO-PHASE FLOW COMPUTER PROGRAM

DELV	Reservoir volume of gas injected during a time-step, G_i , ft^3 .
DFD	Derivative of fractional flow, f' , fraction.
DFDB	Derivative of fractional flow at the front (first injection), f'_f fraction.
DFDM	Maximum fractional flow derivative (drainage), $f'_{\text{md},1}$, fraction.
DFDMW	Maximum fractional flow derivative (imbibition) $f'_{\text{md},2}$, fraction.
DR	Increment of dimensionless radius, r_{iD} , fraction.
DRL	Minimum value of DR, fraction.
DS	Increment of saturation, Statement 83.
DSL	Increment of saturation, Statement 88.
FD	Fractional flow, f_g , fraction.
FDEL	Minimum value of material balance function.
FDWBL	Fractional flow at the lower saturation at the well bore, fraction.
FP	Cumulative volume of fluid produced, Q_p , ft^3 .
FPD	Dimensionless fluid produced, $Q_p/G_{i,\text{max}}$, fraction.
FUN	Material balance function.
F1	Partial material balance function.
G	Volume of gas in reservoir, G , ft^3 .

TABLE XXXI (CONTINUED)

GD	Dimensionless volume of gas injected or produced, $G_{i,2}/G_{i,max}$ or $G_p/G_{i,max}$.
GFD	Ratio of volume of gas re-injected to fluid produced, $G_{i,2}/G_{i,max}$, fraction.
GI	Cumulative volume of gas injected (first injection), G_i , ft ³ .
GI2	Cumulative volume of gas injected (second injection), $G_{i,2}$, ft ³ .
GP	Cumulative volume of gas produced, G_p , ft ³ .
H	Reservoir thickness, h, ft.
IB	Indexing parameter.
IBIE	Defined by Statement 2097.
IBL	Indexing parameter.
ID	Core identification.
IDJP	Defined by Statement 3097.
IE	Indexing parameter.
IL	Critical gas saturation, S_{gc} , per cent.
ILW	Residual gas saturation, S_{gr} , per cent.
ILLU	Defined by Statement 1097.
IMD	Saturation with maximum fractional flow derivative (drainage), $S_{md,1}$, per cent.
IMDW	Saturation with maximum fractional flow derivative (imbibition), $S_{md,2}$, per cent.
IP	Punch index.
ISB	Saturation at the front (first injection) S_f , per cent.
ISBL	Lower saturation at the front, S_{**} , or S_- , per cent.

TABLE XXXI (CONTINUED)

ISBU	Upper saturation at the front, S_* or S_+ , per cent.
ISB1	Upper saturation at the front (withdrawal), S_* , per cent.
ISB2	Lower saturation at the front (withdrawal), S_{**} , per cent.
ISWBL	Lower saturation at the well bore, S_{wb} , per cent.
IU	Maximum gas saturation, S_{max} , per cent.
ILL	Trial lower saturation at the front, S_{**} , or S_- , per cent.
JB	Index used in search for IB.
JH	Index identifying hysteresis case: 1 for non-hysteresis, 2 for $S_{gr} \leq S_f$, 3 for $S_{gr} \geq S_f$.
JP	Flow increment identification.
JWB	Index used in search for ISWBL and ISWBU.
KBT	Breakthrough index: 1 - before, 2 - after.
KIW	Injection-withdrawal index: 1 - injection, 2 - withdrawal.
KJWBB	Defined by Statement 3102.
KP	Punch identification.
KWB	Index used in search for ISWBL and ISWBU.
L	Saturation for DR1, per cent.
M	Injection-withdrawal index: 1 - first injection, 2 - withdrawal, 3 - second injection.
N	Index used in determining M.
P	Porosity, ϕ , fraction.
PIHP	Defined by Statement 34.
RATIO	Interpolation ratio for determining SWBL, fraction.
RB	Radius of the gas water front, r_f , ft.
RB2	Square of RB, r_f^2 , ft ² .

TABLE XXXI (CONTINUED)

RM2	Dimensionless radius of S_{md} , fraction.
RSDW2	Square of dimensionless radius of a saturation, fraction.
RW	Well-bore radius, r_w , ft.
RW2	Square of well-bore radius, r_w^2 , ft ² .
SI	Gas saturation, S_g , fraction.
SWBL	Lower gas saturation at the well bore, fraction.
WGR	Reservoir water-gas ratio, R_{wg} , vol/vol.
WP	Cumulative volume of water produced, W_p , ft ³ .
WPB	Cumulative volume of water produced before breakthrough, ft ³ .
WPD	Dimensionless water production, $W_p/G_{i,max}$.
X	Unnecessary data.

VITA

Edward Glen Woods

Candidate for the Degree of

Doctor of Philosophy

Thesis: AN INVESTIGATION OF CYCLIC, IMMISCIBLE TWO-PHASE FLOW IN
POROUS MEDIA

Major Field: Mechanical Engineering

Biographical:

Personal Data: Born at Sharon, Oklahoma, December 6, 1935, the son of Ted G. and Sylvia C. Woods.

Education: Attended grade school at Seiling, Oklahoma; graduated from Seiling High School, Seiling, Oklahoma, in 1954; received the Bachelor of Science Degree from Oklahoma State University in January 1959; completed requirements for the Master of Science degree in April, 1960; completed requirements for the Doctor of Philosophy degree in April, 1963.

Experience: Employed as a part-time service station attendant from January, 1950 to September, 1954; employed by the Halliburton Oil Well Cementing Company at Odessa, Texas, as a cementing and fracturing truck driver during the summer of 1956 and at the Halliburton Technical Center in Duncan, Oklahoma, as a draftsman during the summer of 1957; employed as a roustabout by the Tidewater Oil Company at Kiefer, Oklahoma, during the summer of 1958; employed by Oklahoma State University as an engineering research assistant from January, 1959, to June, 1960, and from September 1960 to April, 1963; employed by Phillips Petroleum Company production research laboratory, Bartlesville, Oklahoma, as an engineer during the summer of 1960.

Professional Organizations: Engineer-in-training (Oklahoma); Society of Petroleum Engineers of AIME; PI TAU SIGMA.